

Institut für Physik
Arbeitsgruppe Nichtlineare Dynamik

Phase Synchronization Analysis of Event-Related Brain Potentials in Language Processing

Dissertation
zur Erlangung des akademischen Grades
doctor rerum naturalium (Dr. rer. nat.)
im Fach Physik / Nichtlineare Dynamik

eingereicht an der
Mathematisch-Naturwissenschaftlichen Fakultät
der Universität Potsdam

von
Carsten Allefeld

Potsdam, März 2004

Zusammenfassung

Das Forschungsthema Synchronisation bildet einen Schnittpunkt von Nichtlinearer Dynamik und Neurowissenschaft. So hat zum einen neurobiologische Forschung gezeigt, daß die Synchronisation neuronaler Aktivität einen wesentlichen Aspekt der Funktionsweise des Gehirns darstellt. Zum anderen haben Fortschritte in der physikalischen Theorie zur Entdeckung des Phänomens der Phasensynchronisation geführt. Eine dadurch motivierte Datenanalysemethode, die Phasensynchronisations-Analyse, ist bereits mit Erfolg auf empirische Daten angewandt worden.

Die vorliegende Dissertation knüpft an diese konvergierenden Forschungslinien an. Ihren Gegenstand bilden methodische Beiträge zur Fortentwicklung der Phasensynchronisations-Analyse, sowie deren Anwendung auf ereigniskorrelierte Potentiale, eine besonders in den Kognitionswissenschaften wichtige Form von EEG-Daten.

Die methodischen Beiträge dieser Arbeit bestehen zum ersten in einer Reihe spezialisierter statistischer Tests auf einen Unterschied der Synchronisationsstärke in zwei verschiedenen Zuständen eines Systems zweier Oszillatoren. Zweitens wird im Hinblick auf den viel-kanaligen Charakter von EEG-Daten ein Ansatz zur multivariaten Phasensynchronisations-Analyse vorgestellt.

Zur empirischen Untersuchung neuronaler Synchronisation wurde ein klassisches Experiment zur Sprachverarbeitung repliziert, in dem der Effekt einer semantischen Verletzung im Satzkontext mit demjenigen der Manipulation physischer Reizeigenschaften (Schriftfarbe) verglichen wird. Hier zeigt die Phasensynchronisations-Analyse eine Verringerung der globalen Synchronisationsstärke für die semantische Verletzung sowie eine Verstärkung für die physische Manipulation. Im zweiten Fall läßt sich der global beobachtete Synchronisationseffekt mittels der multivariaten Analyse auf die Interaktion zweier symmetrisch gelegener Gehirnareale zurückführen.

Die vorgelegten Befunde zeigen, daß die physikalisch motivierte Methode der Phasensynchronisations-Analyse einen wesentlichen Beitrag zur Untersuchung ereigniskorrelierter Potentiale in den Kognitionswissenschaften zu leisten vermag.

Abstract

The topic of synchronization forms a link between nonlinear dynamics and neuroscience. On the one hand, neurobiological research has shown that the synchronization of neuronal activity is an essential aspect of the working principle of the brain. On the other hand, recent advances in the physical theory have led to the discovery of the phenomenon of phase synchronization. A method of data analysis that is motivated by this finding—phase synchronization analysis—has already been successfully applied to empirical data.

The present doctoral thesis ties up to these converging lines of research. Its subject are methodical contributions to the further development of phase synchronization analysis, as well as its application to event-related potentials, a form of EEG data that is especially important in the cognitive sciences.

The methodical contributions of this work consist firstly in a number of specialized statistical tests for a difference in the synchronization strength in two different states of a system of two oscillators. Secondly, in regard of the many-channel character of EEG data an approach to multivariate phase synchronization analysis is presented.

For the empirical investigation of neuronal synchronization a classic experiment on language processing was replicated, comparing the effect of a semantic violation in a sentence context with that of the manipulation of physical stimulus properties (font color). Here phase synchronization analysis detects a decrease of global synchronization for the semantic violation as well as an increase for the physical manipulation. In the latter case, by means of the multivariate analysis the global synchronization effect can be traced back to an interaction of symmetrically located brain areas.

The findings presented show that the method of phase synchronization analysis motivated by physics is able to provide a relevant contribution to the investigation of event-related potentials in the cognitive sciences.

Contents

1	Introduction	7
1.1	Temporal binding	7
1.2	Synchronization	11
1.3	Aims and outline	13
2	Basic Concepts	15
2.1	Electroencephalography	15
2.2	Event-related potentials	19
2.3	Phase synchronization	24
3	Data Processing and Bivariate Analysis	33
3.1	Reduction of spurious correlations	33
3.2	Determination of the instantaneous phase	36
3.3	Quantification of bivariate phase synchronization and directional statistics	41
4	Statistical Tests for Bivariate Phase Synchronization	47
4.1	Parametric tests	49
4.2	A simple nonparametric test	52
4.3	Bootstrap techniques	53
4.4	Data from time series	55
5	Multivariate Phase Synchronization Analysis	57
5.1	Synchronization cluster analysis	58
5.2	Application to ERP data	61
6	A Language Processing Experiment	67
6.1	Experimental setup and analysis	68
6.2	Results	70
6.3	Discussion	74
7	Conclusion and Outlook	77
A	Language Material	83
	Bibliography	87

Chapter 1

Introduction

The topic of synchronization has recently achieved an outstanding role in neurobiology and cognitive science as well as in nonlinear dynamics. In cognitive neuroscience, synchronization is more and more considered to be one of the basic mechanisms of brain function, from visual perception up to highest cognitive processes. In physics, the long known phenomenon of synchronization of periodic oscillators has in the last years been extended to chaotic systems. These recent advances have led to a cooperation of the two research fields which forms the background of the present thesis.

This chapter gives a short introduction into this converging research. It formulates the main theoretical ideas that have led to the current interest in synchronization processes in neuroscience and summarizes a number of important studies that have been published in this context. This includes the findings of the physical theory of synchronization in nonlinear dynamics and the application of the resulting analysis methods to neurophysiological data. Finally, the chapter states the specific aims of this work and gives an outline of the following.¹

1.1 Temporal binding

Neurobiological research has shown (cf. Engel et al., 1991) that in the visual cortex there exists a hierarchy of neurons that detect increasingly complex features of the scene registered by the eyes. On the simplest level, they just copy the activation patterns of sensory neurons in the retina, but subsequent cells react to contrasts, movements, linear structures in a specific direction, and so on, each in a specific area of the visual field. If one assumes that this hierarchical pattern of accumulating complexity is the functional principle of the whole brain, one has to conclude that at the highest level for each object that is possibly relevant to the organism there exists a single dedicated neuron that detects the special complex combination of properties this object consists of. Since such a scheme leads to an absurdly high number of combinations, it calls for far more neurons than are actually present in the brain (the “combinatorial explosion”), and it implies the strange notion that every contingent item of the world gets hard-coded into the brain (presumably during maturation), which has been caricatured by the idea of the “grandmother neuron”—a neuron that is active if and only if one’s grandmother is present.

On the other hand, for complex perception and cognition it is not sufficient that only basic stimulus features are detected in specialized brain areas. If a number of

¹In this introduction, the understanding of the concepts referred to has to be presumed. Many of them will be explained in Ch. 2.

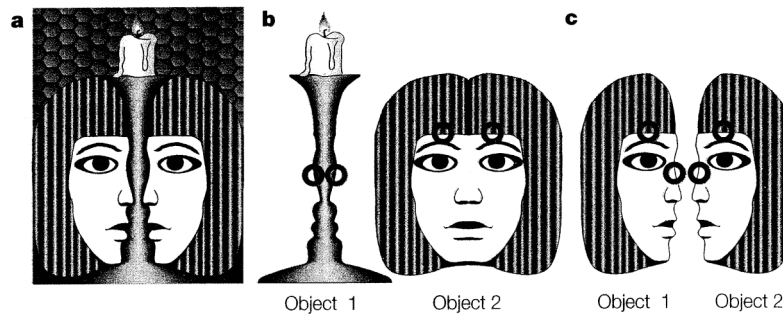


Figure 1.1: The concept of binding, illustrated by a “bistable” image. The image (a) has two possible interpretations: a face partially occluded by a candlestick (b), or two opposing faces (c). Both interpretations are distinguished by the way the edges that are detected at different places (marked by bold circles) are associated with each other to make up a contour—that is, how they are “bound” into object representations. Reproduced with permission from Engel et al. (2001), *Dynamic predictions: Oscillations and synchrony in top-down processing. Nature Reviews Neuroscience*, 2(10), Box 2. Copyright © 2001 Macmillan Magazines Ltd. and © 1990 Palgrave Macmillan.

objects is perceived at the same time, and an activation pattern indicates the presence of a certain set of stimulus features in the perception, there is no information about what features combine with which other features to make up the different objects (the “superposition catastrophe”). For instance, if there is a green ball and a red cube, the detection of “ball”, “cube”, “green”, and “red” could also be interpreted as the presence of a red cube and a green ball. This necessity to specifically combine detected features into object representations is called the *binding problem* (see Fig. 1.1). Because of the combinatorial constraint, binding cannot be achieved by the activity of neurons that are specifically sensitive to certain feature combinations. There has to be a means to encode the belonging-together of low level feature representations directly into the corresponding neuronal activity. That is, the alternative to the representation of an object by a detector neuron is its representation by an assembly of associated neurons that may be distributed over large areas of the brain.

Based on theoretical considerations (cf. von der Malsburg, 1985) as well as animal experiments and an increasing number of findings in human neurophysiological data (see below), it is nowadays widely believed that the mechanism of binding employed in the brain is synchronization, or *temporal binding*. While the activity of single neurons consists of bursts of firing (considered stronger the higher the firing rate is), in most cases these bursts have oscillatory character. According to the theory of temporal binding the activation of an assembly consists in the synchronization of the oscillatory activity of the associated cells. Since this temporal adjustment of firing activity of the cells is not necessarily affecting their individual mean firing rates, synchronization is suitable as a marker of belonging-together of features that are represented by the single neurons.

Though the concept of binding has been introduced in the context of perception to understand the mechanism of sensory integration (of features into an object representation) and segmentation (of one object from another), today the theory of binding has to be seen in the broader context of the *functional integration* of specialized, spatially separated brain areas (cf. Varela et al., 2001). Large-scale cooperation in the brain seems to be necessary to achieve perception-related object representations as well as more complex cognitive processes like the planning of actions, the understanding of music and language, or for being conscious.

References: Von der Malsburg (1985) introduces the idea of dynamic neuronal connectivity patterns as the basis of brain function. Von der Malsburg and Schneider (1986) describe neural synchronization as a means of sensory segmentation under the title of a “Correlation Theory” of brain function. (Interestingly, von der Malsburg (1995) argues that temporal binding is not only present in real brains, but is also efficient in improving the capabilities of artificial neural networks.) Damasio (1990) gives a model of memory retrieval by synchronous activation of distributed neural networks, representing the different modality-related aspects of a recollection in the respective specialized brain areas. Varela (1995) discusses the concept of temporal binding (synchrony) in relation to cognitive operations, wherein distributed cell assemblies underlie the coherence of cognition. Singer (2000) proposes that the brain uses two complementary strategies for representations: single cells specific to frequently occurring items of low complexity and transient cell assemblies for infrequent high-complexity items, while the relatedness of distributed neurons in the latter case is encoded by the synchronization of their responses. Engel et al. (2001) discuss experiments on synchrony in the context of a “dynamicist” idea of top-down processing of stimuli. They give an explanation of the functional role of synchrony (temporal coding) in the operation of the brain, concerning the causes as well as consequences of synchrony. Varela et al. (2001) propose phase synchronization over multiple different frequency bands as a mechanism of large-scale integration in the brain, to enable the emergence of coherent behavior and cognition. Thompson and Varela (2001) discuss the concept of synchronous cell assemblies in the context of their “enactive” approach to the theory of consciousness. Engel and Singer (2001) as well as Singer (2001) investigate the relevance of temporal binding for the understanding of consciousness in the sense of sensory awareness.

Following early theoretical approaches pointing to this direction, it was a number of pioneering studies around 1990 that provided concrete evidence for the existence of a temporal binding mechanism in the brain. These studies were mainly based on single cell and multi-unit recordings in the visual cortex of cats. Engel et al. (1991) give a review of experiments performed by their group (see there for further references). They found oscillations on the spike burst level in the frequency range 40–60 Hz with synchronizations that were specific to neurons with similar feature preferences. Especially compelling was their demonstration (see Fig. 1.2) of a simple form of sensory integration (by synchronization) and segregation (by desynchronization), i.e. direct evidence for the theory of temporal binding. Similar results were obtained by another group; see Eckhorn et al. (1991) for a review and references.

These findings in animal experiments have inspired studies aimed at demonstrating synchronized activity in response to sensory and cognitive processing in humans. Because measurements on the cellular level are strongly invasive and can only in special cases be applied to human subjects, most of the studies have used EEG (electroencephalography, see Sec. 2.1) and similar data. Since EEG signals represent the summed up activity of large local neuron populations, the band power (signal power in a selected frequency band) of the EEG response at a single recording site may be regarded as an indirect measure of synchronization within this population. Terminology related to this interpretation dates back to the investigation of event-related changes in alpha band power starting in the 1970s, so-called event-related desynchronization and synchronization (cf. Pfurtscheller, 1998). In contrast to this, most newer studies have been oriented at the findings in the cat visual cortex and therefore have focused on band power in the gamma range (above 30 Hz).

References: Lutzenberger et al. (1994) find reduced band power for the perception of pseudowords (word-like sounds without a meaning) compared to words in the EEG gamma band; Pulvermüller et al. (1996) repeat this finding for the MEG (magnetoencephalogram) gamma and beta band. Herrmann et al. (1999) report increased EEG gamma band power

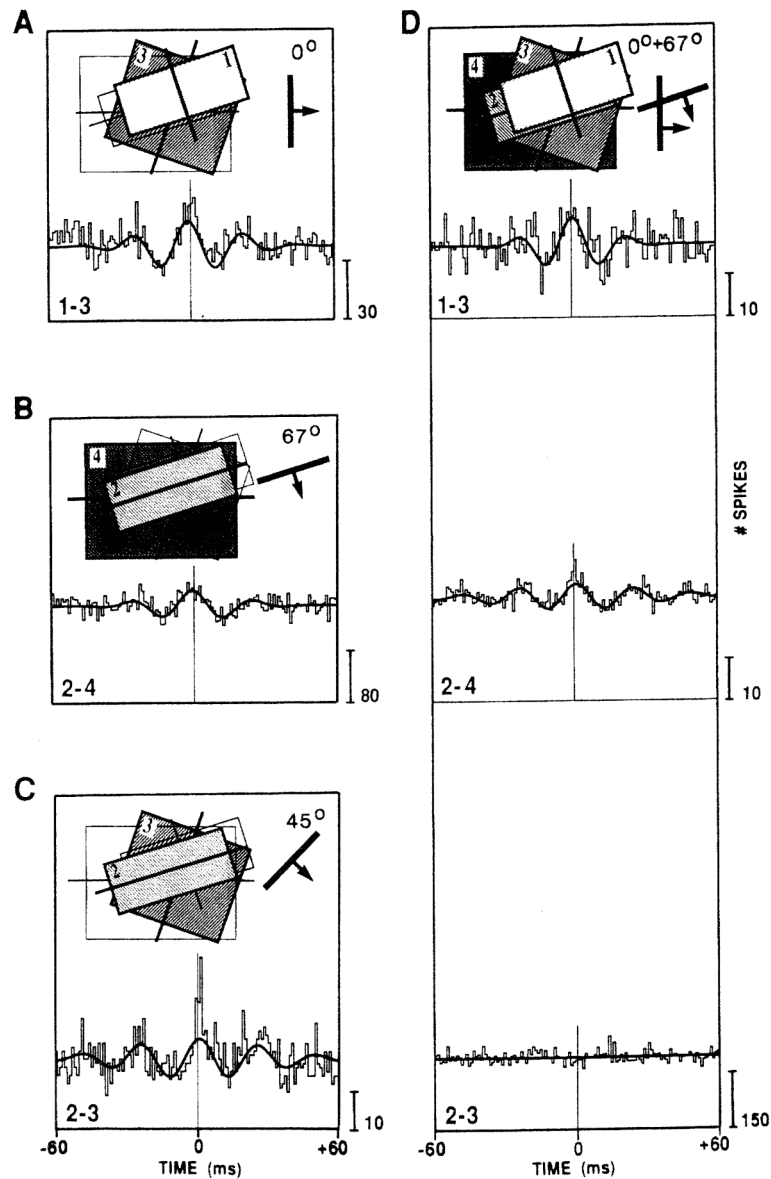


Figure 1.2: Temporal binding in the cat visual cortex. Activity was measured from four cells that are detecting moving bars, with preferences regarding the orientation of the bars of 157° (1), 67° (2), 22° (3), and 90° (4). Cross-correlograms of signals from pairs of cells are shown; an oscillatory cross-correlogram indicates synchronization. A)–C) Moving bars at different orientations cause synchronization between those cells that are activated. D) Two superimposed moving bars at orientations 0° and 67° cause synchronization in cell pairs 1-3 and 2-4, but not between cells 2 and 3. That is, neuron activities are synchronized only if they respond to the same object. Reproduced with permission from Engel et al. (1991), Temporal coding by coherent oscillations as a potential solution to the binding problem: Physiological evidence, Fig. 5. In Schuster, editor, *Nonlinear Dynamics and Neuronal Networks*. Copyright © 1991 Wiley-VCH.

for Kanizsa figures compared to similar visual stimuli without illusory contours. Herrmann and Mecklinger (2000) find increased MEG gamma band power for (visually presented) target stimuli compared to other stimuli. Lachaux et al. (2000) investigate LFP (local field potentials) gamma band responses to stimulation in a visual discrimination task. For further references see Müller (2000), who gives an overview of the findings regarding gamma band responses.

Even if changes in local synchronization are indicated by changes in EEG band power, it still is an indirect measure and results are confounded with changes in the overall activity of the underlying neuron population. Though local synchronization effects like those found in the cat visual cortex cannot be expressly detected in EEG because of its low spatial resolution, EEG data seem to be feasible to investigate long-range synchronization between different brain areas as an indicator of their functional integration. Going a step beyond band power analysis, a number of studies have applied *coherence* (the correlation coefficient applied in the frequency domain) as a linear measure of bivariate synchronization. Coherence gives frequency-specific information on the degree of linear dependency between pairs of signals recorded at different sites. Other than most studies on band power, many of these studies report findings that are not confined to the gamma band.

References: Sarnthein et al. (1998) find increased EEG coherence in the theta band in a delayed response task and relate it to working memory operation. Miltner et al. (1999) report increased EEG gamma band coherence in an associative learning task, between those brain areas that are processing the two classes of stimuli given. Weiss et al. (1999) find different coherence patterns in the EEG alpha-1 and beta-1 band for the processing of concrete vs. abstract nouns and sentence processing vs. pseudo speech. Von Stein and Sarnthein (2000) review several different studies on EEG band power and coherence and argue for a relation between the spatial scale on which synchrony-mediated functional integration takes place and the frequency band of the involved oscillations; these range from the theta to the gamma band. Schack et al. (2000) interpret the phase component of coherence in the EEG alpha-1 band; in the experiment, abstract nouns are visually and auditorily presented to the subject for memorization. Weiss and Müller (2003) give a review of language processing research that is employing coherence: clinical studies on dyslexia, studies on word processing, text processing, and sentence processing.

1.2 Synchronization

By most authors, the mechanism of temporal binding as introduced above is described as synchronization of neuronal oscillations, that is as the dynamical adjustment of the rhythms of different oscillators (see Sec. 2.3). The theory of synchronization processes has a long tradition in physics, having been founded in the 17th century by Huygens for the case of periodic oscillators. In recent years the theory has been updated in the context of nonlinear dynamics and especially regarding the synchronization of chaotic oscillators. (For an introduction and further references, see Pikovsky et al., 2001). Here, Pecora and Carroll (1990) have shown that sufficiently strong coupling may cause two chaotic oscillators to follow identical trajectories (so-called complete synchronization). Subsequent research has led to the discovery by Rosenblum et al. (1996) of a specific form of chaotic synchronization that has become especially important for the investigation of neuronal processes: the phenomenon of *phase synchronization*. In this case, a small coupling of the oscillators causes an adjustment of their phases, while the amplitudes remain uncorrelated and chaotic.

References: The first investigations of phase synchronization and related phenomena have been performed in numerical simulations, mainly employing Rössler oscillators: Ro-

senblum et al. (1997) describe lag synchronization as an intermediate regime between phase and complete synchronization. Pikovsky et al. (1997) give a broad discussion of phase synchronization of chaotic oscillators. Pikovsky et al. (1996) investigate phase synchronization in a population of globally coupled chaotic oscillators and Osipov et al. (1997) in a lattice of chaotic oscillators. Zhou and Kurths (2002) find phase synchronization induced by common noise. Zaks et al. (1999) describe imperfect phase synchronization between nonidentical chaotic oscillators.—Phase synchronization has also been demonstrated in laboratory experiments and in models of as well as empirical data from natural systems, including the human body: Parlitz et al. (1996) observe phase synchronization of chaotic Rössler oscillators implemented in an electronic circuit. Rosa et al. (2000) show chaotic phase synchronization in a plasma discharge tube, DeShazer et al. (2001) in a laser array. Wang et al. (2000) describe phase synchronization and clustering in globally coupled chaotic electrochemical oscillators. Blasius et al. (1999) find phase synchronization in models of spatially extended ecological systems, Lunkeit (2001) in climate models. Paluš et al. (2000) investigate synchronization between the sunspot cycle and the solar inertial motion. Bhattacharya et al. (2001) apply phase synchronization and other nonlinear analysis methods to intensity oscillations of chromospheric bright points. Schäfer et al. (1999) show phase synchronization between the heart beat and the respiration cycle. Tass et al. (1998) demonstrate phase synchronization in MEG and muscle activity in Parkinsonian patients. Laird et al. (2002) describe synchronization between fMRI (functional magnetic resonance imaging) data and the presentation of a stimulus.—For a comprehensive overview of the literature on chaotic synchronization, see Boccaletti et al. (2002).

As noted above, in a number of studies synchronization in EEG has been investigated using the coherence measure. This use can be justified by the observation that in the synchronization of two periodic oscillators, their phases are adjusted to each other while the amplitudes are constant. In this case, synchronization can be detected using coherence because the phase adjustment leads to an increased correlation of the two time series. But, as Tass et al. (1998) point out, synchronization of two oscillators is not equivalent to the linear correlation of two signals that is measured by coherence. If the participating oscillators are chaotic and in the phase synchronized regime, such that their amplitudes are varying with time but are not correlated to each other, the noise inherent in the amplitudes will reduce coherence changes related to synchronization. On the other hand, if the amplitudes of the two oscillators are changing with time in a regular way (for instance, because the number of neurons recruited for the local oscillator increases or decreases) and similar changes take place in both sites, such an amplitude correlation will cause an increase of coherence that is not related to synchronization.²

For these and related reasons, coherence is not to be regarded as a specific measure of synchronization. Because the core of synchronization is the adjustment of phases and not of amplitudes, it should be detected by a measure neglecting amplitude variations (see Sec. 3.3). Such methods of data processing, that are necessary to specifically detect phase synchronization and that are applicable to synchronization in general, are called *phase synchronization analysis*.

References: In the last years, there has been an increasing number of studies in cognitive neuroscience employing measures of phase synchronization for the analysis of EEG and similar data: Rodriguez et al. (1999) show specific patterns of long-range phase synchronization in the EEG gamma band related to the perception of upright vs. upside-down “Mooney” faces (black & white outline pictures of faces). Lachaux et al. (1999) find large-scale and local LFP phase synchronization in a visual discrimination task. Haig et al. (2000) demonstrate a late response in the degree of global and regional EEG gamma band phase

²Empirical evidence supporting these considerations is given by Quiñero et al. (2002), who report that phase synchronization analysis (among other nonlinear methods) differentiates better between different degrees of synchronization in rat EEG than linear measures.

synchronization for task-relevant vs. irrelevant stimuli. Bhattacharya and Petsche (2001) find increased EEG gamma band phase synchrony in musicians while listening to music. Braeutigam et al. (2001) describe events of stimulus-locked MEG gamma band activity associated with a semantic violation. Breakspear (2002) presents evidence of nonlinear contributions to the EEG based on phase synchronization analysis. Chavez et al. (2003) apply network cluster analysis to MEG phase synchronization relations in a binocular rivalry experiment.—Another field in which phase synchronization analysis is effective and increasingly popular is the clinical evaluation of EEG, especially related to epilepsy: Mormann et al. (2000) find changes in phase synchronization before the onset of an epileptic seizure. Jerger et al. (2001) review the effectivity of several different nonlinear measures for seizure prediction and find that phase synchronization provides the most robust indicator. Le Van Quyen et al. (2001b) give an overview of nonlinear methods in seizure prediction including the approach based on phase synchronization. By Lee et al. (2003), EEG phase synchronization analysis is also proposed as a means of investigating the neural basis of schizophrenia.

1.3 Aims and outline

The subject of the present thesis can be specified related to the research summarized above in a number of different respects:

- 1) As a contribution to nonlinear dynamics, this work is analyzing empirical data obtained from a natural system (the human brain), but not investigating details of the theory of synchronization or specific phenomena in numerical simulations of model systems.
- 2) The data are obtained by EEG, and therefore describe the electrical activity of the brain on a relatively large-scale, or coarse-grained level. This is in contrast to studies analyzing signals recorded at single cells or in small neuron populations, by macroelectrodes inside of the skull (LFP), or by MEG.
- 3) This work is interested in synchronization effects correlated with cognitive processes. In this it differs from studies on pathological conditions like epilepsy, where neuronal synchronization comes into view as a mainly physiological phenomenon.
- 4) Accordingly, the data are collected following the experimental paradigm of cognitive science, that is comparing the effects of slightly different versions of a cognitive process. Practically this means that responses are related to different classes of stimuli, each of which is realized many times. This form of EEG recording is called event-related potential (ERP).
- 5) The subject matter of the main experiment is defined by research interests of psycholinguistics. This choice has been determined by the author's cooperation in the interdisciplinary DFG research group "Conflicting Rules", part B1: "Diagnosis in Language Processing". In this respect, this work tries to make theory and methods of physics useful for the purposes of another scientific discipline.
- 6) Regarding methodology, this work is looking for explicit effects of phase synchronization in the EEG. This is in contrast to the use of the band power and the coherence measure, that for reasons given above are only of limited use for the detection of synchronization processes.

The aims of this thesis are twofold: to adapt and apply the methods of phase synchronization analysis to event-related EEG data, and at the same time to contribute to these methods in a way that is also relevant in other fields of application.

The composition of the text is as follows:

In Ch. 2, the concepts underlying this work are introduced. This includes the basics of electroencephalography (Sec. 2.1), the definition of event-related potentials as well as an explanation of the established form of ERP analysis (Sec. 2.2), and the main topics of synchronization theory (Sec. 2.3). Since the research reported in the following lies at the intersection of (at least) two different disciplines, the purpose of this introductory chapter is to lay a common ground for readers with different backgrounds.

Chapter 3 presents elements of the data analysis method used here that are still of a basic nature, but that could have been done in another way: an algorithm employed to reduce correlations in EEG due to mixing (Sec. 3.1), the use of wavelets to determine the instantaneous phase of a time series (Sec. 3.2), and the statistical measure of synchronization strength (Sec. 3.3). These elements represent decisions that continue the specification of the author's approach sketched above.

In the next two chapters, contributions to the methods of synchronization analysis are presented. Chapter 4 discusses a number of different approaches to test for statistically significant changes in synchronization strength between two oscillators. Methods of increasing precision, but also increasing complexity are introduced, explained and checked in numerical simulations.

In Ch. 5, an approach to multivariate phase synchronization analysis is derived and discussed, including a check of the underlying model in a numerical simulation. As a first empirical test of the method, an experiment on the visual processing of illusory contours (Sec. 5.2) was performed. Here, the multivariate analysis proves to deliver useful results in showing the emergence of a synchronization cluster as a response to the visual presentation.

The subject of the last chapter (Ch. 6) are empirical findings obtained by synchronization analysis of event-related potentials in language processing. A classic experiment comparing the effect of a semantic incongruity in a sentence context with that of a physical mismatch (Kutas and Hillyard, 1980b) was replicated. The stimulus presentation is shown to elicit a transient increase of synchronization strength. Each type of deviation causes a specific modification of the basic pattern of synchronization.

Chapter 2

Basic Concepts

In this chapter, the concepts that are defining the subject matter of this work are introduced and explained. The data to be analyzed are obtained by electroencephalography; some technical and physiological aspects of this are described in Sec. 2.1. In the form of event-related potentials (Sec. 2.2), EEG is conceptualized as a random process (with respect to experimental events). The standard method of ERP analysis and its main findings are explained, especially in relation to cognitive processes. This method is to be supplemented by a new analysis procedure that looks for phase synchronization between brain areas. An introduction to the physical theory of synchronization focused on phase synchronization is given in Sec. 2.3.

2.1 Electroencephalography

The electroencephalogram (EEG) is the derivation and recording of time-varying voltages on the human scalp that are generated by the electrical activity of the brain, especially the neocortex (following Nunez, 1995). The (neo-) cortex or “gray matter” is the phylogenetically newest part of the brain; its functions include sensory and cognitive information processing, motor control, and conscious experience. The cortex consists of a thin (2–3 mm) layer of neuronal tissue that is partly stretched out under the skull, partly folded into itself thereby increasing its surface. (Fig. 2.1)

80% of the neurons in the neocortex are so-called pyramidal cells, whose cell bodies are roughly of pyramidal (or rather conical) form. Pyramidal cells and the other neurons in the cortex are locally connected by short-range intracortical fibers (ca. 1 mm long) as well as globally connected by long-range corticocortical fibers (up to 20 cm), the latter making up the “white matter” directly below the cortex. Only a comparatively small amount of fibers comes out of or leads into other parts of the brain. The pyramidal cells are oriented perpendicular to the cortex surface and organized in local groups called columns, as well as larger populations, the so-called macrocolumns of ca. 3 mm diameter and containing 10^5 to 10^6 neurons. (Fig. 2.2)

The electric field of the cortex is caused by the current flows within a pyramidal cell and between it and the neighboring extracellular medium, making the cell an electrical dipole along its axis. Because of their parallel orientation, simultaneous activation of many pyramidal cells generates large correlated dipole layers whose electric field can be measured on the scalp (Fig. 2.1). Since this field reflects the degree of simultaneous activation in the local neuron population, the EEG recorded at a scalp electrode can be regarded as a relatively direct measure of the neocortical

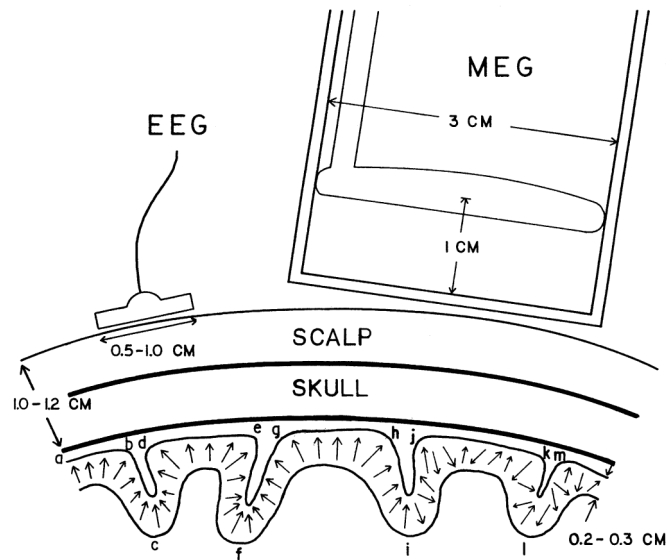


Figure 2.1: Recording of EEG and MEG (magnetoencephalography). The EEG electrode is attached to the scalp surface and separated from the cortex by scalp tissue and skull. The EEG is most sensitive to correlated dipole layers in that parts of the cortex that lie directly under the skull (the so-called gyri; a-b, d-e, g-h). Reproduced with permission from Nunez (1995), *Quantitative states of neocortex*, Fig. 1-4. In Nunez, editor, *Neocortical Dynamics and Human EEG Rhythms*. Copyright © 1995 Oxford University Press.

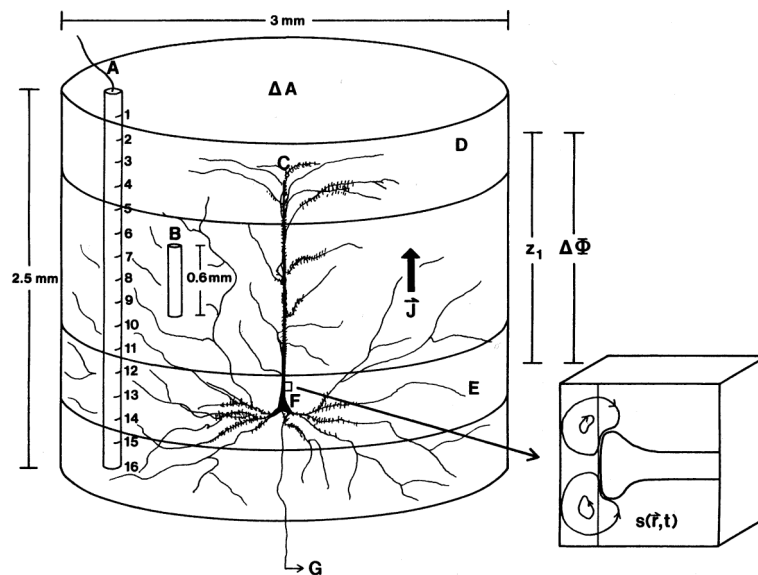


Figure 2.2: A macrocolumn containing up to 10^6 neurons, with one pyramidal cell shown explicitly. The insert shows a synaptic input that is causing microcurrent sources and sinks. In EEG, the effect of the macroscopic net current density \vec{J} of macrocolumns is measured in the form of a potential difference $\Delta\Phi$. From Nunez (1995), Fig. 1-11. Reproduced with permission from Sato, editor, *Magnetoencephalography*, Raven Press. Copyright © 1990 Lippincott Williams & Wilkins.

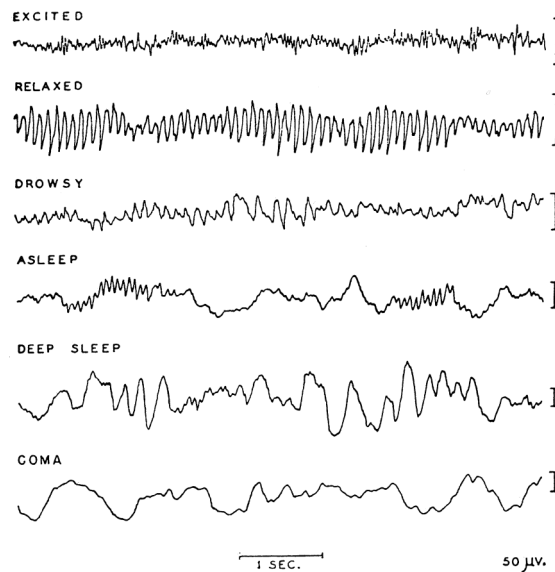


Figure 2.3: Characteristic EEG rhythms, depending on the state of consciousness. From Nunez (1995), Fig. 1-6. Reproduced with permission from Penfield and Jasper, *Epilepsy and the functional Anatomy of the Human Brain*, Little, Brown. Copyright © 1985 Lippincott Williams & Wilkins.

function of the underlying cortex area.

The spatial resolution of EEG lies roughly between 1 and 5 cm. This is markedly lower than the resolution that can be obtained with electrodes directly on the cortex surface (the so-called electrocorticogram applied in brain surgery patients), because scalp electrodes have a distance of about 1 cm from the cortex and because of the low conductivity of the skull that causes a smearing of the potential distribution (Nunez, 1981, Ch. 1 & 8). This loss in resolution between cortex and scalp can in part be compensated for by different methods of postprocessing of EEG data (for a description of the “spherical spline Laplacian” algorithm used in this work, see Sec. 3.1). With high density electrode arrays and efficient postprocessing, the possible resolution of scalp EEG lies in the order of magnitude of macrocolumns, making them the natural theoretical units of cortical dynamics from the point of view of EEG interpretation (Nunez, 1995). For the purposes of this work, this observation also specifies the spatial scale of the neuronal oscillators whose operation is to be examined in synchronization analysis.

The temporal resolution of EEG lies at about 1 ms, its spectral content being in the range from below 1 Hz up to approximately 100 Hz. The spectral composition of EEG depends strongly on the state of consciousness, with a low-amplitude broadband spectrum being typical for awake persons with open eyes or performing cognitive tasks (Fig. 2.3 & Fig. 2.4, “excited”). The EEG spectrum is traditionally differentiated in a number of frequency bands: delta, below 4 Hz; theta, from 4 to 8 Hz; alpha, from 8 to 13 Hz; beta, from 13 to 30 Hz; gamma, beyond 30 Hz (Fig. 2.4). Some of these wave bands are associated with characteristic dominant rhythms, the most prominent being the alpha rhythm, a high-amplitude sinusoidal oscillation of about 10 Hz that is coherent over posterior areas and that is observed in awake but relaxed subjects with closed eyes (Fig. 2.3 & Fig. 2.4, “relaxed”). EEG amplitudes are in the range from 10 to 100 μV (Niedermeyer, 1998).

EEG electrodes are positioned according to the International 10-20 System that originally defined 21 locations but that has been updated by the American Elec-

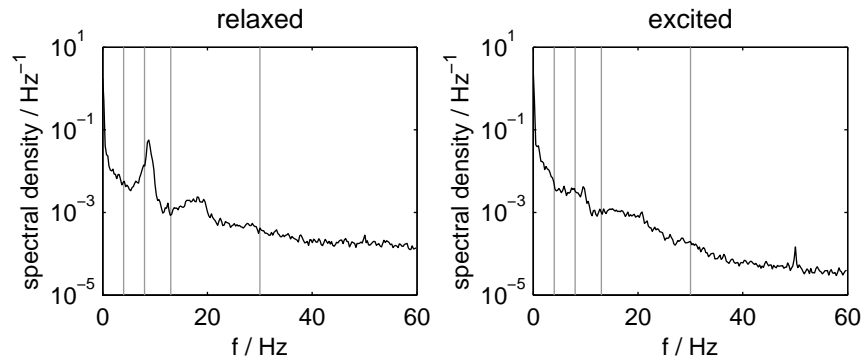


Figure 2.4: EEG power spectral density (electrode CZ). Gray lines indicate the borders between the frequency bands delta, theta, alpha, beta, and gamma. “relaxed”: The subject is resting with closed eyes. Note the strong peak at about 9 Hz corresponding to the alpha rhythm. Even in this relatively coherent case, EEG spectral content is still rather broadband. “excited”: The subject is in a state of perceptual attention and mental operation. The peak at 50 Hz is not caused by neuronal activity but by the disturbance of the measurement by the power line.

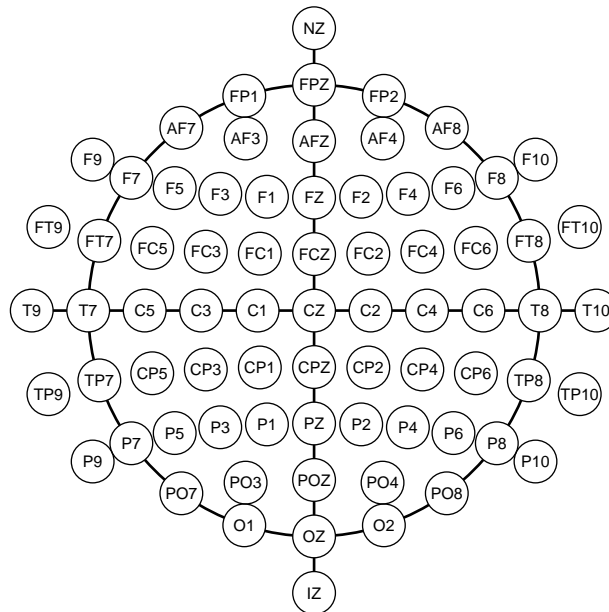


Figure 2.5: The modified combinatorial nomenclature. Letters refer to the main areas of the cortex, the frontal (F), left and right temporal (T), parietal (P) and occipital (O) lobes and include additional designations for the topmost area (C for central) and the foremost region (FP: frontopolar, AF: anterior frontal). These terms are also used in the description of the topography of EEG effects. The number part of the electrode labels indicates the distance from the midline, using odd numbers on the left and even numbers on the right, and is replaced by the letter Z on the midline. NZ and IZ denote the anatomical landmarks, nose bone (Nasion) and back of the skull (Inion). After American Electroencephalographic Society (1991).

troencephalographic Society (1991) to include 75 different placements. The positions of the electrodes are determined relative to anatomical landmarks like the nose bone or the backmost part of the skull and separated by fixed fractions of the distances between these reference points (originally, 10 and 20%) to ensure that an electrode is placed above the same anatomical structure of the brain in subjects with differently sized heads. The electrodes are named according to the modified combinatorial nomenclature (MCN) that uses a combination of letters and numbers to indicate the position (Fig. 2.5). The selection of electrodes actually included in an EEG recording depends on its specific purpose. It can range from just a few electrodes (if one is looking for effects whose topography is known) to a full montage (if as much information as can be obtained is useful, e.g. for localization of cortical sources).

The electrodes are directly attached one-by-one to the scalp or they are embedded in an elastic cap with a predefined montage that is fixed on the subject's head. An electrolyte gel is applied to the attached electrodes to establish a low impedance contact between them and the scalp (usually below 5 k Ω). Leads connected to the electrodes are plugged into an amplifier. In the past the resulting signals have been fed into writing machines producing graphs of the voltage time series on paper; today, they are sampled (at 250 to 1000 Hz) and digitized (up to 32 bits, in units of about 0.1 μ V) and stored on a computer for further processing. Voltages are recorded either between each electrode and a reference electrode placed where almost no brain electrical activity is to be expected, e.g. at the mastoid bones behind the ears (unipolar or reference recording), or between pairs of neighboring electrodes (bipolar recording). Absolute voltage values are in the range of several thousand μ V. (cf. Reilly, 1998; Lopes da Silva, 1998a)

Frequently, the EEG record is contaminated by traces of electric signals that are not generated in the brain. The most important type of those artifacts is that caused by movements of the eyes, because the eye balls constitute electrical dipoles. Eye movements cause strong deflections in the voltage recordings especially for the frontal electrodes, and are monitored by special electrodes positioned close to the eyes (electrooculogram, EOG). Other origins of artifacts include electric activity of muscles in the forehead, the heart beat, as well as disruptions in the skin contact of the electrodes caused by movements of the subject. Most of these artifacts can be identified by visual inspection of the recorded data (in part even by automatic processing), such that the corresponding parts of the record can be marked not to be included in further analysis (so-called rejections). Another type of interference are slow variations in the electrode impedances due to sweating and chemical reactions at the skin surface. For the most part, they can be eliminated by linear detrending over recording segments in the order of seconds to minutes or by a high-pass filter at about 0.1 to 0.5 Hz.

2.2 Event-related potentials

The EEG is continuously generated in the human brain all of the time, accompanying different mental states and different actions. Part of the interest in EEG lies in the fact that characteristics of this ongoing activity can give insight into the general neurological state of a person that can be utilized in the diagnosis of neuronal disorders like epilepsy. In contrast to this, in neuroscience and especially in cognitive research the interesting aspect of EEG is that it can give detailed information about the workings of the brain in a specific situation. Here, the *changes* in EEG related to a certain event like a mental process or the presentation of a stimulus come into focus. The term event-related potential (ERP) denotes the study of EEG in relation to such events that are defined in an experimental setting.

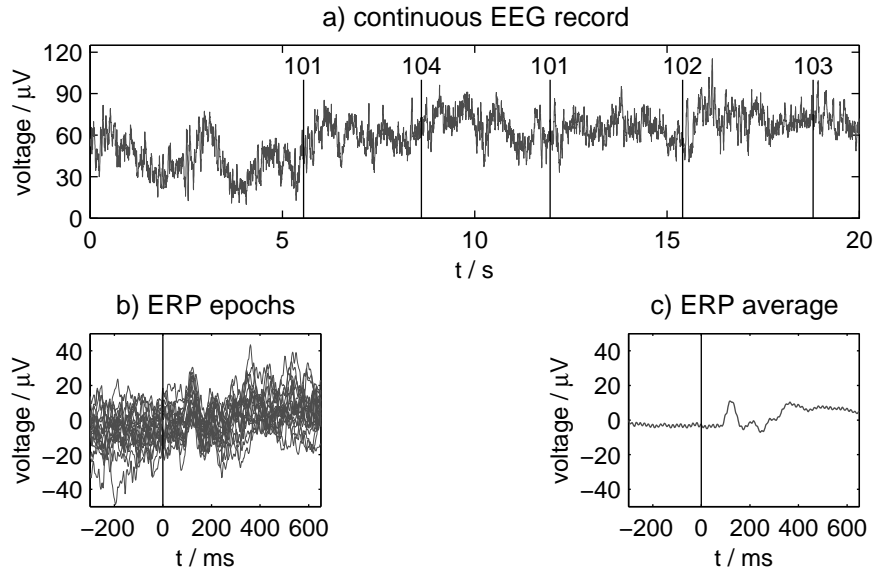


Figure 2.6: Event-related potentials and the ERP average. a) A section of a continuous EEG record at one electrode (OZ). The vertical lines with numerical codes mark the presentation times of different types of stimuli. b) Superimposition of 20 epochs corresponding to one of the stimuli (101) for pre- and poststimulus intervals of lengths $T_{\text{pre}} = 300$ ms and $T_{\text{post}} = 650$ ms. c) Average of 177 epochs. The ERP response is starting about 100 ms after stimulus presentation.

To investigate ERPs, a stimulus or a set of stimuli that are equivalent in a certain respect is repeatedly presented to a subject, and the sections of the EEG record around the time of the stimulus presentation, the so-called epochs, are cut out and collected into an ensemble. If $x(t)$ is the EEG time series and t_i ($i = 1 \dots n$) are the presentation times of a stimulus, then

$$x_i(t) = x(t_i + t) \quad \text{for} \quad -T_{\text{pre}} \leq t \leq T_{\text{post}} \quad (2.1)$$

is the i th epoch for the given lengths of the pre- and poststimulus interval. (In the case of several EEG channels x is to be taken as a vector whose components correspond to the electrodes.) The common method to analyze the epoched data is to calculate the mean over stimulus presentations,

$$\bar{x}(t) = \frac{1}{n} \sum_{i=1}^n x_i(t), \quad (2.2)$$

and to interpret the time course of the result (Fig. 2.6).¹ Specific features of this time course that can be associated with physiological or cognitive processes are called ERP components (see below).

There seems to be no exact, generally accepted definition of the term event-related potential (cf. Lopes da Silva, 1998b). In the common use especially in studies interpreting the epoch average, the mean $\bar{x}(t)$ is looked at as *the* event-related potential, and it is more or less implicitly interpreted as a signal that is generated by a neuron population specifically activated in the processing of the given stimulus, and that is superimposed onto an unchanged “ongoing background EEG” regarded as noise. In this view, the averaging method is just a straightforward way to

¹To compensate for drifts and to prepare the ERP average for comparison between conditions (see below), it is common to additionally perform a “baseline correction”: The time average of the mean over the prestimulus interval is subtracted: $\bar{x}(t) - \int_{-T_{\text{pre}}}^0 \bar{x}(t) dt$.

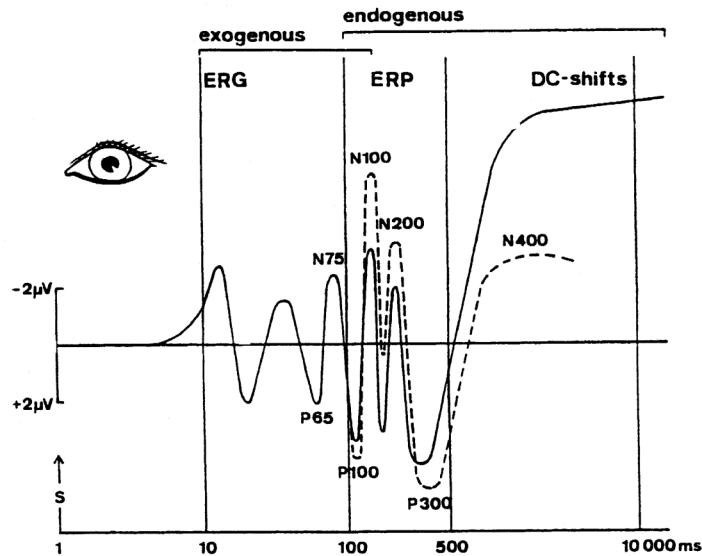


Figure 2.7: Schematic time course of averaged event-related responses to visual stimuli. ERP components are differentiated into exogenous and endogenous, the latter including the N100, P300, and N400 (see text). Longer lasting voltage changes are referred to as DC-shifts (direct current shifts). Note the inverted vertical scale plotting negative voltage to the top, which is customary in ERP research. Reproduced with permission from Altenmüller and Gerloff (1998), *Psychophysiology and the EEG*, Fig. 32.1 A. In Niedermeyer and Lopes da Silva, editors, *Electroencephalography: Basic Principles, Clinical Applications, and Related Fields*. Copyright © 1998 Lippincott Williams & Wilkins.

increase the signal-to-noise ratio of the ERP measurement. Other authors assume that event-related potentials are not just an independent addition to a background EEG, but the result of a transient reorganization of the ongoing activity.² Lopes da Silva (1998b) tries to reflect this controversy in his concept of ERPs as slight EEG changes that are related to a particular event. Though this definition is fairly general, it, too, implicitly refers to an analysis procedure that distinguishes between those changes and some normal state the changes are related to.

A neutral alternative is to consider as an event-related potential just the ensemble of epochs, that is the collection of voltage (potential) recordings that are temporally related to a given event. In the language of statistical time series analysis, the processing of the EEG record to generate epoch ensembles corresponds to the definition of a stochastic process $X(t)$, and each epoch $x_i(t)$ constitutes a realization of this process. As such, the ensemble of realizations is open to a multitude of different data analysis approaches. In this view, the calculation of the ensemble average is just the most basic statistical evaluation that can be applied, the statistical moment of first order. This and any other descriptive statistic can be connected with certain theoretical assumptions, or it can simply be looked at as an empirical quantity that may be correlated with experimental variations. Therefore, even if the common ERP theory of an invariant signal embedded in random noise would prove not to be valid, the findings regarding ERP components would still be valuable.

As noted above, the ERP average exhibits characteristic wave forms (with amplitudes in the range from 2 to 20 μV) that have been shown to correlate with cer-

²Makeig et al. (2002) present results indicating that ERPs are generated by phase-resetting of components of the ongoing brain dynamics. See Penny et al. (2002) for a short review of the recent discussion.

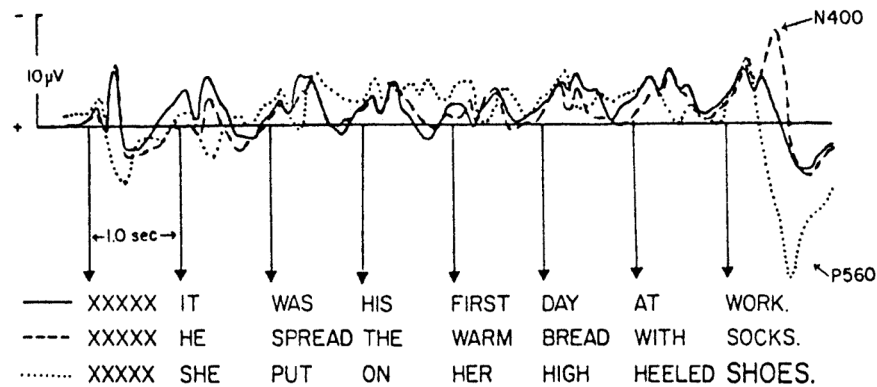


Figure 2.8: The N400 component in the experiment of Kutas and Hillyard. The graph shows the ERP average for the three experimental conditions that are illustrated with a sample sentence below. The presentation of a semantically incongruent noun at the end (dashed line) elicits a negativity around 400 ms compared to a noun that makes sense (continuous line). In the third condition, the noun at the end is semantically congruent but physically deviant (printed in a larger font, dotted line); this elicits a late positivity (“P560”). Reproduced with permission from Kutas and Hillyard (1980b), Reading senseless sentences: Brain potentials reflect semantic incongruity. *Science*, 207. Copyright © 1980 AAAS.

tain physiological or cognitive processes (Fig. 2.7).³ ERP components can be differentiated into “exogenous” and “endogenous”, where the former depend directly on physical properties of the stimulus while the latter are determined by psychological variables and therefore are related to cognitive processes. Exogenous ERP components generally occur up to ca. 100 ms after stimulus presentation, endogenous components after this point. Components are normally named following their polarity (N for negative, P for positive) and their approximate latency, that is the delay of their occurrence relative to the presentation of the stimulus, but they are also distinguished according to their topography (distribution over the scalp) and morphology (shape of the waveform).

The earliest endogenous ERP component is the N100, a negativity with a latency of about 90 to 200 ms. It corresponds to an initial “orienting” response that is the reaction to an unexpected stimulus. The N100 habituates (that is, its amplitude gets smaller over time during an experiment) and it is modulated by the selective attention of the subject. An N100 follows not only the onset but also the offset of a stimulus.

The P300 is the most prominent ERP component. Its latency lies between 280 and 700 ms such that probably the P300 actually consists of a general “late positive complex” of subcomponents. Its common (“oddball”) paradigm is the infrequent presentation of one stimulus embedded in a sequence of many presentations of another stimulus. If the subject attends to the stimuli, the infrequent one elicits a P300 component whose amplitude is inversely related to the stimulus probability.

An important language-related component is the N400 that has originally been found by Kutas and Hillyard (1980b,a). They presented sentences to their subjects, word by word with an interstimulus interval of 1 s. In some of the sentences, the last word was semantically incongruent, that is it did not make sense in the given context. In this case, the ERP response to the last word shows a strong negativity around 400 ms after stimulus presentation compared to a sentence ending with a semantically appropriate word (Fig. 2.8). The N400 has since been demonstrated to show up not only in response to incongruent words, but to reflect a low de-

³The presentation in this and the next paragraphs is following Altenmüller and Gerloff (1998).

gree of semantic expectancy in general. It can be elicited by printed, spoken, as well as sign language and occurs not only with words in sentences, but also in a so-called priming paradigm, where a single word presented first provides the semantic context for a second one (cf. Altenmüller and Gerloff, 1998). Though it is an ERP component specific to language, which is generally associated with areas in the left hemisphere of the brain, the N400 shows no preponderance on the left but is broadly distributed temporoparietally⁴ on both sides (Friederici, 1995).

In the description of the N400 component, a detail has already been mentioned that is generally important in the utilization of ERP averages and other quantities for the purposes of cognitive science. Up to now, ERP components have been presented as absolute responses to a given stimulus. But in the context of the experiment of Kutas and Hillyard (1980b), the response to the semantically incongruent noun can only be interpreted in comparison to the response to a noun that fits into the sentence. That means the N400 observed here is a *relative* negativity.

Generally speaking, each trial of an experiment—the presentation of a stimulus or a sequence of presentations that form a unit, like the parts of a sentence—belongs to one of the so-called conditions of an experiment. These experimental conditions correspond each to a different stimulus (in the simplest case) or to classes of stimuli that are equivalent in a certain respect within each group and define certain variations between groups. EEG epochs are sorted into ensembles according to the experimental condition of the trial, and the average ERP (or other quantities) are calculated for each condition separately. Important for the interpretation of the experimental results is then the *difference* in the stimulus response for the different experimental conditions that is caused by a small variation of the stimulus class.⁵ This difference can be quantified on a generic scale by relating it to the variation over trials or over subjects, determining its statistical strength.

The reason for this approach is that the ERP response to a set of stimuli presented in an experiment does not solely correspond to those specific aspects that the experimenter has in mind, but includes a manifold of operations necessary for stimulus processing as well as the “background” activity of the brain that is not related to the stimulus at all. Part of this may be reduced by the averaging technique or other statistical procedures, diminishing the impact of random influences or of the individual features of a stimulus belonging to a class. But still much of the remaining activity is related to stimulus processing in general, for instance character recognition or retrieval of lexical information. These processes are common to all experimental conditions, and so the part corresponding to their experimentally relevant aspects can only be filtered out by comparing the responses in the conditions.

The experiment of Kutas and Hillyard defines three experimental conditions, the first containing normal sentences ending with a semantically appropriate noun, the second sentences with a semantic incongruity, and a third group of sentences with a noun that fits in but is shown in a larger font (Fig. 2.8). Looking at the ERP average elicited by the terminal noun (the so-called critical item) in the second condition (dashed line), there is an early negative peak that can be labeled as an N100 component, but that is apparently not related to the semantic incongruity because it shows up in almost exactly the same form in the control condition (continuous line). The N400 component observed here is therefore to be taken as the negativity of the average in the “semantic incongruity” experimental condition relative to the average in the control condition.

As noted above, event-related potentials may be conceptualized as stochastic

⁴For an explanation of this and related terms used to describe the topography of ERP components, see Fig. 2.5.

⁵See Coles and Rugg (1995). Analogous considerations are valid for the cognitive sciences in general; for an introduction into experimental design, see Campbell and Stanley (1963).

processes, the epoch ensembles being samples of realizations. The ERP average is the traditionally most important statistic of the process used in its analysis, and accordingly there is a large number of studies presenting averages in different experimental contexts, defining ERP components and associating them with brain processes. Nonetheless, the mean is just one of the moments of a stochastic process and there are other statistics possibly illuminating different aspects of brain dynamics. Some of these have been employed in ERP analysis for quite some time, most notably the calculation of event-related nonstationary band power, determining effects of so-called event-related desynchronization and synchronization (ERS / ERD, cf. Pfurtscheller, 1998; Altenmüller and Gerloff, 1998). Despite their name, these effects do not refer to the observation of synchronization processes in the strict sense. Their labels are based on the notion that changes in band power at a single electrode are caused by variations in the strength of local synchronization in the neuron population subserving it, generating a stronger or weaker collective effect at the scalp.

More recent alternative evaluation methods of ERPs are inspired by concepts of nonlinear dynamics, like the approach of beim Graben (2001), who encodes ERP epochs into symbol strings and applies entropy measures of complexity to determine the symbolic dynamics of ERPs (see also beim Graben et al., 2000). In a similar way, the subject matter of the present work is to apply the theory of phase synchronization to event-related potentials. Here, instead of calculating the mean of voltages, event-related phase synchronization is analyzed by computing the frequency-specific instantaneous phase of ERP epochs (Sec. 3.2) and quantifying the peakedness of the distribution of the phase difference between electrodes as a measure of the statistical strength of phase synchronization (Sec. 3.3). The physical theory underlying this approach will be introduced in the next section.

2.3 Phase synchronization

Synchronization is a subject of physics with a long tradition, going back to its discovery by Huygens in 1665. It is an essentially nonlinear phenomenon that can be observed in a multitude of technical as well as natural systems, including the human brain. The presentation in this section follows the monograph by Pikovsky et al. (2001). It is aimed at the notion of phase synchronization as the reference point of the analyses presented in this work.

In general terms, synchronization is the adjustment of the rhythms of self-sustained oscillators due to coupling. A self-sustained oscillator is a dynamical system that generates oscillations out of itself, rather than adhering to an externally provided rhythm. A classic example of a periodic self-sustained oscillator is the pendulum clock. It possesses an internal energy reservoir in the form of weights and uses that energy to generate the periodic motion of its pendulum. Amplitude and frequency of this oscillation are specific properties of the clock mechanism and as such are constant within certain bounds.

In the theoretical description, a periodic oscillator corresponds to the *limit cycle* of a nonlinear dynamical system (cf. Pikovsky et al., 2001, Ch. 7). Combining the different variables describing the system state into a vector \vec{x} , the dynamics of a system can generally be described by the differential equation $\dot{\vec{x}} = \vec{f}(\vec{x})$. If this equation possesses a periodic solution with period T_0 ,

$$\vec{x}_0(t) = \vec{x}_0(t + T_0),$$

that attracts neighboring system states, this solution is called a limit cycle (Fig. 2.9). The *phase* ϕ of the oscillator is a coordinate along the limit cycle (a function of \vec{x})

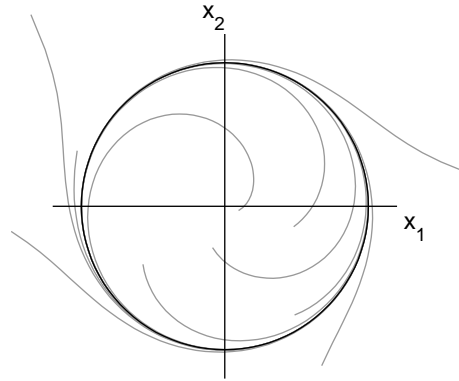


Figure 2.9: The limit cycle (black) of a two-dimensional dynamical system ($\vec{x} = (x_1, x_2)$). Neighboring trajectories (gray lines) approach the cycle and join the periodic motion along it.

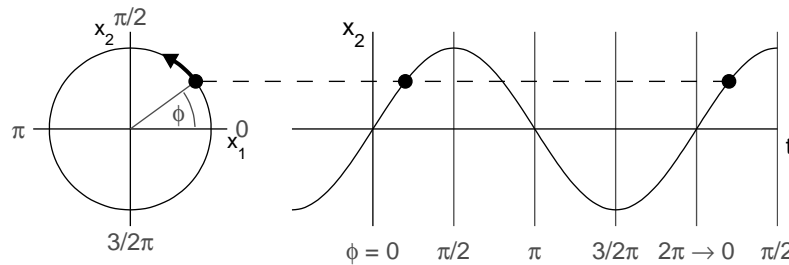


Figure 2.10: The phase on a circle-shaped limit cycle with uniform motion is the angle between a fixed direction (e.g. positive x_1 axis) and the current system state (\bullet). The motion on the circle corresponds to a sinusoidal time series. Periodically recurring system states (\bullet connected with dashed line) are assigned the same value of the circular phase by resetting it after increasing with time over a period of 2π .

whose value is uniformly increasing with time, gaining 2π with every oscillation:

$$\dot{\phi} = \text{const.} = \omega_0, \quad \text{where} \quad \omega_0 = \frac{2\pi}{T_0}. \quad (2.3)$$

The constant derivative of the phase ω_0 is called the natural frequency of the oscillator.⁶ In the simplest case of a circle-shaped limit cycle with uniform motion the phase is the angle within the circle between the current system state and an arbitrary reference direction (Fig. 2.10). The complementary coordinate in the radial direction is called amplitude.

In the notion of phase that has just been established there is an ambiguity. On the one hand, the phase is an ever-increasing variable that describes the continuing oscillations on the limit cycle. With every oscillation the phase gains 2π , such that the integral part of $\phi/2\pi$ can be seen as the number of full oscillations the system has performed. This may be called the linear aspect of the phase. On the other hand, the motion described by the phase is periodic, and the system states of a periodic oscillator corresponding to phases ϕ , $\phi + 2\pi$, $\phi + 4\pi$, ... are physically identical so that these values are equivalent. In this respect, calculations and comparisons concerning the phase have to be taken modulo 2π . (The circular aspect

⁶Normally, the quantity $f = 1/T$ (where T is the period) is called the frequency of an oscillation. In this and the following methodological sections, by the term frequency the author is referring to the *angular frequency* $\omega = 2\pi f$ instead, which is directly specifying the increase of the phase per time unit.

of the phase.) Since consecutive intervals of length 2π are equivalent, it is often convenient to wrap the linear phase into one of these intervals, e.g. $[0, 2\pi[$ (the fractional part of $\phi/2\pi$) or $[-\pi, \pi[$. In the following, the linear and the circular interpretation of phase (including phase differences) will not be distinguished explicitly as long as the relevant aspect can be concluded from the context. With time series, a linear phase can be reconstructed from the circular phase by “unwrap-
ing”, i.e. shifting the phase time series by 2π at each discontinuity.

Because the limit cycle is stable, deviations from it in the radial direction will be compensated quickly, while modifications of the phase will be retained. Therefore, if the periodic oscillator is subjected to a small external force \vec{p} of strength ϵ that depends on the system state and varies with time,

$$\dot{\vec{x}} = \vec{f}(\vec{x}) + \epsilon \vec{p}(\vec{x}, t),$$

this force will mainly affect the phase. Because the amplitude remains unchanged, the modified dynamics of the system can be described in terms of phase only:

$$\dot{\phi} = \omega_0 + \epsilon Q(\phi, t), \quad (2.4)$$

where Q represents the effect of the force on the phase.

Two self-sustained oscillators A and B can be bidirectionally coupled if each of them exerts a force on the other one. Since the time dependence of these forces bears on the respective oscillator’s phase, the dynamics of phases $\phi_{A,B}$ can be written as

$$\dot{\phi}_A = \omega_A + \epsilon Q_A(\phi_A, \phi_B), \quad \dot{\phi}_B = \omega_B + \epsilon Q_B(\phi_B, \phi_A),$$

where $\omega_{A,B}$ are the natural frequencies of the uncoupled oscillators (corresponding to $\epsilon = 0$) and the functions $Q_{A,B}$ represent the coupling forces. These equations can be further simplified if the natural frequencies are close to each other, $\omega_A \approx \omega_B$. Approximating by time-averaging over fast variations in the coupling forces one retains only the resonant terms in the Fourier expansion of $Q_{A,B}$ (cf. Pikovsky et al., 2001, Ch. 7 & 8). As a result, the phase dynamics depends on the difference of the oscillator phases only:

$$\dot{\phi}_A = \omega_A + \epsilon q_A(\phi_A - \phi_B), \quad \dot{\phi}_B = \omega_B + \epsilon q_B(\phi_B - \phi_A).$$

Introducing the *phase difference* $\Delta\phi = \phi_B - \phi_A$ as a new variable, its dynamics can be described by

$$\dot{\Delta\phi} = \Delta\omega + \epsilon q(\Delta\phi), \quad (2.5)$$

where $\Delta\omega = \omega_B - \omega_A$ is the difference between the natural frequencies (the “detuning”) and $q(\Delta\phi) = q_B(\Delta\phi) - q_A(-\Delta\phi)$ is the coupling function that is 2π -periodic in $\Delta\phi$.⁷ This is the basic equation describing the phenomenon of bivariate synchronization which is further analyzed in the following.

Synchronization sets in if the frequency detuning is not too large or the coupling is strong enough. If the extremal values of $q(\Delta\phi)$ are denoted by $q_{\min, \max}$, the synchronization condition is given by the inequality

$$-\epsilon q_{\max} < \Delta\omega < -\epsilon q_{\min}, \quad (2.6)$$

defining a triangular synchronization region in the space of parameters $(\epsilon, \Delta\omega)$. In this case, the dynamics of the phase difference has a stable fixed point $\Delta\phi_s$ and after a transition time the phase difference stays constant:

$$\Delta\phi \rightarrow \Delta\phi_s = \text{const.}, \quad \phi_B = \phi_A + \Delta\phi_s.$$

⁷Synchronization is also possible if the natural frequencies are close to a rational ratio different from 1: $\omega_A/\omega_B \approx m/n$, where $m, n \in \mathbb{N}$. In this case of $m : n$ synchronization Eq. 2.5 still holds with $\Delta\phi = m\phi_B - n\phi_A$, $\Delta\omega = m\omega_B - n\omega_A$, and $q(\Delta\phi) = mq_B(\Delta\phi) - nq_A(-\Delta\phi)$.

Equation 2.5 also holds for the phase difference between an oscillator (B) and an external periodic force (A) acting onto it. This can be seen as an extreme case of asymmetric coupling, $q_A = 0$.

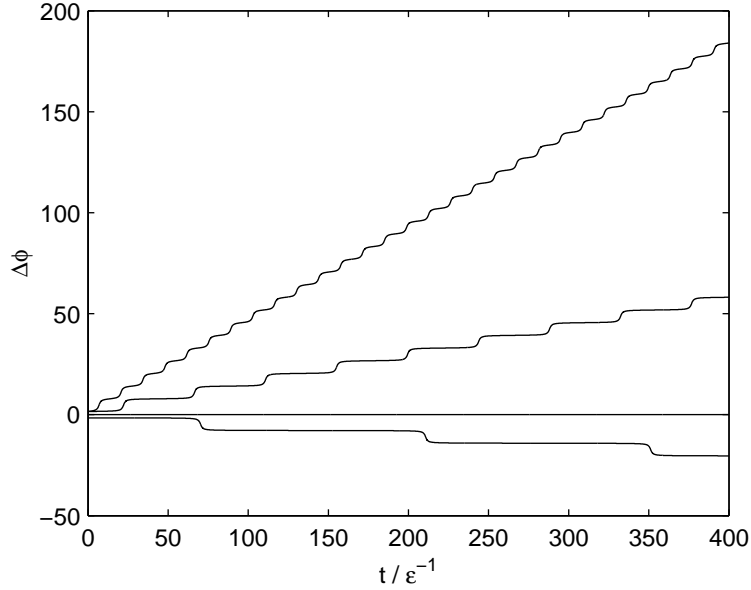


Figure 2.11: Dynamics of the phase difference with the coupling $q(\Delta\phi) = -\sin(\Delta\phi)$ for different frequency detunings $\Delta\omega = -1.001, 0, 1.01, 1.1 \epsilon$ (from bottom to top). In the synchronized regime $|\Delta\omega| \leq \epsilon$ the phase difference is constant. Close to the synchronization transition it is nearly constant for most of the time, interrupted by phase slips $\pm 2\pi$ occurring with a constant period (here $T_{\Delta\phi} \approx 140, \infty, 44.3, 13.7 \epsilon^{-1}$, corresp.). Time is given in units of ϵ^{-1} , frequency in units of ϵ . After Pikovsky et al. (2001), Fig. 7.5.

Here, synchronization manifests itself in a fixed relation of the two oscillator phases, a phenomenon that is called *phase locking*. The rhythms of the oscillators are perfectly adjusted to each other, implying that their instantaneous frequencies are identical, the so-called *frequency entrainment* $\dot{\phi}_B = \dot{\phi}_A$.

This is an idealized result due to the approximations that were made in the derivation of the phase difference dynamics. In general in the synchronized regime the phase difference is not constant but performs small oscillations around a constant value. The phases are not exactly locked to each other, but still the phase difference is *bounded* within one oscillation cycle:

$$\Delta\phi_{\min} \leq \Delta\phi \leq \Delta\phi_{\max} \quad \text{with} \quad \Delta\phi_{\max} - \Delta\phi_{\min} < 2\pi \quad (2.7)$$

(cf. Rosenblum et al., 1996). Though in this case the instantaneous frequencies $\dot{\phi}_{A,B}$ are not identical, the condition of frequency entrainment still holds for time-averaged frequencies,

$$\Omega_B = \Omega_A \quad \text{with} \quad \Omega_{A,B} = \lim_{t \rightarrow \infty} \frac{\phi_{A,B}(t) - \phi_{A,B}(0)}{t}, \quad (2.8)$$

because the contribution of the oscillating phase difference vanishes in the limit.

If the synchronization condition (Eq. 2.6) is not met, the phase difference increases (or decreases) all the time. Close to the transition to synchronization it stays almost constant for long periods of time, but then performs a full cycle rather quickly, gaining (or losing) 2π . These *phase slips* (Fig. 2.11) occur regularly, giving rise to a difference of the average oscillator frequencies of

$$\Delta\Omega = \Omega_B - \Omega_A = \frac{2\pi}{T_{\Delta\phi}}, \quad \text{where} \quad T_{\Delta\phi} = \int_0^{2\pi} \frac{d\Delta\phi}{\Delta\omega + \epsilon q(\Delta\phi)}$$

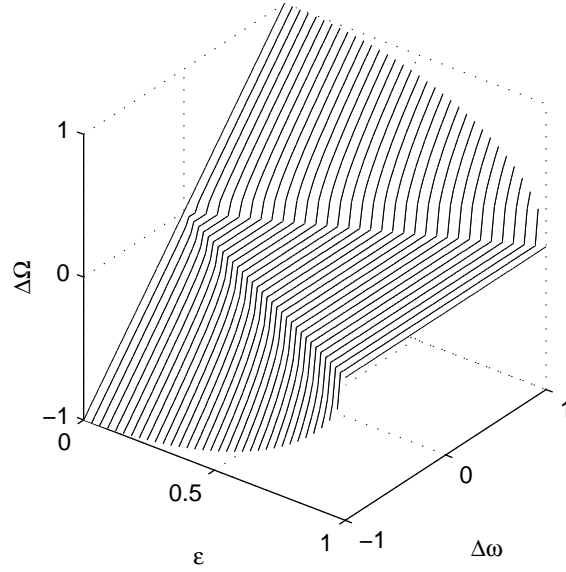


Figure 2.12: The synchronization diagram shows the difference of the average frequencies $\Delta\Omega$ as a function of the coupling strength ϵ and the frequency detuning $\Delta\omega$. If the oscillators are not coupled ($\epsilon = 0$) the average frequency difference is just the detuning, $\Delta\Omega = \Delta\omega$. For larger coupling strength $\epsilon > 0$, the range of detunings for which synchronization is achieved (frequency entrainment, $\Delta\Omega = 0$) increases linearly, forming the triangular synchronization region. In the unsynchronized state, $\Delta\Omega$ is different from zero but still smaller than $\Delta\omega$. The diagram was calculated for sine coupling, $q(\Delta\phi) = -\sin(\Delta\phi)$.

is the fixed period of the phase slips. Close to the transition points at $\Delta\omega_c = -\epsilon q_{\min,\max}$ the average frequency difference depends on the difference of the natural frequencies according to

$$\Delta\Omega \cong \pm \sqrt{|\Delta\omega^2 - \Delta\omega_c^2|}.$$

The full dependence of $\Delta\Omega$ on ϵ and $\Delta\omega$ including the synchronization region is depicted in Fig. 2.12 for the case of sine coupling.

Up to this point, synchronization has been considered in the case of deterministic periodic oscillators only. In contrast, most natural systems are exposed to irregular external perturbations. The straightforward way to include such influences in the model is to add a noise term to the phase difference dynamics (cf. Pikovsky et al., 2001, Ch. 9):

$$\dot{\Delta\phi} = \Delta\omega + \epsilon q(\Delta\phi) + \xi(t), \quad (2.9)$$

where ξ represents mean-free noise ($\langle \xi(t) \rangle = 0$). By this, Eq. 2.5 is turned into a Langevin equation describing a stochastic process. Now, in addition to the frequency detuning, the coupling has also to overcome the effect of the noise to achieve synchronization. If the noise is strong enough, it can drive the phase difference out of one cycle into the next one, causing a sequence of irregular phase slips. The phase difference is then performing a random walk from cycle to cycle, that is biased into one direction if the detuning is different from zero (Fig. 2.13a). For unbounded noise this is possible (with a small probability) even for arbitrarily high coupling strengths. In this case the phase difference is not bounded, and synchronization in the sense that has been introduced above (Eq. 2.7) can not be achieved. Still the coupling has an effect on the phase difference dynamics that

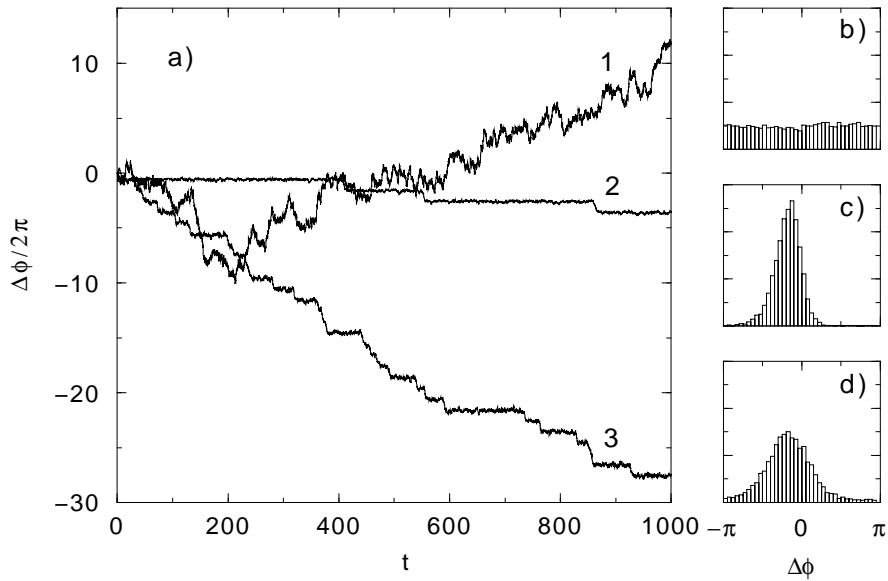


Figure 2.13: The dynamics of the phase difference of coupled noisy oscillators. a) The linear phase difference performing a random walk. 1: The oscillators are uncoupled. 2: Coupled oscillators with small noise and moderate frequency mismatch; there are rare phase slips of -2π . 3: Stronger noise than for curve 2, phase slips are occurring frequently. b)–d) Histograms of the circular phase difference, corresponding to curves 1–3. In the uncoupled case the distribution is uniform. Stronger noise is smoothing out the peak caused by coupling. Reproduced with permission from Pikovsky et al. (2001), *Synchronization: A Universal Concept in Non-linear Sciences*, Fig. 9.2. Copyright © 2001 Cambridge University Press.

can be recognized in the probability distribution of the circular phase difference (Fig. 2.13b–d). In Sec. 3.3, this effect will be used to introduce a statistical measure of synchronization strength as an alternative to the strict definition.

Not only noisy, but also chaotic oscillators can be synchronized (cf. Pikovsky et al., 2001, Ch. 10). The main issue in this case is to obtain a suitable definition of the phase of such a system. A common example of a chaotic oscillator is the Rössler system (Fig. 2.14). Here, in place of a limit cycle we find a tangle of trajectories forming the chaotic attractor. Though in the projection onto the x, y -plane it resembles a smeared circle-shaped limit cycle, in this case it is not possible to introduce a variable in the state space that is uniformly increasing with time. Still, there are a number of different methods to calculate a quantity whose properties are close to that of the phase of a periodic oscillator and that can be utilized to analyze chaotic synchronization; some of them are discussed in greater detail in Sec. 3.2. A simple approach is to define

$$\phi = \arctan \frac{y}{x} \quad \text{and} \quad A = \sqrt{x^2 + y^2}, \quad (2.10)$$

that is, to take the angle⁸ around the origin in the projection plane as the phase, and correspondingly the distance from the origin as the instantaneous amplitude A .

An important phenomenon of chaotic synchronization can be observed with

⁸The arctan is the common formulation of this definition, though this function only gives values in the range $[-\frac{\pi}{2}; \frac{\pi}{2}]$. To obtain the full circular phase, one should use $\phi = \arg(x + iy)$ or the equivalent `atan2(y, x)` function of many computer languages.

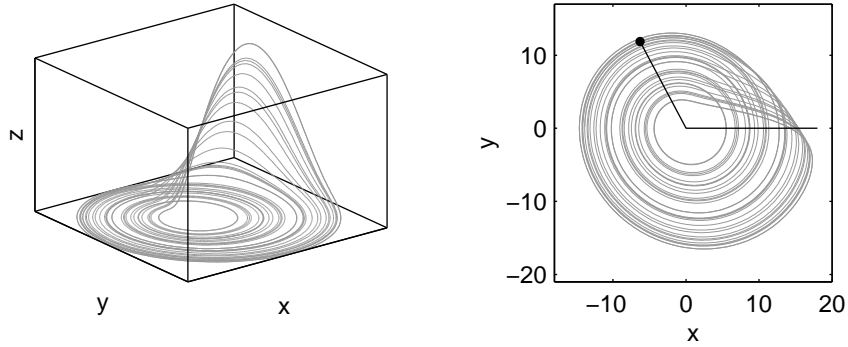


Figure 2.14: The attractor of the Rössler oscillator for standard values of the parameters (Eqs. 2.11). The right panel is showing the projection onto the x, y -plane. The angle between the positive x axis and a particular system state (\bullet) is indicated, which is one possible definition of the phase of this chaotic oscillator.

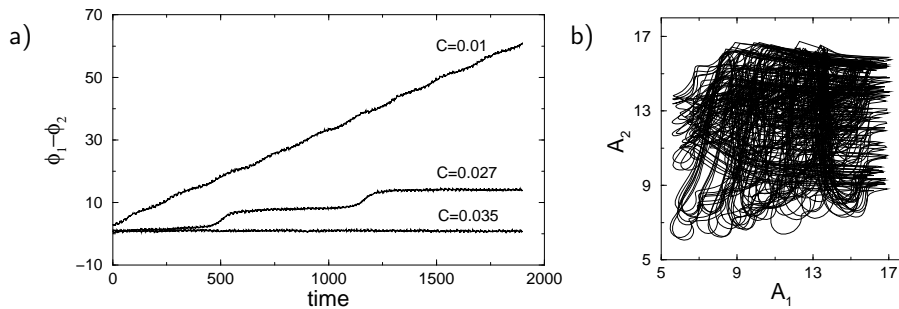


Figure 2.15: Phase synchronization of coupled Rössler oscillators (Eqs. 2.11 with $\omega_{1,2} = 1 \pm 0.015$). a) The phase difference $\phi_1 - \phi_2$ of the oscillators over time. For coupling strength $C = 0.035$ there are no phase slips. b) In the synchronized regime the amplitudes A_1, A_2 remain chaotic and are almost uncorrelated. Reproduced with permission from Rosenblum et al. (1996), Phase synchronization of chaotic oscillators. *Physical Review Letters*, 76, Fig. 1. Copyright © 1996 American Physical Society.

two coupled Rössler oscillators 1 and 2:

$$\begin{aligned}\dot{x}_{1,2} &= -\omega_{1,2} y_{1,2} - z_{1,2} + C(x_{2,1} - x_{1,2}), \\ \dot{y}_{1,2} &= \omega_{1,2} x_{1,2} + 0.15 y_{1,2}, \\ \dot{z}_{1,2} &= 0.2 + z_{1,2}(x_{1,2} - 10).\end{aligned}\tag{2.11}$$

The parameters $\omega_{1,2}$ determine the natural frequencies of the two oscillators, while C is the strength of their coupling. For a small frequency mismatch $\omega_2 - \omega_1$ and a coupling that is also small but strong enough to overcome the detuning this system reaches a synchronized regime where the phase difference seems to be bounded (Fig. 2.15a). Interestingly, the dynamics of the two oscillators is still chaotic and their amplitudes are uncorrelated (Fig. 2.15b). This specific regime in the dynamics of two coupled chaotic oscillators has been found by Rosenblum et al. (1996). The authors have called it *phase synchronization* to distinguish this form of synchronization from other types that can be obtained with stronger coupling, like the perfect coincidence of the two oscillators' states. In the system of coupled Rössler oscillators with $\omega_1 = \omega_2$, in contrast to complete synchronization, phase synchronization can be achieved with very small coupling.

The phase dynamics of a chaotic oscillator like the Rössler system can be described by a dependency of the instantaneous frequency on the chaotic amplitude (cf. Rosenblum et al., 1996):

$$\dot{\phi} = \omega_0 + F(A).$$

Because the dynamics of the amplitude can formally be made independent of the phase,⁹ its effect on the phase can be regarded as an external irregular influence (cf. Pikovsky et al., 2001, Ch. 10). Therefore, the chaotic aspect of the phase dynamics can effectively be treated as noise, so that chaotic synchronization can be described in the framework of synchronization of noisy periodic oscillators (Eq. 2.9).

In the preceding, the basic mechanisms of bivariate synchronization have been described for the cases of periodic, noisy and chaotic oscillators. Concluding, the author wants to remark that the notion of phase synchronization has a threefold meaning. Firstly, the term phase synchronization analysis used in the title of this work denotes the approach to the processing of empirical data, in which phases are calculated and their statistical properties are evaluated while the corresponding amplitudes are disregarded (Sec. 3.3). This approach is, secondly, grounded on the notion that synchronization in the sense of adjustment of rhythms is always “phase synchronization”, because the rhythm of an oscillator is to be described in terms of a phase. Thirdly, this approach is further motivated and justified by the finding of the concrete phenomenon that occurs in coupled chaotic oscillators, that weak coupling may effect a boundedness of the phase difference while the amplitudes remain free. Because weak coupling affects the phases but not the amplitudes, it can be detected by phase synchronization analysis, removing the noise inherent in the amplitudes.

⁹This is achieved by turning the amplitude dynamics into a discrete-time map, where the time points are determined by the return of the circular phase to a chosen value (corresponding to a Poincaré section in state space). Because at these time points the phase has a pre-determined value, the future evolution of the amplitude is determined only by its own current value.

Chapter 3

Data Processing and Bivariate Analysis

While the previous chapter has described the data to be analyzed and the physical theory underlying this analysis, the present chapter goes into the details of the procedures of data processing that are applied. Though these sections are still concerned with basic methodical aspects, in contrast to the preceding sections they already contain relevant decisions that have been made in order to adapt method and data to each other. Their sequence follows the logical order of the processing steps. Section 3.1 describes a remedy to the problems (with respect to synchronization analysis) caused by the low spatial resolution of raw EEG by interposing a step of data decorrelation. Section 3.2 continues the discussion of the definition of an oscillator's phase started in Sec. 2.3. It introduces the wavelet transform as a method to obtain an instantaneous phase from measured time series and explains why in the case of EEG data this method is to be preferred over others. The final section (3.3) establishes the statistical measure of bivariate synchronization strength that is applied in this work. Its choice in preference over other approaches is accounted for by an excursion into the statistics of directional data.

3.1 Reduction of spurious correlations

EEG is a problematic type of data for the calculation of correlations and other quantifications of dependency between signals from different locations, including phase synchronization. The reason for this is that the voltage time series measured at a given scalp site does not solely correspond to the activity of the neuron population directly underneath, but is a combination of influences that can be widespread in the cortex. Therefore, a high level of baseline correlations between different sites is to be expected that does not correspond to correlated activity within the brain.

There are two causes for this. Firstly, the electric potentials produced by the dynamically changing currents in the neural tissue can not be measured as such, but have to be related to a *reference*. EEG recordings are measurements of voltages, that is differences of the electric potential at different places. The common approach to this problem is to put the reference electrode at a place where one can expect to find only very weak local electric activity like the ear lobes, the mastoid bones behind the ears, the neck, or the nose. But, as Nunez et al. (1997) have shown based on numerical simulations, measurements are reference-dependent even if the relevant neural field sources are not close to the reference electrode, and so practically there is no such thing as a "quiet reference". Because the variations of the potential

at the reference electrode are included in the voltage measurements at every other electrode this activity can lead to spuriously high correlations that are uniformly distributed over the scalp.

The other cause of spurious correlations is more localized. It is due to *volume conduction*, the circumstance that currents generated by cortical activity are passively spread over the scalp because of the lower conductivity of the skull (Nunez, 1981, Ch. 1). This leads to a smearing of the electric potential as it can be found under the skull (the dura potential). Measurements at neighboring electrodes are highly correlated because the current spread acts as a mixing-in of activity from the surrounding areas. As an active reference electrode can induce spurious long-range correlations, volume conduction leads to spuriously high short-range correlations.

There are a number of methods aimed at reducing these spurious correlations with different levels of sophistication. Regarding the reference electrode problem, as part of the postprocessing of EEG recordings one can compute an improved reference and re-reference the data according to it; possibilities include the mean of the two ear lobe voltages, or the average over all electrode sites. For volume conduction, detailed models of the electric properties of the cortical and scalp tissue and the skull can be designed to simulate their effect on the dura potential and reconstruct it from the scalp voltage measurements. But according to Nunez et al. (1997), it is an approach in between that delivers very good results, namely the surface spline Laplacian, the calculation of the surface Laplacian of spline-interpolated scalp measurements. This method is able to completely remove reference problems, and though it does not directly aim at recovering inner surface potentials, simulations have shown that with dense electrode arrays it provides an excellent estimate of dura potentials (cf. Nunez, 1995).

According to Nunez (1981, Ch. 8), more than the scalp potential itself it is the density of currents flowing into the scalp from below that is indicative of the location of neuronal generators (cf. Perrin et al., 1987). Therefore it is interesting to look at the sources and sinks of the resulting currents that are tangential to the scalp surface, i.e. the surface divergence of the current density \vec{j} . This quantity is commonly called *source current density*:

$$\text{SCD} = \vec{\nabla}_{\text{surface}} \cdot \vec{j}$$

(where $\vec{\nabla}_{\text{surface}}$ is the surface component of the Nabla operator). The current density represents the Ohmic current corresponding to the potential gradient

$$\vec{j} = -\sigma \vec{\nabla} \Phi$$

(where σ is the conductivity of the scalp and Φ the electric potential), and therefore

$$\text{SCD} = -\sigma \Delta_{\text{surface}} \Phi$$

(where Δ_{surface} is the surface component of the Laplace operator). Since the measured voltages $U = \Phi - \Phi_0$ are the potential with respect to a (spatially) constant reference Φ_0 and the Laplacian is a spatial derivative, the SCD can be calculated on the voltages,

$$\text{SCD} = -\sigma \Delta_{\text{surface}} U. \quad (3.1)$$

The source current density does not depend on the reference potential Φ_0 any more, and because the surface Laplacian acts as a spatial high-pass filter, local correlations are reduced.

To apply the Laplacian, the voltages U_i measured at the electrode locations \vec{r}_i have to be interpolated to obtain a continuous function on the scalp surface. The

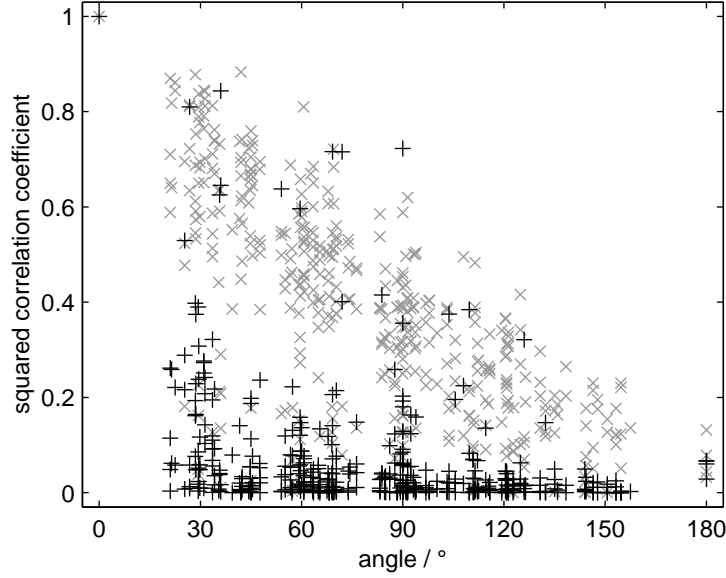


Figure 3.1: Reduction of correlations in experimental data by the spherical spline Laplacian algorithm with $m = 4$. The squared correlation coefficient of signals is plotted for each pair of electrodes within a set of 30 against the spherical angle between the electrodes. For raw data (gray \times) a strong dependence of the correlation on the electrode distance is visible that is largely removed after processing (black $+$).

available methods to calculate the surface Laplacian (cf. Nunez et al., 1997) differ in the type of interpolation used. The author is following the approach of Perrin et al. (1989) that is characterized by a simple, straightforward mathematical ansatz. They assume that the scalp surface is approximately spherical with a radius normalized to unity and assign idealized positions to the electrodes. These are obtained by transferring the procedures of electrode localization of the International 10-20 System (Sec. 2.1) onto the unit sphere (cf. Lagerlund et al., 1993). With electrode locations $\vec{r}_i = \hat{r}_i$ for electrodes $i = 1 \dots N$, the voltage on the whole sphere surface is interpolated by

$$U(\hat{r}) = c_0 + \sum_{j=1}^N c_j g_m(\hat{r} \cdot \hat{r}_j), \quad (3.2)$$

where c_0 to c_N are the interpolation coefficients that have to be chosen such that $U(\hat{r}_i) = U_i$ and $\sum_{i=1}^N c_i = 0$, and

$$g_m(z) = \frac{1}{4\pi} \sum_{l=1}^{\infty} \frac{2l+1}{l^m(l+1)^m} P_l(z) \quad (3.3)$$

is the spherical spline function of order m ; $P_l(z)$ denotes the l^{th} degree Legendre polynomial.

Since for the spherical geometry holds

$$\Delta_{\text{surface}} \propto \Delta_{\theta, \phi} = \frac{1}{\sin \theta} \frac{\partial}{\partial \theta} \sin \theta \frac{\partial}{\partial \theta} + \frac{1}{\sin^2 \theta} \frac{\partial^2}{\partial \phi^2}$$

where θ and ϕ denote the angles in a spherical coordinate system and

$$\Delta_{\theta, \phi} P_l(\cos \theta) = -l(l+1) P_l(\cos \theta),$$

the surface Laplacian of this spline interpolation has the same form as the interpolation itself, and for the source current density estimation follows:

$$\text{SCD}(\hat{r}) = -\sigma \Delta_{\text{surface}} U(\hat{r}) \propto -\Delta_{\theta, \phi} U(\hat{r}) = \sum_{j=1}^N c_j g_{m-1}(\hat{r} \cdot \hat{r}_j).$$

The value of the last term evaluated at the electrode positions,

$$L_i = \sum_{j=1}^N c_j g_{m-1}(\hat{r}_i \cdot \hat{r}_j) \quad (3.4)$$

is then used in place of the original recordings U_i for the subsequent analysis.

The calculation is computationally cheap, because for given electrode positions the relation between $\vec{U} = (U_i)$ and $\vec{L} = (L_i)$ can be written as a matrix multiplication. With $\vec{C} = (c_i)$ for $i = 1 \dots N$, $G = (g_m(\hat{r}_i \cdot \hat{r}_j))$, \vec{T} denoting a column vector of ones, and I denoting the identity matrix, the interpolation condition is fulfilled by

$$\vec{C} = G^{-1} \left(I - \vec{T} \frac{\vec{T}^+ G^{-1}}{\vec{T}^+ G^{-1} \vec{T}} \right) \vec{U} \quad \text{and} \quad c_0 = \frac{\vec{T}^+ G^{-1}}{\vec{T}^+ G^{-1} \vec{T}} \vec{U},$$

where $+$ is the transposition operator. Therefore the calculation of the Laplacian can be written as $\vec{L} = \mathcal{L} \vec{U}$, where

$$\mathcal{L} = HG^{-1} \left(I - \vec{T} \frac{\vec{T}^+ G^{-1}}{\vec{T}^+ G^{-1} \vec{T}} \right),$$

with $H = (g_{m-1}(\hat{r}_i \cdot \hat{r}_j))$. The author has chosen $m = 4$ for the spline order based on the recommendation of Perrin et al. (1989) and experiments with empirical data (Fig. 3.1).¹

3.2 Determination of the instantaneous phase

To be able to apply phase synchronization analysis to empirical data, it is necessary to assign an instantaneous phase $\phi(t)$ to the measured scalar time series $x(t)$. In the literature there is no generally adopted method to do so, but a number of methods that are more or less adapted to specific situations. In this section two basic approaches are presented that have a well-founded mathematical background, the analytic signal method and the wavelet method, and their close relationship is detailed. Based on this systematic presentation some of the procedures that have been used by other authors are commented on.

As has been explained in Sec. 2.3, the notion of phase stems from the theory of the periodic oscillator corresponding to a limit cycle in a nonlinear dynamical system. Here the phase describes the periodicity of the system's behavior and in the simplest case equals an angle in state space. If the movement on the limit cycle is not uniform or the shape of the trajectory is not circular, the phase can still be unambiguously defined as a periodic variable whose value is constantly increasing in time, corresponding to the evolution of the system state along the limit cycle. For chaotic dynamics with a complex attractor geometry it is generally not possible to

¹For a comment on the possible use of generic methods like independent component analysis (ICA; cf. Ziehe and Müller, 1998) as a preprocessing step for synchronization analysis to reduce mixing-related dependencies in EEG data, see Ch. 7.

consistently define such a variable.² Nonetheless, in many cases an approximate definition can be found, based on the observation that the attractor in a certain planar projection can be considered as a limit cycle that has been “smeared out” but still clearly orbits around a center. In this situation, the direct way to define a phase is to take the angle in the projection plane with respect to the orbit’s center.

In empirical data often the full state of the oscillatory system is not accessible, but only one scalar observable. Also, because the data are noisy and/or nonstationary, methods to reconstruct the state space from an observable (cf. Kantz and Schreiber, 1997) do not give usable results. In this case it is necessary to determine the phase based not on the system state, but directly on the measured signal $x(t)$. A general framework to do so is to transform the real valued signal into a complex signal $z(t)$ and to consider the argument of the complex value (corresponding to the angle in the complex plane) as the instantaneous phase of the signal: $\phi(t) = \arg z(t)$. Different methods of phase definition then reduce to differences in the applied transform $x(t) \rightarrow z(t)$.

Real valued signals may be characterized as such by their symmetry in the frequency domain: $\tilde{x}(-\omega) = \tilde{x}(\omega)^*$, where \tilde{x} is the Fourier transform of x and $*$ denotes the complex complement. Since the range of negative frequencies $\omega < 0$ is totally redundant, the most direct way to obtain a complex signal without losing any of the signal’s information is to delete the negative frequency components by applying a linear filter with a transfer function of

$$\tilde{f}(\omega) = 2 \Theta(\omega) = \begin{cases} 0 & \omega < 0 \\ 2 & \omega \geq 0 \end{cases},$$

where Θ is the Heaviside step function (cf. Carmona et al., 1998, Sec. 1.1.2). The result of this transform is called the *analytic signal*; it can also be written as a convolution

$$z(t) = (x * f)(t) \quad \text{with} \quad f(t) = \delta(t) + \frac{i}{\pi t}. \quad (3.5)$$

The analytic signal is a common tool in signal processing. In phase synchronization analysis this approach has been introduced by Rosenblum et al. (1996).

The real part of the analytic signal is identical to the original real valued signal, $\text{Re}(z(t)) = x(t)$. Its imaginary component is called the *Hilbert transform* H of x , so that

$$z(t) = x(t) + iHx(t), \quad \text{where} \quad Hx(t) = \frac{1}{\pi} \text{P.V.} \int_{-\infty}^{\infty} \frac{x(t')}{t - t'} dt'$$

and P.V. denotes the principal value integral. The effect of the Hilbert transform can be described as the application of a $\pi/2$ phase lag separately to all frequency components. Therefore, it transforms any cosine signal $\cos(\omega t)$ into the sine and the analytic signal is the corresponding complex harmonic $\exp(i\omega t)$, which means that the resulting phase $\phi(t) = \omega t$ is identical to the one commonly assigned to a sinusoidal oscillation. The approach is equally successful if the spectrum of the given signal shows only a single narrow peak because the underlying process deviates only weakly from a harmonic oscillation, like it is the case for instance with the Rössler system (for standard values of the parameters; see Fig. 2.14). Pikovsky et al. (1997) have shown that the instantaneous phase of this chaotic oscillator is well-defined in the sense that the analytic signal approach, the definition based on an angle in state space (Eq. 2.10), as well as a third method using a Poincaré section give very similar values and equivalent results in the phase synchronization analysis.

²In the language of nonlinear dynamics, at every place in state space the phase increases in that local direction that corresponds to the zero Lyapunov exponent, which is always present in the Lyapunov spectrum of a time-continuous autonomous system (Pikovsky et al., 1997). Still, these local directions can not necessarily be merged to globally define the phase as a variable in state space.

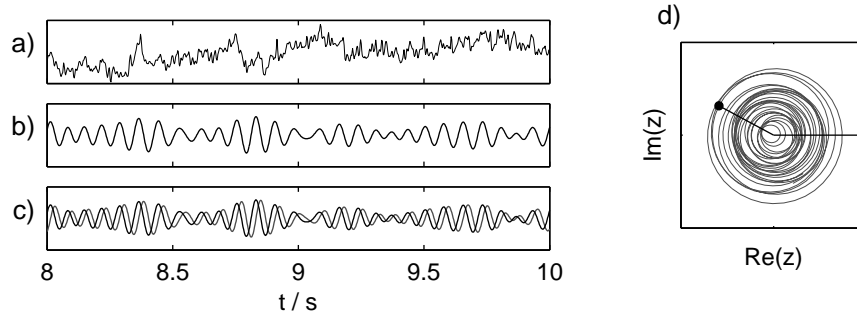


Figure 3.2: Determination of the instantaneous phase from data. a) A section of a continuous EEG record at one electrode; the measured data are scalar, real-valued, and broadband (noisy). b) The data have been filtered with a band-pass for 13 Hz, the result is an amplitude-modulated sinusoidal wave. c) The Hilbert transform has been applied to obtain the imaginary part (gray line) of the analytic signal complementing the given real part (black line, equals b). d) The transformed signal $z(t)$ performs orbits in the complex plane, so that the instantaneous phase can be defined as an angle.—The transform $a \rightarrow c$ has actually been done by convolution with a complex Morlet wavelet for $\eta = 10$, scaled such that the center frequency is $\omega = 2\pi \cdot 13$ Hz.

On the other hand, for many complex natural systems the signals that can be obtained do not have such a simple composition. Especially for EEG, the measured data are a superposition of a large number of components with extremely different frequencies (Sec. 2.1), and those oscillations that are engaged in the synchronization processes that are of interest in the given experimental context make up only a small part of the broadband signal. In this case, it is necessary to apply a band-pass filter to emphasize the signal components in a specific frequency band (Fig. 3.2).³ In many cases it is not known in advance which frequencies characterize the oscillatory processes one is looking for and so the band-pass has to be applied several times in versions that are adjusted to the different frequencies. A framework for such signal analysis at different frequencies retaining a high temporal resolution is given by wavelet theory.

A wavelet (following Mallat, 1998, Sec. 4.3) is a function $\Psi(t)$ with zero mean

$$\int_{-\infty}^{\infty} \Psi(t) dt = 0$$

that is normalized according to a square norm:

$$\langle \Psi | \Psi \rangle = \int_{-\infty}^{\infty} \Psi(t) \Psi^*(t) dt = 1$$

($\langle \cdot | \cdot \rangle$ denotes the scalar product of two complex-valued functions). The *wavelet transform* W analyzes a signal x by correlating it with so-called time-frequency atoms that are rescaled (parameter s) and translated (parameter u) versions of the wavelet:

$$Wx(u, s) = \langle x | \Psi_{u,s} \rangle = \int_{-\infty}^{\infty} x(t) \Psi_{u,s}^*(t) dt \quad (3.6)$$

$$\text{with } \Psi_{u,s}(t) = \frac{1}{\sqrt{s}} \Psi\left(\frac{t-u}{s}\right).$$

³For the case of MEG/EMG signals, cf. Tass et al. (1998).

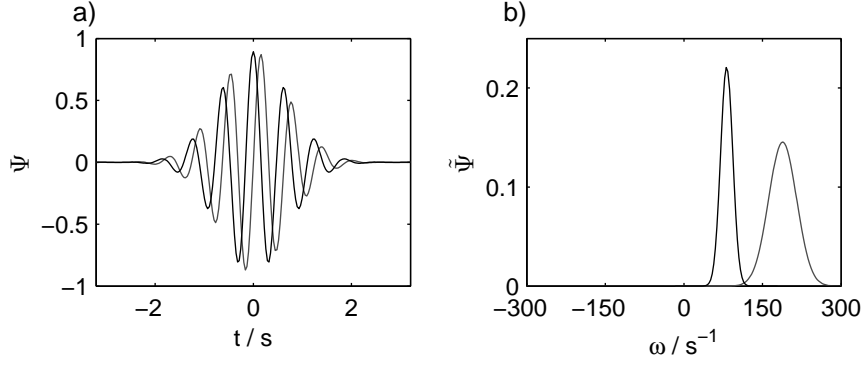


Figure 3.3: a) The complex Morlet wavelet for $\eta = 10$ (black line: real part, gray line: imaginary part). b) Transfer functions of the filters corresponding to a convolution with a scaled Morlet wavelet for two different scales, $s = \eta/\omega$ with $\omega/2\pi = 13\text{ Hz}, 30\text{ Hz}$. The filter with the higher center frequency also has a larger bandwidth (increased time and reduced frequency resolution). Note that the value of the transfer functions for $\omega < 0$ is practically 0, such that the calculation of the analytic signal implicit in the filtering is almost perfect.

For a fixed scale s , the transform can be written as a convolution

$$Wx(u, s) = (x * \Psi_s)(u) \quad \text{with} \quad \Psi_s(t) = \frac{1}{\sqrt{s}} \Psi^* \left(-\frac{t}{s} \right)$$

that is, as a filter with a transfer function of $\tilde{\Psi}_s(\omega) = \sqrt{s} \tilde{\Psi}^*(s\omega)$.

A wavelet is called analytic if $\Psi(t)$ is an analytic signal, i.e. if it does not contain any negative frequency components ($\tilde{\Psi}(\omega) = 0$ for $\omega < 0$). In this case, the wavelet transform $Wx_s(u)$ as a function of u is the analytic signal corresponding to $x(t)$ that has additionally been filtered according to the scale s . That means the analytic wavelet transform comprises the effect of a band-pass filter and of the Hilbert transform (Fig. 3.2).

In this work, the Gabor⁴ or complex *Morlet wavelet* is used (Fig. 3.3a). It is a complex harmonic modulated with a Gaussian-shaped envelope:

$$\Psi(t) = \sqrt[4]{\frac{2}{\pi}} \exp(-t^2) \exp(i\eta t) \quad (3.7)$$

(Carmona et al., 1998, Sec. 4.3.1). This wavelet is not strictly analytic, but for the relevant applied case $\eta > 5$ it is analytic in a very good approximation. The constant parameter η distinguishes variants of the wavelet and has to be chosen according to the purpose of the application (see below).

The time-frequency atoms of the Morlet wavelet transform are

$$\Psi_{u,s}(t) = \sqrt[4]{\frac{2}{s^2\pi}} \exp\left(-\frac{(t-u)^2}{s^2}\right) \exp\left(i\eta\frac{t-u}{s}\right).$$

Considering the modulus squared of the atom

$$|\Psi_{u,s}(t)|^2 = \sqrt{\frac{2}{s^2\pi}} \exp\left(-2\frac{(t-u)^2}{s^2}\right)$$

⁴Interestingly, the two approaches to the definition of an instantaneous phase discussed in this section have a common source: The analytic signal was introduced by Gabor in the same study (Gabor, 1946) that presented an early form of a wavelet-based time-frequency analysis.

as a distribution over time, one can see that it is localized around $t = u$ with a precision of $\sigma_t = s/2$. In the frequency domain the wavelet is also Gaussian-shaped, and the transfer function corresponding to the wavelet transform is

$$\tilde{\Psi}_s(\omega) = \sqrt{s} \tilde{\Psi}^*(s \omega) = \sqrt{\frac{s^2}{2\pi}} \exp\left(-\frac{1}{4}(s \omega - \eta)^2\right) \quad (3.8)$$

(Fig. 3.3b). Considering now the modulus squared of the transfer function

$$|\tilde{\Psi}_s(\omega)|^2 = \sqrt{\frac{s^2}{2\pi}} \exp\left(-\frac{1}{2}s^2 \left(\omega - \frac{\eta}{s}\right)^2\right)$$

as a distribution over frequency, one can see that the time-frequency atom is localized around $\omega = \eta/s$ with a precision of $\sigma_\omega = 1/s$.

The Morlet wavelet transform corresponds to the parallel application of a number of Gaussian band-pass filters with different center frequencies (a “filter bank”). The scaling implicit in the wavelet transform leads to a constant ratio of center frequency to bandwidth $\omega/\sigma_\omega = \eta$. Because of this, the frequency resolution of the analysis $\sigma_\omega = \omega/\eta$ gets finer with decreasing center frequency and the time resolution $\sigma_t = \eta/2\omega$ gets finer with increasing center frequency. The constant combined time-frequency resolution of the Morlet wavelet is $\sigma_t \sigma_\omega = \frac{1}{2}$, which is the optimum of the general uncertainty relation $\sigma_t \sigma_\omega \geq \frac{1}{2}$ for time-frequency analyses (Mallat, 1998, Sec. 2.3.2). The tradeoff between time and frequency resolution can be adjusted by the parameter η .

Since the Morlet wavelet is approximately analytic, the wavelet transform encompasses the calculation of the analytic signal and the application of band-pass filters in an elegant way. Other than the analytic signal approach, the wavelet transform $Wx(u, s)$ gives not only one complex signal $z(t)$, but one for every scale s : $z_s(t) = Wx(t, s)$. Because the scale corresponds to a frequency $\omega = \eta/s$, this can be used to define a frequency-specific complex signal $z(t, \omega) = Wx(t, \eta/\omega)$ and, accordingly, a frequency-specific instantaneous phase:

$$\phi(t, \omega) = \arg z(t, \omega) = \arg Wx\left(t, \frac{\eta}{\omega}\right). \quad (3.9)$$

This definition of the phase based on the complex Morlet wavelet will be used as the basis of the synchronization analyses presented in the following chapters.

The wavelet transform has been used in a large number of studies analyzing empirical data, including EEG (cf. Lopes da Silva, 1998a). For instance, Tallon-Baudry et al. (1996) have used it for computing a time-frequency energy density $E(t, \omega) = |z(t, \omega)|^2$ of event-related potentials as well as indices of phase locking (but without calculating an instantaneous phase; see also Braeutigam et al., 2001). In the context of phase synchronization analysis, Rodriguez et al. (1999) resp. Lachaux et al. (1999) have used a Morlet wavelet and advocated it as an alternative to the analytic signal, but have redundantly combined it with a band-pass filter for the same frequency band. On the other hand, DeShazer et al. (2001) have modified the analytic signal approach by using a Gaussian transfer function in place of the Heaviside, thereby effectively computing a Morlet wavelet transform but without relating their method to wavelet theory. Similarly Haig et al. (2000) have computed instantaneous phases by using one component of a windowed Fourier transform of the signal, which is equivalent to a wavelet transform that is confined to a single frequency η with a wavelet of the form $\Psi(t) = \exp(i \eta t) g(t)$, where g is the window function. Though Le Van Quyen et al. (2001a) had empirically compared the wavelet method with the one using combined band-pass and analytic signal, finding that there are only small differences, and though some

of the authors had already recognized the close relationship between the analytic signal and wavelet transform approaches, the first study contributing to the field of phase synchronization analysis to correctly state the mathematical relations was Quian Quiroga et al. (2002).

A special case in synchronization analysis is Schack et al. (2000) and related studies (Weiss and Müller, 2003; Weiss et al., 2004). To obtain frequency- and time-dependent phases for two channels, the authors fit a two-dimensional ARMA (autoregressive moving average) model to the data that features time-varying parameters. It is questionable whether this laborious procedure provides an advantage over the more direct, mathematically elegant and transparent approach of the wavelet transform. Moreover, the authors interpret a constant phase difference between oscillators as an indicator of the “speed of information transfer”. Such an interpretation corresponds to an understanding of the observed process in terms of signal propagation, but not of synchronization, where the most important cause for a phase lag is a difference in the natural frequencies of two oscillators.

3.3 Quantification of bivariate phase synchronization and directional statistics

In Sec. 2.3 synchronization has been introduced as a phenomenon occurring in coupled self-sustained oscillators and has originally been defined as the boundedness of the phase difference (Eq. 2.7). It has also been stated that in noisy oscillators it is possible that this condition is never exactly met, even though the coupling has a clear effect on the probability distribution of the circular phase difference (Fig. 2.13). Although the basic phenomenon of chaotic phase synchronization observed in coupled Rössler oscillators consists also in a bounded phase difference, for other chaotic oscillators irregular phase slips similar to the noisy case may occur (imperfect synchronization, cf. Pikovsky et al., 2001, Ch. 10). Still another and in practice the most important reason why it may be impossible to observe a bounded phase difference is noise that is affecting the data acquisition. Strong measurement noise is common in many types of empirical data, and this is clearly the case for EEG. In all of these circumstances, the original definition of (phase) synchronization has to be replaced by a quantitative statistical concept. In this perspective, phase synchronization is a gradual phenomenon whose strength corresponds to the degree of dynamical dependence between the phases of the two oscillators. This section introduces the basic measure of bivariate phase synchronization that will be used subsequently, and it gives an overview of the mathematical background and statistical properties of this measure.

In the bivariate case,⁵ we are concerned with a system that consists of two self-sustained oscillators, A and B. For each of them a phase ϕ_A , ϕ_B is defined (Sec. 3.2). The oscillators are coupled to each other such that the phase difference $\Delta\phi = \phi_B - \phi_A$ tends to a preferred value (in the most simple case, to 0). This tendency is disturbed by dynamical noise or by chaos—that both can conceptionally be considered in the framework of stochastic dynamics—and the determination of the phases is subject to measurement noise. Therefore the phase difference is a random variable characterized by a probability distribution which is empirically accessible in the form of a number of realizations $\Delta\phi_j$, $j = 1 \dots n$ (a sample). In the examination of a single time series of a phase difference $\Delta\phi(t)$, the different time points may be looked at as these (statistically dependent) realizations. In the context of this work about synchronization analysis of event-related potentials (Sec. 2.2) the realizations correspond to the epochs of an experimental condition,

⁵An approach to multivariate statistical phase synchronization analysis will be introduced in Ch. 5.

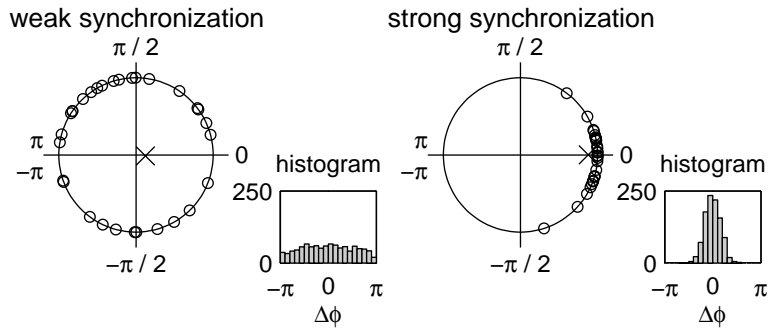


Figure 3.4: The measure of synchronization strength \bar{R} . If points on the unit circle (\circ) are assigned to the values of the phase difference $\Delta\phi_j$ in a sample, \bar{R} can be visualized as the distance between the center of gravity of the points (\times) and the circle center. Weak synchronization corresponds to a nearly uniform distribution of the phase difference and a small value of the measure (here, $\bar{R} = 0.12$), strong synchronization to a distribution concentrated on one side and a high \bar{R} value (here, 0.88). (Histogram and \times -location are based on 1000 samples, of which 30 are plotted on the circle.)

while time is treated as an additional independent parameter of the nonstationary process.

Tass et al. (1998) have introduced a measure of synchronization strength that quantifies the deviation of the phase difference distribution from a uniform one. It is based on the Shannon entropy S of the phase difference distribution, estimated on a sample histogram with N equal bins. The measure is then defined to be the normalized entropy

$$\frac{S_{\max} - S}{S_{\max}} \quad \text{with} \quad S_{\max} = \log N$$

that can obtain values in the range from 0 corresponding to the uniform distribution (no synchronization) to 1 corresponding to a δ distribution (perfect synchronization). The entropy measure has been successfully used by the authors to observe neural and muscular synchronization processes in MEG and EMG data. Nonetheless, it has some disadvantages: the definition includes a parameter (the number of histogram bins N) whose value has to be appropriately chosen, and the binning procedure makes the calculation of the entropy measure computationally expensive, which is important in the processing of large amounts of data.

In this work another measure of synchronization strength is used whose computation is much more straightforward, the *mean resultant length*:

$$\bar{R} = \left| \frac{1}{n} \sum_{j=1}^n \exp(i\Delta\phi_j) \right|. \quad (3.10)$$

\bar{R} also takes on values in the range from 0 to 1, describing a continuum between no and perfect phase synchronization. But in contrast to the entropy measure, \bar{R} does not quantify the general nonuniformity of the distribution but the magnitude of its (single) peak (Fig. 3.4).⁶ Under different names, the mean resultant length has been used as a measure of bivariate synchronization in a number of studies analyzing EEG data (Rodriguez et al., 1999; Lachaux et al., 1999; Mormann et al., 2000;

⁶Because of this, the use of \bar{R} as a synchronization measure presumes that the phase difference distribution is unimodal, which may be seen as drawback against the entropy measure. On the other hand a multimodal distribution is an indicator of $m:n$ synchronization (Sec. 2.3, Fn. 7). If the locking ratio defining $\Delta\phi$ is correctly chosen, the distribution of the generalized phase difference should be essentially unimodal.

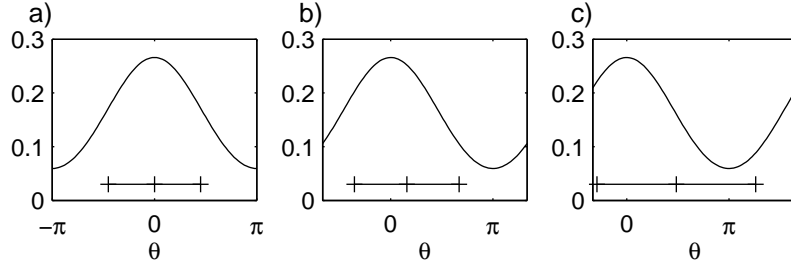


Figure 3.5: Linear statistics of a circular random variable. The same circular distribution is mapped onto three different intervals on the line, yielding different values for mean and standard deviation (indicated by the horizontal bar). a) $[-\pi, \pi[\rightarrow 0 \pm 1.42$. b) $[-\frac{2}{3}\pi, \frac{1}{3}\pi[\rightarrow 0.49 \pm 1.61$. c) $[-\frac{1}{3}\pi, \frac{2}{3}\pi[\rightarrow 1.52 \pm 2.44$.

Quián Quiroga et al., 2002). The \bar{R} statistic has also been applied directly to phases as a global measure of phase synchronization in a population of oscillators (Haig et al., 2000). For the author, the most important property of the mean resultant length is that it has a well elaborated background of mathematical theory, describing its statistical properties. This background is the field of *directional statistics*.

Directional statistics (Mardia, 1972; Mardia and Jupp, 2000) deals with a special type of random variable which is defined on a circular scale, such that values whose difference is an integral multiple of a certain period (in general 2π) are regarded the same, and for convenience all values are wrapped into a single period. The circular phase difference $\Delta\phi$ (Sec. 2.3) is an example of such a random variable; another example are directions in space which are a common object of investigations in science, for instance the directions of the flight of birds or that of geologic formations. For the purposes of this discussion the *circular random variable* may be generically denoted by θ .

To such a variable standard linear statistical measures and moments like mean and variance are not applicable, because they yield different values depending on the way the values of the circular variable are mapped onto a linear scale (Fig. 3.5). Instead of these classical moments, directional statistics studies the statistical properties of the values of trigonometric functions applied to the circular variable θ , the *trigonometric moments* of order p ($p = 1, 2, \dots$) of its distribution

$$\alpha_p = \langle \cos p\theta \rangle \quad \text{and} \quad \beta_p = \langle \sin p\theta \rangle.$$

The combined complex form of cosine and sine moments $\alpha_p + i\beta_p$ is equivalent to the characteristic function of the distribution (its Fourier transform). The first element of this series is of special importance, because the polar components

$$\mu = \arg(\alpha_1 + i\beta_1) \quad \text{and} \quad \varrho = |\alpha_1 + i\beta_1| \quad (3.11)$$

can be regarded as indices of the *mean direction* of the distribution and of its *concentration* onto this mean direction, respectively. (Mardia and Jupp, 2000, Sec. 3.4)

These are the theoretical moments of the circular distribution. The corresponding quantities on a sample θ_j ($j = 1 \dots n$) are

$$a_p = \frac{1}{n} \sum \cos p\theta_j \quad \text{and} \quad b_p = \frac{1}{n} \sum \sin p\theta_j,$$

which are estimators of the moments α_p and β_p . The components of the first empirical moment are

$$\bar{C} = a_1 = \frac{1}{n} \sum_{j=1}^n \cos \theta_j \quad \text{and} \quad \bar{S} = b_1 = \frac{1}{n} \sum_{j=1}^n \sin \theta_j$$

or, in polar representation,

$$\bar{\theta} = \arg(\bar{C} + i\bar{S}) \quad \text{and} \quad \bar{R} = |\bar{C} + i\bar{S}| = \left| \frac{1}{n} \sum_{j=1}^n \exp(i\theta_j) \right|.$$

Since \bar{R} is the length of the mean of the unit vectors corresponding to the sample values it is called mean resultant length. \bar{R} is an estimator of the population moment ϱ and as such an empirical measure of the concentration of the underlying distribution. (Mardia and Jupp, 2000, Sec. 2.2 ff.) Applied to a sample of the phase difference distribution of two oscillators, it turns into a measure of synchronization strength.

Since \bar{R} is based on a finite sample of the distribution, it is just an estimate of the true concentration ϱ . To be able to assess the precision of this estimation or to perform a statistical test (see Ch. 4) it is necessary to know about the distribution of \bar{R} as a random variable. Because of the simple definition of this statistic, it is possible to derive basic properties of its sampling distribution. Since \bar{C} and \bar{S} are sums of identically distributed contributions, due to the central limit theorem their asymptotic ($n \rightarrow \infty$) joint distribution is a two-dimensional normal. The moments of this distribution depend on the trigonometric moments of θ :

$$\begin{aligned} \langle \bar{C} \rangle &= \alpha_1 & \langle \bar{S} \rangle &= \beta_1 \\ n \operatorname{var} \bar{C} &= \frac{1}{2}(1 + \alpha_2 - 2\alpha_1^2) & n \operatorname{var} \bar{S} &= \frac{1}{2}(1 - \alpha_2 - 2\beta_1^2) \\ n \operatorname{cov}(\bar{C}, \bar{S}) &= \frac{1}{2}(\beta_2 - 2\alpha_1\beta_1) \end{aligned} \quad (3.12)$$

For $\varrho > 0$, the transformation from (\bar{C}, \bar{S}) to $(\bar{R}, \bar{\theta})$ is locally linear, and so \bar{R} is asymptotically normally distributed, too. If the distribution of θ is symmetrical about 0, it holds

$$\langle \bar{R} \rangle = \alpha_1 + \frac{1 - \alpha_2}{4\alpha_1 n} + O(n^{-3/2}) \cong \alpha_1 = \varrho \quad \text{and} \quad n \operatorname{var} \bar{R} \cong \frac{1}{2}(1 + \alpha_2 - 2\alpha_1^2).$$

For the uniform distribution ($\varrho = 0$), $2n\bar{R}$ is asymptotically distributed as χ_2^2 . (Mardia and Jupp, 2000, Sec. 4.8) Beyond this, the sampling distribution of \bar{R} can only be specified if something is known about the distribution of θ .

In linear statistics the normal distribution plays a central role, which is justified by its special statistical properties. In its place in directional statistics there are two similar but different distributions, each of them sharing some of these properties (Mardia and Jupp, 2000, Sec. 3.5). The first is the *von Mises distribution* $M(\mu, \kappa)$, defined by the probability density function (Fig. 3.6a)

$$p_M(\theta; \mu, \kappa) = \frac{1}{2\pi I_0(\kappa)} \exp(\kappa \cos(\theta - \mu)). \quad (3.13)$$

I_p denotes the modified Bessel function of the first kind of order p . μ specifies the mean direction of the distribution and κ its concentration; the moments are

$$\alpha_p = \frac{I_p(\kappa)}{I_0(\kappa)} \cos(p\mu), \quad \beta_p = \frac{I_p(\kappa)}{I_0(\kappa)} \sin(p\mu),$$

and especially

$$\varrho = A(\kappa) \stackrel{\text{Def}}{=} \frac{I_1(\kappa)}{I_0(\kappa)}.$$

For a centered von Mises distribution $M(0, \kappa)$ with $\kappa > 0$, the moments of the sampling distribution of \bar{R} are

$$\langle \bar{R} \rangle \cong A(\kappa) \quad \text{and} \quad n \operatorname{var} \bar{R} \cong 1 - A(\kappa)^2 - \frac{A(\kappa)}{\kappa}.$$

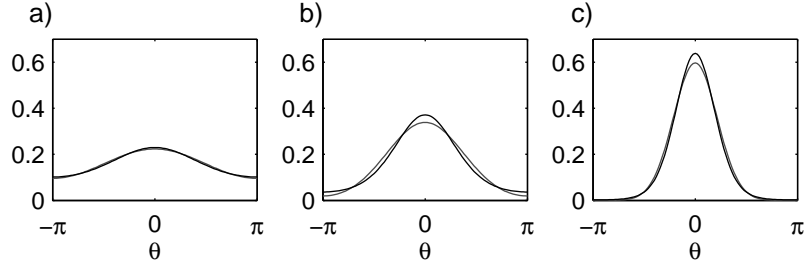


Figure 3.6: The probability distribution functions of the centered von Mises (black line) and wrapped normal (gray line) distributions for three values of the concentration moment ϱ . a) $\varrho = 0.2$: $M(0, 0.41)$, $W(0, 1.79)$. b) $\varrho = 0.5$: $M(0, 1.16)$, $W(0, 1.18)$. c) $\varrho = 0.8$: $M(0, 2.87)$, $W(0, 0.67)$.

Main properties of the von Mises distribution in analogy to the normal distribution are that it is the one with maximum entropy for fixed moments ϱ and μ (that is, it is the best estimate of a distribution if only these moments are known) and the one under which the sample moment $\bar{\theta}$ is the maximum likelihood estimator of a shifting parameter like μ .

For the application in the context of phase synchronization it is of special importance that the simplest stochastic model of phase synchronization, deriving from Eq. 2.9 with detuning $\Delta\omega = 0$, coupling $q(\Delta\phi) = -\sin(\Delta\phi)$, and $\xi(t)$ being standard normal white noise:

$$\dot{\Delta\phi} = -\epsilon \sin(\Delta\phi) + \xi(t), \quad (3.14)$$

the so-called von Mises process, results in a stationary solution that is a von Mises distribution: $\Delta\phi \sim M(0, 2\epsilon)$.

The second circular distribution corresponding to the linear normal one is the *wrapped normal distribution* $W(\mu, \sigma)$ with the probability density (Fig. 3.6b)

$$p_W(\theta; \mu, \sigma) = \frac{1}{\sqrt{2\pi}\sigma} \sum_{k=-\infty}^{k=\infty} \exp\left(-\frac{1}{2} \frac{(\theta - \mu + 2\pi k)^2}{\sigma^2}\right). \quad (3.15)$$

Again μ specifies the mean direction of the distribution and σ its dispersion. The moments are

$$\alpha_p = \varrho^{p^2} \cos(p\mu), \quad \beta_p = \varrho^{p^2} \sin(p\mu) \quad \text{with} \quad \varrho = \exp\left(-\frac{1}{2}\sigma^2\right).$$

For a centered wrapped normal distribution $W(0, \sigma)$, the moments of the sampling distribution of \bar{R} are

$$\langle \bar{R} \rangle \cong \varrho \quad \text{and} \quad n \text{ var } \bar{R} \cong \frac{1}{2}(1 - \varrho^2)^2 \quad \text{with} \quad \varrho = \exp\left(-\frac{1}{2}\sigma^2\right).$$

Main properties of the wrapped normal distribution corresponding to those of the normal distribution are that it is additive and that there exists a central limit theorem which describes convergence to the wrapped normal distribution.

The von Mises and the wrapped normal distribution can be related to each other by equating their concentration moments $A(\kappa) = \varrho = \exp(-\frac{1}{2}\sigma^2)$. For extreme values $\varrho \rightarrow 0$ or $\varrho \rightarrow 1$ they converge to each other and to the uniform or δ distribution, respectively. For intermediate values the peak of the von Mises distribution is sharper (Fig. 3.6). Since the von Mises and the wrapped normal distribution are closely related to basic statistical properties of circular random variables,

there is some possibility that empirical distributions of circular random variables may be described sufficiently well by one of them, including the phase difference of coupled oscillators (see Sec. 4.1). Even if this is may not be so, they retain their importance as paradigmatic circular random distributions.

The concepts and insights of directional statistics are used at several places in the following chapters. Chapter 4 describes a number of hypothesis tests concerning \bar{R} which rely in different degrees on the properties summarized above. Chapter 5 introduces an approach to multivariate phase synchronization based on the idea of a synchronization cluster that is specified in terms of directional statistics.

Chapter 4

Statistical Tests for Bivariate Phase Synchronization

In Sec. 3.3, a statistical measure of phase synchronization strength has been introduced and its background in the theory of directional statistics has been given. As detailed there, the measure of synchronization strength \bar{R} is an estimator of the trigonometric moment ϱ of the phase difference distribution, quantifying the magnitude of its peak. Since such a statistical measure is in itself a random variable, a deviation of its empirical value from zero (corresponding to no synchronization) does not suffice to state an effect of phase synchronization. This means that a statistical test has to be applied.

In the literature, there are some approaches to test for the significance of a measured synchronization level (cf. Paluš, 1997; Paluš and Hoyer, 1998; Tass et al., 1998; Rodriguez et al., 1999; Lachaux et al., 1999; Mormann et al., 2000; Bhattacharya et al., 2001). Though these studies differ in the exact specification of the null hypothesis, in all cases it corresponds to a system state of no synchronization. In practice this null hypothesis often proves to be too strong (to be too easily rejected), because there is a base level of synchronization which is always present in the system. Therefore the test is not able to distinguish between different system states. Moreover, most of these approaches¹ do not include a theoretical analysis of their test statistic, and calculate critical values based on the method of surrogate data, whose statistic validity (not only in this context) has recently been challenged.²

This chapter presents tests improving this situation in three respects:

- 1) A measure known from the context of directional statistics is used and its simple and defined statistical properties are utilized (see Sec. 3.3).

¹An exception are Mormann et al. (2000), who apply a Rayleigh test for uniformity (cf. Mardia and Jupp, 2000) to the phase difference distribution.

²Surrogate data (cf. Kantz and Schreiber, 1997, Sec. 7.1) have been introduced into nonlinear data analysis by Theiler et al. (1992). They are random data conforming to the null hypothesis of the test, that have been generated by processing the original time series. The classic and still most widely used method is that of phase randomization in the frequency domain (FT-based surrogates) that generates data according to the null hypothesis of a circular (with respect to the time variable), linear, Gaussian, stationary random process.

While this null hypothesis seems not to be really adequate in the context of testing for synchronization, recent research by Mammen and Nandi (2004) has led to even more severe objections. Especially for FT-based surrogates they have been able to show that critical values estimated from surrogate data do not asymptotically stabilize. So even though FT-based surrogate data tests are valid (i.e., result in correct rejection probabilities) for circular stationary Gaussian processes, for many test statistics the variance of the estimated critical value is of the same order of magnitude as the variance of the test statistic itself. This means that a surrogate data test may operate essentially on chance level.

- 2) A two-sample approach is used, testing against the null hypothesis that the synchronization strength is the same in the two samples.
- 3) Testing procedures based on proven statistical theory are used. In the non-parametric case, they rely on resampling techniques.

A number of tests is presented that differ in generality and precision, but also in computational complexity. The different tests are graded with respect to their applicability and usefulness in a given situation and their correctness is checked in numerical simulations.

In contrast to the other parts of this work, this chapter is not directly aimed at the processing of EEG data. On the one hand, the testing procedures described here are applicable in all fields concerned with statistical analysis of bivariate phase synchronization, regardless of the type of data. On the other hand, in the following chapters the multivariate character of EEG will come into focus, and the statistics that become relevant there and which will be the subject of significance testing will be quantities derived, but different from the bivariate measure \bar{R} and will have different properties. Still, some of the insights and methods that are described in this chapter will be utilized again at later points.³

The two-samples test setup

The mean resultant length (see Sec. 3.3)

$$\bar{R} = \left| \frac{1}{n} \sum_{j=1}^n \exp(i \Delta\phi_j) \right|$$

is a measure of phase synchronization based on a sample $\Delta\phi_j$ of size n ($j = 1 \dots n$) of the phase difference $\Delta\phi = \phi_B - \phi_A$ of two coupled oscillators A and B. It reflects the synchronization strength in a certain state of the system. Since only in special cases it makes sense to compare against a state of unsynchronized behavior, it is necessary to obtain a reference level of synchronization. This is given by a second sample of the phase difference from another state of the same system of two oscillators. For each of the samples $\Delta\phi_{1,j}$, $\Delta\phi_{2,j}$ the value of the measure \bar{R}_1 , \bar{R}_2 is calculated, and the question to be answered by the test is whether the difference of these two values is significant.

The corresponding *null hypothesis* is that the population values of the synchronization measure are equal,

$$H_0 : \varrho_1 = \varrho_2.$$

The test decides if this hypothesis is to be rejected or accepted based on the given information (the samples), and the important part of the test design is to ensure that the probability for erroneous rejection of the null hypothesis, the so-called error of the first kind, does not exceed a chosen value, the *significance level* α of the test.

In the given form the different tests to be presented in the following assume that both samples are of equal size, but they are easily generalized to different sample sizes n_1 and n_2 . Initially, all of the tests assume that the samples consist of independent values, that is they are obtained from independent realizations of the process of phase synchronization. In this way the number of samples is also the number of degrees of freedom inherent in the data (in total $2n$). This is a strong constraint, and so in the last section some of the tests are generalized to the case of partly dependent samples, so that the data from the underlying time series can be fully utilized.

³An earlier version of the work presented in this chapter is being published as Allefeld and Kurths (2004b).

Accuracy and power of the tests

In several respects, the quality of the tests will be judged on theoretical grounds. But in many cases the performance of a test cannot be theoretically deduced. Therefore the tests have been checked in a numerical simulation using random numbers generated according to the wrapped normal distribution with the specified ϱ .⁴ The essential parameter to be calculated is the probability for the rejection of the null hypothesis. If the null hypothesis $\varrho_1 = \varrho_2$ is true, this probability is called *error of the first kind*, which has to be equal to or at least smaller than the significance level. For the general case in which both ϱ s are arbitrarily chosen it is called the *power function*, because the power of the test to recognize a situation not conforming to the null hypothesis corresponds to this probability for $\varrho_1 \neq \varrho_2$.

Figure 4.1 presents the results of the simulations. Two samples of size $n = 100$ from the wrapped normal distribution for the given values of ϱ_1 and ϱ_2 have been generated, the respective test for a significance level of 5% has been performed and the relative frequency of rejection as an estimator of the probability has been calculated in 4000 repetitions. Panel a) shows the rejection probability depending on ϱ with $\varrho_1 = \varrho_2 = \varrho$ (error of the first kind), panel b) depending on ϱ_1 with $\varrho_2 = 0$, and panel c) the same for $\varrho_2 = 0.4$ and $\varrho_2 = 0.8$ (three sections through the two-dimensional power function). Since the scale is much smaller in panel a), the randomness of the probability estimation appears stronger here; the horizontal black lines mark the mean \pm s.d. to be expected from a binomial distribution.⁵

In Fig. 4.1a it can be seen that all of the tests are valid for all values of ϱ in the sense that the chosen significance level is not exceeded (within the accuracy of the simulation). On the other hand, four of the tests show errors that in the vicinity of $\varrho = 0$ lie strongly below α . This leads to a decreased power of these tests for testing against $\varrho_2 = 0$, as can be seen in panel b). For higher values of ϱ_2 , this weakness is no longer relevant; the different lines are almost indistinguishable. What can also be seen in panel c) is that the power of the tests increases (the valley of the power function gets narrower) for those higher values. The following sections will refer to these results in more detail.

4.1 Parametric tests

A direct way to construct a test is to assume that the distribution of $\Delta\phi$ belongs to a certain family which can be described by a small number of parameters, of which the concentration moment ϱ is the most important. This is the approach taken by Mardia in his monographs on directional statistics (Mardia and Jupp, 2000; Mardia, 1972). It is mathematically justified, but it will be seen that its applicability is rather limited.

As has been derived in Sec. 3.3, \bar{R} is asymptotically normally distributed for $\varrho > 0$. Based on the assumption that $\Delta\phi$ follows one of the two standard circular distributions, the moments of the corresponding sampling distributions of \bar{R} can be calculated. For the von Mises distribution $M(\mu, \kappa)$, they are

$$\langle \bar{R} \rangle \cong A(\kappa), \quad n \text{ var}(\bar{R}) \cong 1 - A(\kappa)^2 - \frac{A(\kappa)}{\kappa}$$

⁴For a definition of the wrapped normal distribution, see above Eq. 3.15. It is important to note that except for the parametric test there is nothing in the derivation of the test procedures that relies on the specific properties of this distribution. For the numerical simulation it has been necessary to choose a specific distribution family, and the wrapped normal has been chosen because random numbers are easily obtained and because it can be considered as a typical circular random distribution. Calculations based on the von Mises distribution produced equivalent results.

⁵s.d. = standard deviation

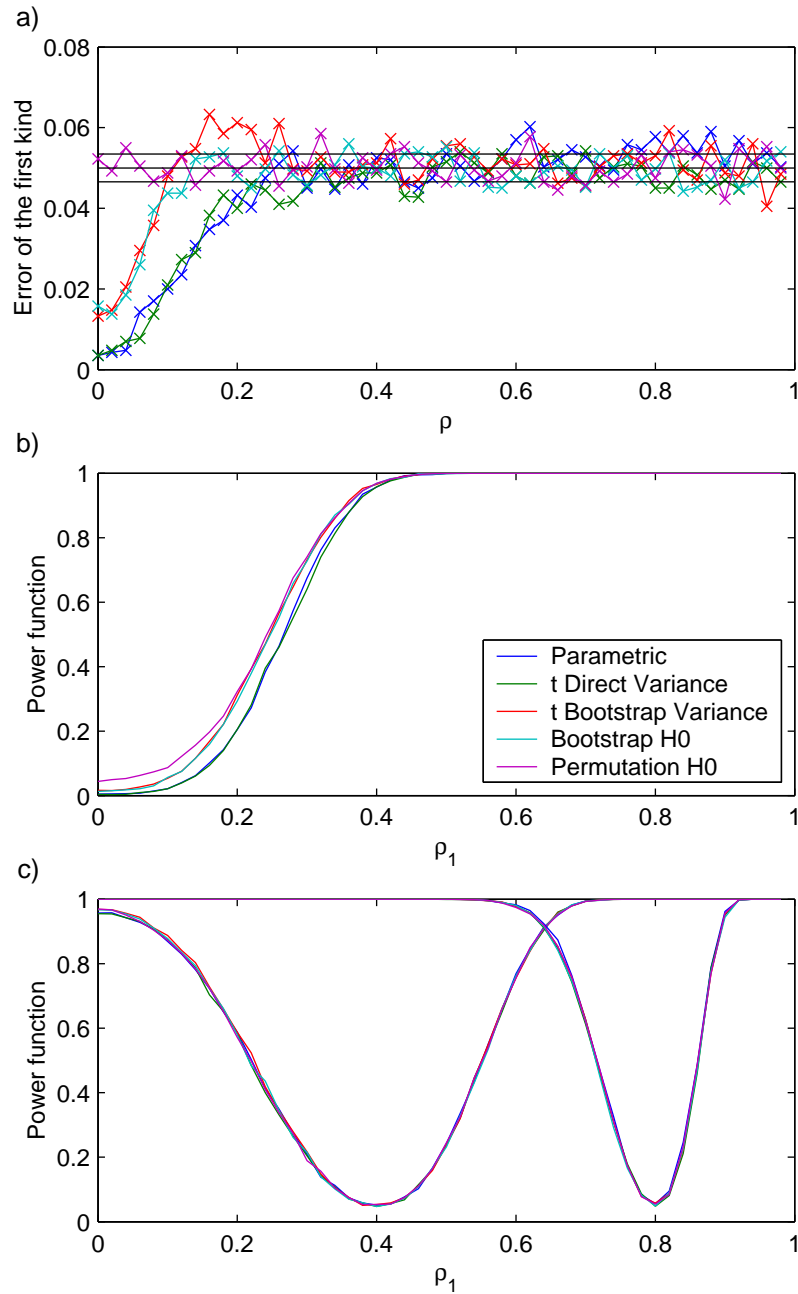


Figure 4.1: Investigation of the properties of the presented tests in a numerical simulation based on wrapped normally distributed samples of size $n = 100$. a) Empirical error of the first kind in samples conforming to the null hypothesis $\varrho_1 = \varrho_2 = \varrho$. b) Power function for testing against a sample with $\varrho_2 = 0$. c) Power functions for testing against a sample with $\varrho_2 = 0.4$ and $\varrho_2 = 0.8$, respectively. Each probability has been estimated based on 4000 simulations of the test for a significance level of $\alpha = 5\%$.

with $A(\kappa) = I_1(\kappa)/I_0(\kappa)$. For the wrapped normal distribution $W(\mu, \sigma)$ holds

$$\langle \bar{R} \rangle \cong \varrho, \quad n \operatorname{var}(\bar{R}) \cong \frac{1}{2}(1 - \varrho^2)^2$$

with $\varrho = \exp(-\frac{1}{2}\sigma^2)$; in both cases, plus terms of order $1/n$.

Following Mardia and Jupp (2000), a *variance-stabilizing transformation* is used to define a suitable test statistic. Such a transformation can be defined for a statistic Z on a sample of a random variable which follows a distribution with a parameter a . The moments of the statistic are functions of this parameter:

$$\langle Z \rangle = f(a) \quad \text{and} \quad n \operatorname{var}(Z) = g(a).$$

Now, if the transformation

$$h(x) = \int_0^x \frac{1}{\sqrt{g(f^{-1}(x))}} dx$$

is applied to the statistic Z , the result is a quantity with an approximately constant variance: $n \operatorname{var}(h(Z)) \cong 1$.

In the case of the statistic \bar{R} on a von Mises or a wrapped normal distribution, the corresponding transformations are

$$h_M(x) = \int_0^{A^{-1}(x)} \sqrt{A'(\kappa)} d\kappa \quad \text{and} \quad h_W(x) = \sqrt{2} \operatorname{artanh} x, \quad (4.1)$$

respectively.⁶ Interestingly, the latter is up to a factor identical to the variance-stabilizing transformation of the linear correlation coefficient, the Fisher Z transform (Sheskin, 1997).

The result of these transformations is now used to perform a test for a significant difference of the synchronization measure in the two samples $\bar{R}_{1,2}$. Under the null hypothesis $\varrho_1 = \varrho_2$ the statistic

$$\sqrt{\frac{n}{2}} (h(\bar{R}_2) - h(\bar{R}_1)) \quad (4.2)$$

follows asymptotically a standard normal distribution. The hypothesis of equal synchronization strength in the two samples has to be rejected if the modulus of this quantity exceeds a certain value, which is given by the quantiles of the normal distribution for a chosen significance level (i.e., a Gauss test is to be performed).

The variance-stabilizing transformation test is applicable if both samples follow the supposed distribution and if the sample size is large enough so that the asymptotic approximation can be applied. An additional restriction follows from the presupposition $\varrho > 0$ in the derivation of the sampling distribution of \bar{R} ; for a finite sample size it is necessary that circa $\varrho_{1,2} > 3/\sqrt{2n}$. For smaller values, the asymptotic distribution assumption as well as the variance estimation implicit in the test are no longer correct. In Fig. 4.1 (blue lines) it can be seen that this leads to a decrease of the error of the first kind below the significance level and a corresponding suboptimal power for testing against $\varrho_2 = 0$. Still, the test seems to be valid in all cases.

To check if the parametric test based on the von Mises or the wrapped normal distribution is applicable to typical phase difference distributions caused by synchronization, they are compared to simulation results from a classic example, two

⁶The first integral can not be written in a closed form, but can be calculated numerically.

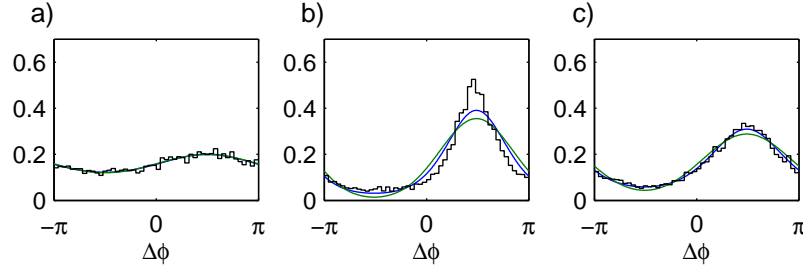


Figure 4.2: Histograms of the phase difference distribution of two coupled Rössler oscillators in a numerical simulation (black), with fitted von Mises (blue) and wrapped normal (green) probability distribution functions. a) Weak coupling $\epsilon = 0.005$. b) Stronger coupling $\epsilon = 0.015$. c) Stronger coupling with additional measurement noise of s.d. 5.

coupled chaotic Rössler oscillators (see Eqs. 2.11):

$$\begin{aligned}\dot{x}_{A,B} &= -\omega_{A,B} y_{A,B} - z_{A,B} + \epsilon(x_{B,A} - x_{A,B}), \\ \dot{y}_{A,B} &= \omega_{A,B} x_{A,B} + a y_{A,B}, \\ \dot{z}_{A,B} &= f + z_{A,B}(x_{A,B} - c),\end{aligned}$$

where $a = 0.15$, $f = 0.2$, $c = 10$, with a small frequency mismatch $\omega_{A,B} = 1 \mp 0.01$. Phases are defined to be $\phi_{A,B} = \arctan y_{A,B}/x_{A,B}$.

Figure 4.2 shows the distribution of the phase difference (which depends on the strength of the coupling ϵ) in a numerical simulation. For a small value of $\epsilon = 0.005$, the resulting distribution may be well described by a fitted von Mises as well as a wrapped normal distribution (a). If the coupling is increased to $\epsilon = 0.015$, the peak of the distribution is sharper than both of the fitted distributions (b). To make the simulation more realistic for empirical data, artificial measurement noise in phase space has been added (two-dimensional normal in the (x, y) -plane with s.d.= 5). As a result, the distribution for the stronger coupling may again be described by a fitted von Mises distribution, but not as well by a wrapped normal distribution (c). It seems that measurement noise may improve the applicability of the standard distributions in phase synchronization systems.

As can be seen from this, there surely are synchronization phase differences which can be described by one of the standard normal distributions, but this is not always the case. Not only that the parametric test may be inapplicable; to be precise, one would have to perform a separate test for goodness of fit in each case. Though the parametric approach of Mardia is elegant and simple, it is therefore necessary to look for a nonparametric means to test for phase synchronization.

4.2 A simple nonparametric test

There is a classic nonparametric approach in statistics which is designed to test for a significant difference of the means of two samples, the t -test. Mean values and variances are calculated from the samples and the difference of the means is divided by the standard deviation of its estimation, resulting in the t statistic. If the sample values are normally distributed, t is distributed according to a Student distribution with $f = 2(n - 1)$ degrees of freedom (Sheskin, 1997).

Formally, it is possible to write the equation for \bar{R} in the form of a mean value:

$$\bar{R} = \frac{1}{n} \sum \cos(\Delta\phi_j - \bar{\theta}) \quad \text{with} \quad \bar{\theta} = \arg \sum \exp(i\Delta\phi_j).$$

Correspondingly the variance of the estimation can be directly calculated:

$$s_{\bar{R}}^2 \cong \frac{1}{n(n-1)} \sum (\cos(\Delta\phi_j - \bar{\theta}) - \bar{R})^2. \quad (4.3)$$

With this, a t -like statistic is defined as

$$t = \frac{\bar{R}_1 - \bar{R}_2}{\sqrt{s_{\bar{R},1}^2 + s_{\bar{R},2}^2}}. \quad (4.4)$$

This approach has two faults: The randomness of the mean direction $\bar{\theta}$ of the phase differences is neglected, which leads to deviations especially for small values of ϱ and therefore inaccuracies in the calculation of the variance $s_{\bar{R}}^2$; and the distribution of $\cos(\Delta\phi_j - \bar{\theta})$ is certainly not normal.

However, the t -test proves to be very robust against deviations from the distribution assumption for large samples, and so one can approximately assume that the given statistic is distributed like a standard t random variable. Based on this, the hypothesis of equal concentration has to be rejected if the modulus of this quantity exceeds a certain value, which is given by the quantiles of the t_f distribution with $f = 2(n-1)$ for a chosen significance level. In this approximation, the test is applicable for a sufficiently large sample size.

The advantage of this approach is that it is generally applicable, but at the expense of theoretical accuracy. Despite of this, in the simulation (Fig. 4.1, green lines) the test proves to have properties very similar to those of the parametric test for the wrapped normal distribution. The tests presented in the following are non-parametric with increasing accuracy, but also increasing computational demands, and so the simple t -test may be an option where precision is not that important.

4.3 Bootstrap techniques

The basis of the two testing approaches presented so far is the theoretical derivation of statistical properties of the used measure. This is also the cause for their limitations, because either the specific distribution of $\Delta\phi$ has to be known or the applied approximations are not generally valid. There is a group of computational techniques introduced by Efron and Tibshirani (1993) under the name *bootstrap* that make it possible to investigate those statistical properties empirically, replacing theory by the use of computer power. In the following some of these techniques will be used, but in a way that additionally includes general theoretical knowledge about \bar{R} to reduce the computational expense.

The basic idea is to generate “bootstrap replications” of the statistic of interest, and to calculate its variance and other properties on the set of these replications. To compute the sampling distribution of the statistic \bar{R} , it is necessary to somehow estimate the underlying distribution of the sample values, the population distribution of the random variable $\Delta\phi$. The best available knowledge about this distribution is the sample $\Delta\phi_j$ itself, and so the best (nonparametric) estimate of the population is a discrete distribution with probability $1/n$ for each of the sample values. To generate new samples according to this estimate, one simply has to draw values from the original sample with replacement. Formally, if k_j ($j = 1 \dots n$) are uniformly distributed independent integer random numbers in the range $1 \dots n$, then $\Delta\phi_{k_j}$ is a bootstrap replication of the sample, and the statistic calculated on this sample is a bootstrap replication of \bar{R} . This technique is called *resampling*.

As a variant of the bootstrap, it is also possible to use a parametric estimate of the distribution of $\Delta\phi$. The parameters of the distribution are estimated from the

sample, and the replications of the sample are taken from random numbers following the distribution with those parameter values. For the present application, this would not be a relevant improvement over the parametric approach explained above; it would increase the complexity of the computations but only marginally improve the accuracy of the test. But the special form of the statistic of interest, \bar{R} , makes it possible to perform a “parametric” bootstrap at an intermediate level. As has been shown in Sec. 3.3, the asymptotic joint distribution of (\bar{C}, \bar{S}) is two-dimensional normal, and the parameters of this distribution depend on the first and second trigonometric moments of the distribution of $\Delta\phi$. This description is an approximation based on the central limit theorem, but it is very good also for relatively small sample sizes (about $n \geq 30$); it is valid for every distribution of $\Delta\phi$ and for all values of ϱ . With this, it is possible to generate parametric bootstrap replications of \bar{R} in a very direct way: The moments⁷ α_1 , α_2 , β_1 , and β_2 are estimated from the sample by the empirical moments, replications of (\bar{C}, \bar{S}) are generated according to the corresponding two-dimensional normal distribution (see Eqs. 3.12), and the replication of \bar{R} is calculated as $\bar{R} = \sqrt{\bar{C}^2 + \bar{S}^2}$. In this way, it is not necessary to generate replications of the sample itself, which drastically reduces the computation time (in calculations performed by the author, up to a factor 40). Such an improvement in speed is especially important if the quantiles of the sampling distribution are to be calculated.

Bootstrap t -test

A very straightforward application of these techniques is to modify the t -test by replacing the direct variance estimation (Eq. 4.3) by the variance estimated from bootstrap replications. About 200 replications are generated for \bar{R}_1 and \bar{R}_2 each, and the variance of these replications is used as $s_{\bar{R},1}^2$ and $s_{\bar{R},2}^2$, respectively, in Eq. 4.4. In this way, the inaccuracy of the direct variance estimation is removed.

The consequence of this becomes visible in the simulation (Fig. 4.1, red lines). The threshold for ϱ below which the error of the first kind is smaller than necessary gets nearer to 0, and therefore the power of the test is increased. But the theoretical objections to the application of the t -test remain valid, and this improved version is still just a low-precision approximation.

Bootstrap H_0 simulation

Another approach is to use the bootstrap techniques to simulate the distribution of the test statistic $|\bar{R}_1 - \bar{R}_2|$ under the null hypothesis. The underlying assumption is that if $\varrho_1 = \varrho_2$, then the distributions of $\Delta\phi_1$ and $\Delta\phi_2$ are also the same. This same distribution gets estimated by the distribution of the *combined sample* $\Delta\phi_{0,k}$, $k = 1 \dots 2n$, where

$$\Delta\phi_{0,k} = \begin{cases} \Delta\phi_{1,k} & \text{for } k \leq n, \\ \Delta\phi_{2,(k-n)} & \text{for } k > n. \end{cases} \quad (4.5)$$

Bootstrap H_0 “replications” for \bar{R}_1 and \bar{R}_2 are generated by resampling or via the “parametric” approach from this combined sample (but with sample size n), and the replication of $|\bar{R}_1 - \bar{R}_2|$ is calculated. About $200/\alpha$ values (4000 for $\alpha = 5\%$) are generated, and the 200th largest of them is used as the rejection threshold of the test. That is, the null hypothesis is to be rejected if the actual value of $|\bar{R}_1 - \bar{R}_2|$ exceeds this threshold.

It is important to see that the generated \bar{R} values are not replications of the value on the original sample, but that they correspond to a distribution according to the null hypothesis, which is simulated by the union of the two samples. The

⁷Not to be confounded with the significance level of the test α .

theoretical basis of this test is much better than that of the bootstrap t -test, because there is no assumption for the distribution of the test statistic, but this distribution is simulated explicitly. However, in the simulation (Fig. 4.1, cyan lines) their performances seem to be essentially the same, and this at a much higher computational expense. Like before, there is a range of small ϱ values for which the error of the first kind is smaller than necessary, decreasing the power of the test. The cause for this is that the bootstrap H_0 simulation is not exact. This is improved in the next section.⁸

The permutation test

According to Efron and Tibshirani (1993), the bootstrap simulation of the null hypothesis distribution of a statistic like $\bar{R}_1 - \bar{R}_2$ is not exact, because the properties of the original sample are not preserved. In the general bootstrap case this cannot be achieved, because to preserve them exactly would make impossible the random variation that is necessary to estimate the sampling distribution. But in the two-samples situation it is possible to introduce random variation and still preserve the statistical properties of the combined sample representing the null hypothesis distribution. The trick is to generate new samples $\Delta\phi_{1,j}$ and $\Delta\phi_{2,j}$ by randomly exchanging sample values between them. That is, the new samples are the first and second half of a random permutation of the combined sample $\Delta\phi_{0,k}$. Formally, if k_ℓ is a random permutation of the integers $1 \dots 2n$, then the “replication” of \bar{R}_1 is calculated on $\Delta\phi_{0,k_\ell}$ with $\ell = 1 \dots n$ and of \bar{R}_2 on $\Delta\phi_{0,k_\ell}$ with $\ell = (n+1) \dots 2n$. The following calculation is the same as for the bootstrap H_0 . Such a testing procedure for the comparison of two samples is called a *permutation test*; it is very similar to the standard bootstrap approach, but is much older than bootstrap theory.⁹

The theoretical accuracy of this test is reflected in the simulation results (Fig. 4.1, magenta lines). The permutation test is the only one that perfectly adheres to the chosen significance level for all values of ϱ . Accordingly, its power for testing against $\varrho_2 = 0$ is the highest of all tests presented, which is especially important for small differences in ϱ . The price of this superior performance is the high computational effort. Since every two simulated samples as well as the sample values in them are not independent of each other because of the permutation underlying their selection, the computation cannot be cut short by the intermediate parametric step introduced above for the bootstrap computations. The permutations have really to be carried out and the replications of the test statistic have to be calculated directly from the generated samples.

4.4 Data from time series

As has been mentioned in the beginning, in the form presented all of the tests presume that the sample values in every sample are independent of each other, and that means they have to be obtained from independent realizations of the process of phase synchronization. The phase difference in a given realization is a function of time, $\Delta\phi(t)$. There are a number of different realizations of the process, $\Delta\phi_j(t)$, $j = 1 \dots n$, and each of the sample values has to be obtained from another realization, typically corresponding to the same time point t_0 : $\Delta\phi_j = \Delta\phi_j(t_0)$. This is

⁸In addition to the tests based on bootstrap variance estimation and H_0 simulation, it is possible to perform a test based on bootstrap confidence intervals. These methods proved to be unreliable in the simulation and therefore have been left out.

⁹See Efron and Tibshirani (1993), Ch. 15. For a practically oriented introduction to permutation tests in many variations, see Good (1994). The proof of exactness of permutation tests can be found in Lehmann (1997).

necessary because in this way the sample size n is also the number of degrees of freedom inherent in the data. If one would use time series data from consecutive time points, the amount of statistical dependency reducing the number of degrees of freedom below the sample size would not be known. In the case of the parametric tests, the simple t -test, and the “parametric” bootstrap tests this number directly enters into the equations, determining the variance of the test statistic.

In the case of the resampling-based version of the bootstrap tests, the situation is slightly different. Here, the aim is to produce replications of the sample that have the same statistical properties as the original. Since resampling works by drawing with replacement, the new sample values are statistically independent, and by making the size of the new samples equal to n , the equivalence is granted. This would no longer work if one simply put partly dependent data into the original samples used for resampling, because the structure of those dependencies would be destroyed in the resampling process.

But there is a version of resampling which takes this into account. If the realization of the process $\Delta\phi_j(t)$ is sampled at certain time points t_m , then the original sample gets a two-dimensional structure: $\Delta\phi_{jm} = \Delta\phi_j(t_m)$. The resampling now has to be performed in a way that does not destroy the dependency structure within the rows (constant j). This is accomplished by simply treating each row as a single vector-valued sample value $\vec{\Delta\phi}_j = (\Delta\phi_{j\bullet})$, and to perform the resampling by drawing from the set of these row vectors in the original sample. The same method can be used to adapt the permutation test to partly dependent data.

In this way, the full information from time series data can be utilized in the test, increasing its power. The number of realizations that is needed to distinguish two states in a test is decreased because of the increased statistical power inherent in each sample value. But it is important to see that one still needs multiple independent realizations of the process; if the sample just contains one vector sample value, there is nothing to resample or to permute.¹⁰

Since in this case the parametric bootstrap can no longer be used but the resampling has actually to be performed, the advantage in terms of computational expense of the bootstrap H_0 simulation versus the permutation test gets lost, and so practically the latter is the method of choice because of its superior accuracy. Eventually, the bootstrap t -test may still be an alternative, if it is known in advance that all ϱ values are sufficiently different from zero.

¹⁰For recent approaches to the adaptation of resampling methods to single-realization time series data, see Härdle et al. (2003).

Chapter 5

Multivariate Phase Synchronization Analysis

The basic form of statistical phase synchronization analysis as it has been introduced in Sec. 3.3 applies only to the bivariate case. Two autonomous oscillators are coupled to each other, and the effect of the coupling is registered in the dynamics of the oscillators' phases, especially in the distribution of their phase difference. EEG data, on the other hand, are essentially multivariate. There is a large number of common electrode sites on the scalp, and unless there is very clear information on the location of the neuronal oscillators relevant in a given experimental context, a reduction of the number of EEG channels taken into consideration for synchronization analysis would be artificial.

The literature on EEG synchronization analysis is characterized by this lack of appropriate methods. Because until now statistical phase synchronization analysis was constrained to the bivariate case, the examination of empirical multivariate data has been accomplished by the simple repeated application of bivariate synchronization measures. For instance, Rodriguez et al. (1999) tested for significant increases and decreases in the strength of phase synchronization between EEG signals obtained in a visual attention task, separately for each pair of electrodes, and displayed the results as colored lines between the sites in a schematic map of the scalp. This approach gives detailed information on the topographic structure of synchronization relations, but it has at least two drawbacks: The visualization can get incomprehensible if a large number of lines has to be drawn, and this analysis in itself gives no information on a common integrating structure that may be present in the data. In the other extreme, Haig et al. (2000) computed an index of global phase synchronization which is meant to indicate synchronization phenomena between all recording sites at once, but fails to give topographic details and effectively destroys much of the information present in the data.

The assessment of synchronization processes in multivariate data requires a genuinely multivariate method of phase synchronization analysis. In this chapter, the author introduces his approach to such a method, that combines the global with the topographically detailed perspective. To this end, the concept of a statistical phase synchronization cluster is introduced and a method to identify this structure in a given data set is derived. In contrast to studies concerning the dynamics and stability of clusters of perfect (phase) synchronization and the coexistence and interaction of multiple clusters (e.g. Osipov and Kurths, 2001), the present chapter tries to describe the form of a single statistical cluster, in which the oscillators participate in different degrees, ranging from no to perfect agreement with the cluster dynamics. The goal is to derive a general structure whose application to empirical

data can be seen as a generic multivariate analysis in the field of phase synchronization.¹

5.1 Synchronization cluster analysis

In statistical phase synchronization analysis, the relevant information is given by the phase ϕ_{ik} of the N oscillators $i = 1 \dots N$ in a number of realizations $k = 1 \dots n$ of the stochastic process that is considered. The strength of synchronization between each two oscillators i and j can be quantified by the measure introduced in Sec. 3.3:

$$\bar{R}_{ij} = \left| \frac{1}{n} \sum_k \exp(i(\phi_{jk} - \phi_{ik})) \right|. \quad (5.1)$$

The objective of multivariate phase synchronization analysis is to derive from this matrix (\bar{R}_{ij}) of bivariate indices some information about the synchronization state of the whole of N oscillators.

In the following, the approach of *synchronization cluster analysis* will be presented in three steps. The general definition of a synchronization cluster is followed by its concretization in a specific dynamical model, which in turn motivates a generally applicable method of data analysis. Each step does not directly derive from the preceding, but introduces a significant modification.

The concept of a synchronization cluster

The basic idea is to conceive of the oscillators as constituting a cluster in which they participate in different degrees c_i . The cluster consists of a common rhythm, a mean of the oscillations of the single oscillators, and it is described by the dynamics of a cluster phase.

In each realization, this *reference phase of the cluster* is defined as a circular weighted mean of the oscillator phases,

$$\Phi_k = \arg \sum_j c_j \exp(i\phi_{jk}), \quad (5.2)$$

while the *participation indices* c_i are calculated as a (monotonously increasing) function of the synchronization strength between an oscillator and the cluster,

$$c_i = f(\bar{R}_{iC}) \quad \text{with} \quad \bar{R}_{iC} = \left| \frac{1}{n} \sum_k \exp(i(\phi_{ik} - \Phi_k)) \right|. \quad (5.3)$$

In this way, the participation index quantifies both how close an oscillator follows the common rhythm as well as how important it is in its contribution to the cluster.

A self-consistent solution of this set of equations would represent a synchronization cluster analysis of the given data set ϕ_{ik} . A problem for this ansatz is that while the definition of the cluster phase Φ is quite straightforward, it is not obvious which function f should be chosen for the relation between the \bar{R}_{iC} and the c_i .

A dynamical perspective

To fill this gap, a look at the process leading to the formation of a synchronization cluster may be helpful. The model given below does not maintain the generality of

¹An earlier version of the work presented in this chapter is being published as Allefeld and Kurths (2004a).

the first approach, but clarifies the dynamical meaning of the statistical quantities introduced above. This concretization will also lead to a modification of the given ansatz.

The model consists of an ensemble of *coupled noisy phase oscillators*,

$$\dot{\phi}_i = \omega_0 + \sum_j k_{ij} \sin(\phi_j - \phi_i) + \xi_i, \quad (5.4)$$

where the coupling coefficients can be written as a product, $k_{ij} = c_i c_j$. It can be seen as a generalization of the von Mises process (Eq. 3.14).² The ξ_i are taken to be mutually independent Gaussian white noises with the same variance, normalized to unity by an appropriate choice of the time unit. Because the coupling matrix factorizes, the differential equations can be decoupled by a *mean field* approach such that

$$\dot{\phi}_i = \omega_0 + c_i \mathcal{M} \sin(\Phi - \phi_i) + \xi_i,$$

where

$$\mathcal{M} = \left| \sum_j c_j \exp(i\phi_j) \right| \quad \text{and} \quad \Phi = \arg \sum_j c_j \exp(i\phi_j) \quad (5.5)$$

are the amplitude and the phase of the mean field, respectively. By this transformation, the coupling between oscillators has been formally replaced by a coupling to the mean field. If the number of oscillators is large enough and the system is in its stationary state, the mean field is approximately independent of the dynamics of the individual oscillators, and so it can be treated as a common external driving with a constant amplitude $\mathcal{M} = \langle \mathcal{M} \rangle$.

The phase of the mean field Φ can be eliminated from the equations by looking at the phase difference between an oscillator and the mean field, $\Delta\phi_i = \phi_i - \Phi$. Its dynamics obtains the form

$$\Delta\dot{\phi}_i = -c_i \mathcal{M} \sin(\Delta\phi_i) + \xi_i.$$

That means that the multivariate generalization of the von Mises process given above can be reduced to a number of one-dimensional von Mises processes independent of each other. The stationary distribution resulting from this dynamics is a von Mises distribution, $\Delta\phi_i \sim \mathcal{M}(0, 2c_i\mathcal{M})$, and the corresponding population value of the oscillator-mean field synchronization strength is

$$\varrho_{iC} = |\langle \exp(i\Delta\phi_i) \rangle| = A(2c_i\mathcal{M}) \quad \text{with} \quad A(\kappa) = I_1(\kappa)/I_0(\kappa).$$

Since this derivation assumes that the system reaches a stationary state, its prediction has been checked in numerical simulations of the model system (Eq. 5.4). One of the results is shown in Fig. 5.1, demonstrating that theoretical and empirical distributions of the $\Delta\phi_i$ agree well with each other.

The parts of this dynamical model can be easily identified with those of the original approach. The synchronization cluster corresponds to the mean field, which effectively rules the dynamics of the individual oscillators, and the cluster phase Φ_k is a realization of the phase of the mean field Φ . The ‘‘participation’’ of an oscillator in the cluster is given by the coefficient c_i , which specifies its contribution as well as its coupling to the mean field. And the oscillator-cluster synchronization strength \bar{R}_{iC} is an empirical estimator of ϱ_{iC} , which depends on the participation index.

²It can also be related to the well-known Kuramoto model (Kuramoto, 1984; Strogatz, 2000). The differences are: The strength of the coupling between two oscillators k_{ij} is not the same for each pair of oscillators, but has the form of a factorizable matrix. The natural frequencies of the oscillators are identical. And, replacing this source of incoherence, the dynamics has been complemented by a stochastic part.

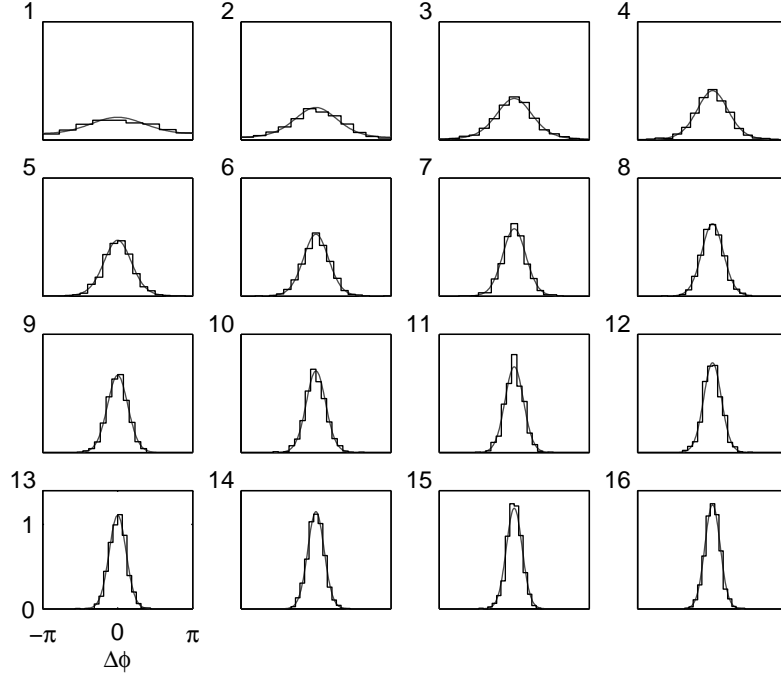


Figure 5.1: Results of a numerical simulation of the model system (Eq. 5.4) with $N = 16$ and $c_i = 0.05 i$. Each plot corresponds to the oscillator whose index i is given at the upper left corner. Histograms (black lines) show the distributions of the $\Delta\phi_i$ after $t = 20$ (starting from random initial conditions) in 1000 independent realizations of the process. They are in good agreement with the theoretical distributions (gray lines).

As a modification of the original concept of a synchronization cluster, the relation between c_i and q_{iC} is not a simple function, but additionally depends on the amplitude of the mean field \mathcal{M} , whose value in the stationary state is a result of the couplings of all oscillators in the cluster to each other. Because of the form of \mathcal{M} as a weighted sum it can be used to define a normalized index of the overall cluster strength

$$r_{\text{Cluster}} = \frac{1}{\sum |c_j|} \mathcal{M} = \left| \frac{1}{\sum |c_j|} \sum_j c_j \exp(i \phi_j) \right|$$

(values from 0 to 1), which can be seen as a generalization of the global synchronization index $r_{\text{Global}} = \left| \frac{1}{N} \sum \exp(i \phi_j) \right|$ used by Haig et al. (2000). Its expectation value can be expressed as a weighted mean of the q_{iC} :

$$\langle r_{\text{Cluster}} \rangle = \frac{1}{\sum |c_j|} \sum_j |c_j| q_{jC}.$$

The data analysis algorithm

The dynamic approach did not lead to a simple specification of the function f , and the first definition of the cluster phase (Eq. 5.2) is only in a specific model identical to the phase of the mean field (Eq. 5.5). But the dynamical perspective enables us to modify the idea of synchronization cluster analysis in a way that is much more generally applicable. It is based on another theoretical observation. For the

population values of the bivariate synchronization indices \bar{R}_{ij} holds

$$\varrho_{ij} = |\langle \exp(i(\phi_j - \phi_i)) \rangle| = |\langle \exp(i(\Delta\phi_j - \Delta\phi_i)) \rangle|.$$

If in the given dynamics it is possible to introduce in some specific way a mean field, then the dynamics of the phase differences are decoupled. If additionally each oscillator is driven by noise independent of that acting on the other oscillators, then $\Delta\phi_i$ and $\Delta\phi_j$ become independent random variables, and so

$$\varrho_{ij} = |\langle \exp(i\Delta\phi_j) \rangle| |\langle \exp(-i\Delta\phi_i) \rangle| = \varrho_{iC} \varrho_{jC} \quad \text{for } i \neq j \quad (\varrho_{ii} = 1),$$

that is, the synchronization matrix (apart from the diagonal) factorizes.

This leads to a version of synchronization cluster analysis in which the quantity to be estimated from the data is no longer the participation index c_i , which depends on the specific dynamics, but the strength of the synchronization between an oscillator and the cluster ϱ_{iC} . Like c_i , this quantity is a measure of the degree of participation of the oscillator in the cluster.

The corresponding algorithm is as follows: \bar{R}_{ij} is an empirical estimate of $\varrho_{ij} = \varrho_{iC} \varrho_{jC}$ which is asymptotically normally distributed (see Sec. 3.3), $\bar{R}_{ij} \sim N(\varrho_{ij}, \sigma_{ij}^2)$. A maximum likelihood estimation of the ϱ_{iC} then reduces to minimizing the sum of square weighted errors

$$\sum_{i,j>i} E_{ij}^2 \quad \text{with} \quad E_{ij} = \frac{\bar{R}_{ij} - \varrho_{iC} \varrho_{jC}}{\sigma_{ij}},$$

where

$$\sigma_{ij} = \frac{1}{\sqrt{2n}} (1 - \varrho_{iC}^2 \varrho_{jC}^2)$$

is based on the assumption that due to the central limit theorem the difference of two independent circular random variables can in sufficiently good approximation be described by a wrapped normal distribution. The residual errors can then be used to check whether the model may be applied to the given data set. In the following, the estimate of ϱ_{iC} based on this algorithm will be denoted by \bar{R}_{iC} .

In this form, synchronization cluster analysis is independent of most of the details of the dynamical model used for its motivation. The basic premises that are relevant to this approach are that the dynamics of the oscillators can be decoupled by introducing a mean field and that its stochastic part is independent for each of them. In this sense, the factorization of the matrix of bivariate synchronization indices \bar{R}_{ij} by estimating the synchronization strengths to the cluster ϱ_{iC} can be regarded as the generic multivariate phase synchronization analysis aimed at in the beginning. This does not mean that it is necessarily applicable to every data set, since there still are specific assumptions. But even in cases where the applied structure is not perfectly adequate, it may serve as a first approximation and specific deviations from the applied model may be detected by large values of the residual errors E_{ij} . Another favorable characteristic of this analysis is that its result maintains a direct relation to the bivariate synchronization indices: An approximation of the synchronization strength between two oscillators \bar{R}_{ij} is given by the product of the estimates of the synchronization strengths to the cluster $\bar{R}_{iC} \bar{R}_{jC}$. In the following we will see that the method can be successfully applied to EEG data.

5.2 Application to ERP data

To obtain data to check the applicability of the method described in the last section, a test experiment was performed. Though the main aim of this work is to

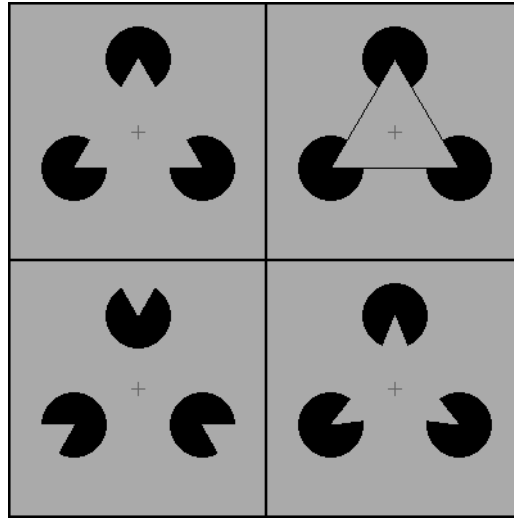


Figure 5.2: The stimuli: Kanizsa, Triangle, Non-Triangle, and Target. The cross at the center is used to suppress eye movements. The first three stimuli define the experimental conditions.

analyze ERPs in language processing, for reasons of simplicity and robustness of the effects a visual attention experiment following Tallon-Baudry et al. (1996) was chosen for this purpose. In this experiment, four different stimuli (Fig. 5.2) were presented on a computer screen. The stimuli corresponding to experimental conditions consisted of a Kanizsa triangle with an illusory contour (“Kanizsa”; cf. Kanizsa, 1976), a similar shape with triangle edges drawn (“Triangle”), and a shape consisting of the same parts as the Kanizsa without forming an illusory contour (“Non-Triangle”). The task of the subject was to count silently the number of occurrences per experimental block of the fourth stimulus (“Target”, a variant of the Kanizsa), to ensure that he/she remained attentive. The idea of this experimental setup is that the perception of a Kanizsa figure, consisting of three elements that are non-contiguous but that belong together and define a virtual triangle-shaped contour, requires an increased effort of visual binding (see Ch. 1).

Data was obtained from one female subject of 23 years, right-handed and with normal vision. Stimuli were presented in a randomized order for 700 ms with a random interstimulus interval of 2–3 s. There were eight blocks of 90 stimulus presentations each. EEG was recorded with a sampling rate of 500 Hz at 30 electrodes (see Fig. 5.6, rightmost panel) and artifact-free epochs (Sec. 2.2) from –300 ms to 650 ms relative to the stimulus presentation were selected for processing. The scalp current density estimation procedure described in Sec. 3.1 was applied and frequency-specific instantaneous phases $\phi(t, f)$ were calculated by the Morlet wavelet method with $\eta = 10$ (Sec. 3.2).³ The resulting data were reduced to epochs from –150 ms to 500 ms to remove boundary effects.

For each experimental condition, frequency, and time instant separately, the phases ϕ_{ik} at an electrode i in a trial k were taken as input to the procedures of phase synchronization analysis described above. That is to say, the electrodes were assumed to represent autonomous oscillators and the epochs were treated as realizations of the process.

Though the synchronization cluster analysis reduces an $N \times N$ matrix to a vector with N elements, in combination with the variation of time, frequency, and

³In this section and the following chapter that are describing experimental results, frequencies will be given as $f = \omega/2\pi$ instead of the angular frequency ω .

experimental condition there is still a very large amount of information to be assessed. This can be reduced by selecting a specific frequency (see below), but because there is no prior information one first needs to get an overview of the processes in the different frequency bands. For this purpose, three measures of the *overall synchronization strength* were calculated for each frequency and time instant:

- 1) The *bivariate mean*, the mean of the bivariate synchronization indices for all pairs of electrodes,

$$\frac{2}{N(N-1)} \sum_{i,j>i} \bar{R}_{ij}, \quad (5.6)$$

- 2) the *threshold ratio*, that is the ratio of electrode pairs with an \bar{R}_{ij} whose t -statistic difference from the value at -150 ms exceeds a certain threshold, corresponding to a significance test at a level of 5% (see Sec. 4.2), and
- 3) an estimate of the expectation value of the *cluster strength*:

$$\frac{1}{\sum_j A^{-1}(\bar{R}_{jC})} \sum_j A^{-1}(\bar{R}_{jC}) \bar{R}_{jC}. \quad (5.7)$$

These quantities can be conveniently displayed in time-frequency plots.

The results for the Kanizsa condition are shown in Fig. 5.3. All of the quantities reveal two distinct increases in synchronization related to the stimulus presentation, one below 10 Hz with a latency of 100–200 ms, and a second one around 13 Hz and a latency of about 300 ms. Interestingly, there seem to be no synchronization effects in the higher frequency bands. The increased values of bivariate mean and cluster strength around 50 Hz are a result of a direct influence of the power line onto the EEG voltage recordings; this effect disappears in the threshold ratio which describes the difference to the prestimulus level.

For a more detailed examination of the analysis results, the author chose the band around 13 Hz of the higher-frequency response. Since the cluster analysis delivers indices \bar{R}_{jC} attributed to the electrodes, their values can be displayed in a conventional scalp map to give an easily apprehensible representation of the topographic information obtained. Figure 5.4 shows the time evolution of the synchronization topography for the Kanizsa condition. The emergence of the synchronization cluster around 150 ms can clearly be seen. Its distribution seems to be almost constant until its disappearance at 450 ms and involves mainly parietal as well as right frontotemporal areas, with a maximum in the left parietal region.

Figure 5.5 shows a comparison of the overall measures in the three different experimental conditions. All the measures indicate that there is a difference between the Kanizsa condition and the two other conditions. A bootstrap-based⁴ statistical analysis of the threshold ratio at 300 ms shows strong significance $p = 0.007$ for the difference between Kanizsa and Triangle and standard significance $p = 0.05$ for the difference between Kanizsa and Non-Triangle conditions; for the other two measures the statistical differences are weaker. Disregarding scaling, the information given by bivariate mean and cluster strength seems to be almost the same. This suggests that the generic analysis giving the \bar{R}_{jC} should not be complemented by the cluster strength, that relies on further details of the dynamical model, but by the seemingly equivalent bivariate mean. The threshold ratio gives a slightly different time structure; because of its definition, there is no apparent difference between conditions in the prestimulus interval (and even until 200 ms poststimulus).

⁴Variances of the measures were calculated for each condition separately by generating bootstrap replications of the set of epochs (cf. Efron and Tibshirani, 1993), and p -values corresponding to a t -test were computed.

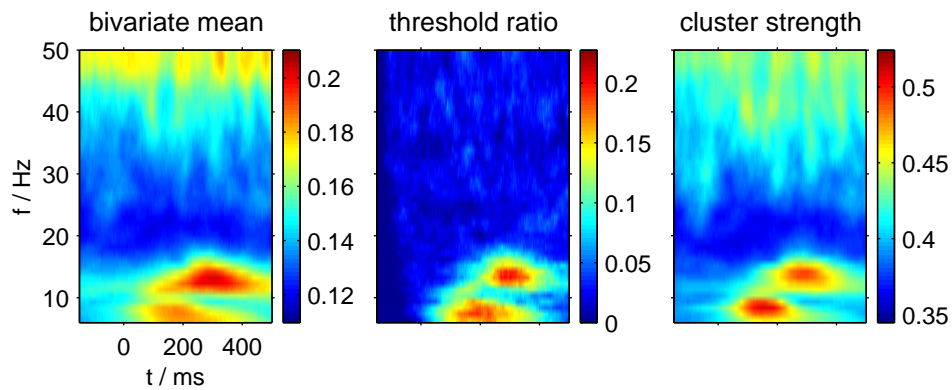


Figure 5.3: Time-frequency plots for the Kanizsa condition of the three measures of the overall synchronization state: bivariate mean, threshold ratio, and cluster strength (see text for definitions). All three measures show a similar pattern of increased synchronization related to the stimulus presentation.

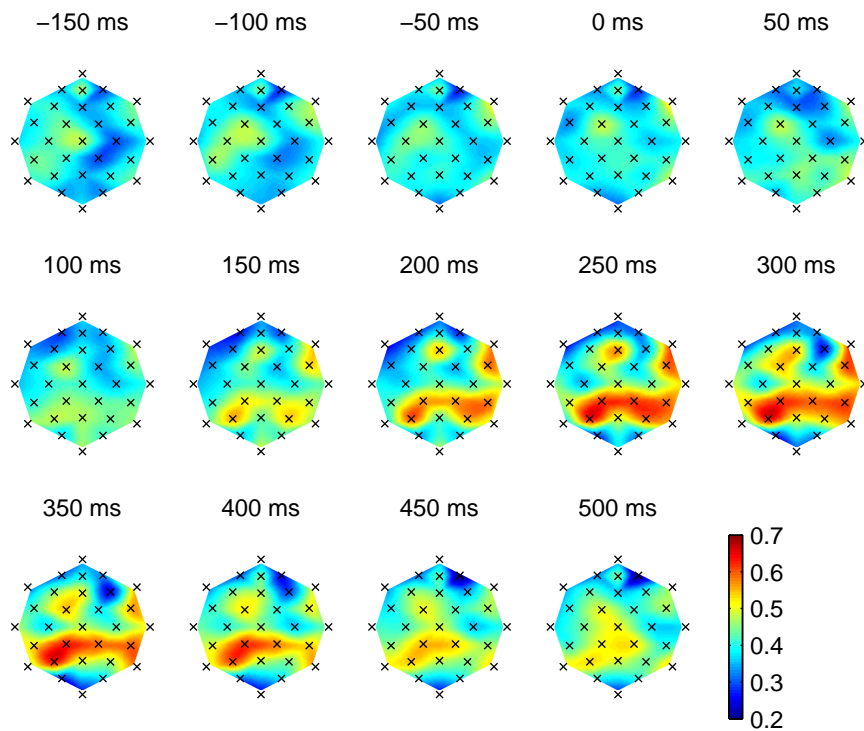


Figure 5.4: Time evolution of the cluster synchronization topography at $f = 13$ Hz for the Kanizsa condition. The continuous colors correspond to an interpolation of the \bar{R}_{IC} -values attributed to the electrodes, whose positions are marked by \times -symbols. For a chart of the electrode names, see Fig. 5.6.

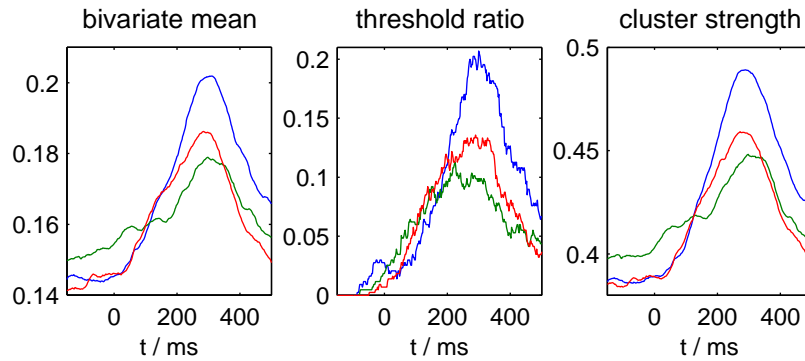


Figure 5.5: Comparison of the time courses at $f = 13$ Hz of the measures of overall synchronization, bivariate mean, threshold ratio, and cluster strength, for the three experimental conditions: Kanizsa (blue), Triangle (green), and Non-Triangle (red).

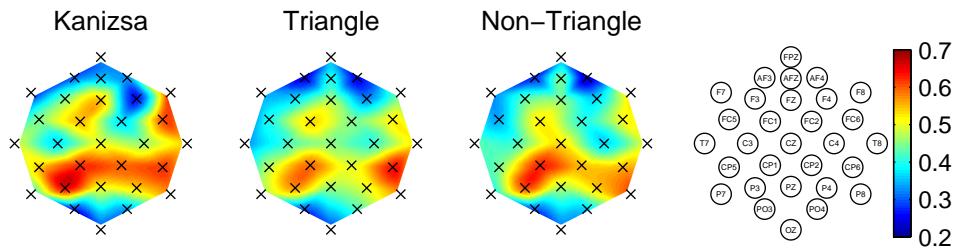


Figure 5.6: Comparison of the synchronization topography at $f = 13$ Hz and $t = 300$ ms for the experimental conditions. The rightmost panel gives the MCN names (Sec. 2.1) of the electrodes included in the recording.

The different synchronization clusters in the three conditions at 300 ms are shown in Fig. 5.6. The basic topography seems to be the same in all conditions, with overall higher values in the Kanizsa condition. The corresponding residual errors E_{ij} are between -0.32 and 0.58 s.d.; these small values show that there is a basic agreement between the assumptions underlying the analysis and the empirical data.

These results indicate that the approach to multivariate phase synchronization analysis introduced in this chapter can be successfully applied to ERP data. Since the main purpose of the experiment was to provide a test case for the method, the results shall only briefly be interpreted in relation to neuronal processes: The mainly parietal distribution of the observed cluster fits in nicely with the location of visual areas in the backmost part of the brain. The different strengths of overall synchronization in the conditions can be understood in such a way, that the perception of the Kanizsa triangle *requires* increased synchronization related to visual binding—in contrast to the triangle with physically present edges—and allows binding to be *successful*—in contrast to the Non-Triangle, where no virtual contour can be constructed.

While the focus of this chapter has still been on methodology, the next chapter will present the main empirical results on language processing.

Chapter 6

A Language Processing Experiment

In the preceding chapters, the theoretical and methodical foundations of phase synchronization analysis have been described and methodical contributions to this field have been presented, including a first test application of these methods to EEG data. In this final chapter of the thesis, its main empirical aim comes into focus: the investigation of synchronization processes related to language processing.

The first ERP effect that has been specifically associated with language comprehension was found by Kutas and Hillyard (1980b); it is the N400 component that has already been briefly described in Sec. 2.2. The N400 consists of a negativity in the ERP average that occurs about 400 ms after the presentation of a word stimulus that is inappropriate in the given semantic context. Kutas and Hillyard presented English sentences to their subjects in which the last word, a noun, was either semantically inappropriate, physically deviant, or both (see Fig. 2.8). By this design they were able to show that the response to a semantic deviation, the N400, is clearly distinct from the effect of an otherwise unexpected stimulus, a positivity that is usually called P300. The physical variation in their experiment, the use of a larger font size, elicited a late positive complex that was called “P560” by the authors.¹

Since these early findings, a number of other ERP components has been identified that provide information on different aspects of language processing. Friederici (1995, 2002) discusses them in the context of a three-stage model of language comprehension. The first phase results in an initial syntactic structure that is based on word category information only. This process is reflected in an early left anterior negativity (ELAN) about 200 ms after stimulus presentation. After the full lexical information has become available, in the second phase semantic information (corresponding to the N400) as well as the syntactic properties of the words are processed, the latter being reflected in a left anterior negativity (LAN) that also occurs around 400 ms. Finally, in the third phase syntactic and semantic aspects are mapped onto each other. If this integration fails, syntactic reanalysis or repair is induced, eliciting a late centroparietal positivity (called P600).

Irrespective of the substantial progress in the neurophysiological investigation of language processing that has been made in the last two decades, resulting in detailed models like that of Friederici briefly sketched above, the findings of Kutas and Hillyard are still of central importance. The N400 is one of the best known and reliably reproduced language-related ERP components. Because of this, for the purposes of this thesis the classic study of Kutas and Hillyard (1980b) was

¹For a detailed discussion of their findings, see also Kutas and Hillyard (1980a).

replicated, to provide a basis for a first exploration of neuronal synchronization processes in language comprehension. Their experiment was modified insofar as the physical variation consisted in a change of the font color instead of the font size, and the sentences were in German. Nonetheless the basic experimental design was the same and as we will see, the findings of Kutas and Hillyard have been reproduced.

6.1 Experimental setup and analysis

In the experiment,² German language sentences of the form “Der Priester wurde geholt.” (“The priest was called.”) were visually presented word-by-word to the subject on a computer screen. In these sentences the terminal verb either made sense, or it did not, and the verb was either presented in the same color as the beginning of the sentence (green or red), or in the other color. The combination of these two variations defines the four experimental conditions. After each sentence a probe word was presented. By this, the subject was prompted to indicate by a button press if this word occurred in the preceding sentence in the same way, including color. The purpose of this was to check if the sentence had been perceived correctly.

The conditions of the experiment are:

- 1) the *control* condition,
- 2) the *semantic incongruity* condition,
- 3) the *physical mismatch* condition, and
- 4) the *combined* condition.

Figure 6.1 shows sample trials belonging to the four conditions. In (1) the sentence is completed by the verb “geholt”, which makes sense. In (2) this is substituted by the verb “asphaltiert”. This verb would make sense in another sentence, “Die Straße wurde asphaltiert.” (“The road was asphalted.”), but not here; in this context the verb is semantically incongruent. In both (1) and (2), the whole sentence is shown in a uniform color. The sentence in (3) is identical to that of (1), but here the beginning is shown in green, while the verb is in red color; thus the verb is physically mismatching. In (4) both manipulations are combined: the sentence contains an inappropriate verb and it is colored differently. The last column of Fig. 6.1 shows sample probe words; in (1) and (2) the subject should answer “did occur”, in (3) and (4), “did not occur”.

The language material (see App. A) used in the experiment consisted of 52 pairs of sentences. They were chosen such that by exchanging the terminal verbs in each pair a semantic incongruity is generated. Each of the 4 resulting sentences was shown in matching and mismatching colors, such that there were 416 different trials in total, 104 of them for each condition. The trials were presented in a randomized order, divided into eight blocks of 52 trials each. To familiarize the subject with the experimental procedure, there were two warm-up blocks of 12 trials each.

In a trial, a warning stimulus “x x x x” was presented for 500 ms followed by 300 ms with a blanked screen. The words of the sentence were presented for 400 ms each, with 100 ms in between. After the verb a pause of 800 ms was interposed, followed by the presentation of the probe word. Then the subject had 3.5 s to give an answer. The screen was blanked for 1 s before the next trial started.

²The experimental setup and language material were adopted in a modified form from Friederici et al. (1999). Special care was taken to achieve a balanced design to rule out alternative explanations of the effects.

1	x x x x x	Der Priester wurde geholt.*	geholt
2	x x x x x	Der Priester wurde asphaltiert.†	asphaltiert
3	x x x x x	Der Priester wurde geholt.	Priester
4	x x x x x	Der Priester wurde asphaltiert.	asphaltiert

*The priest was called.

†The priest was asphalted.

Figure 6.1: Sample trials illustrating the four experimental conditions of the experiment, including its warning (second column), sentence (third column), and probe word (fourth column) parts.

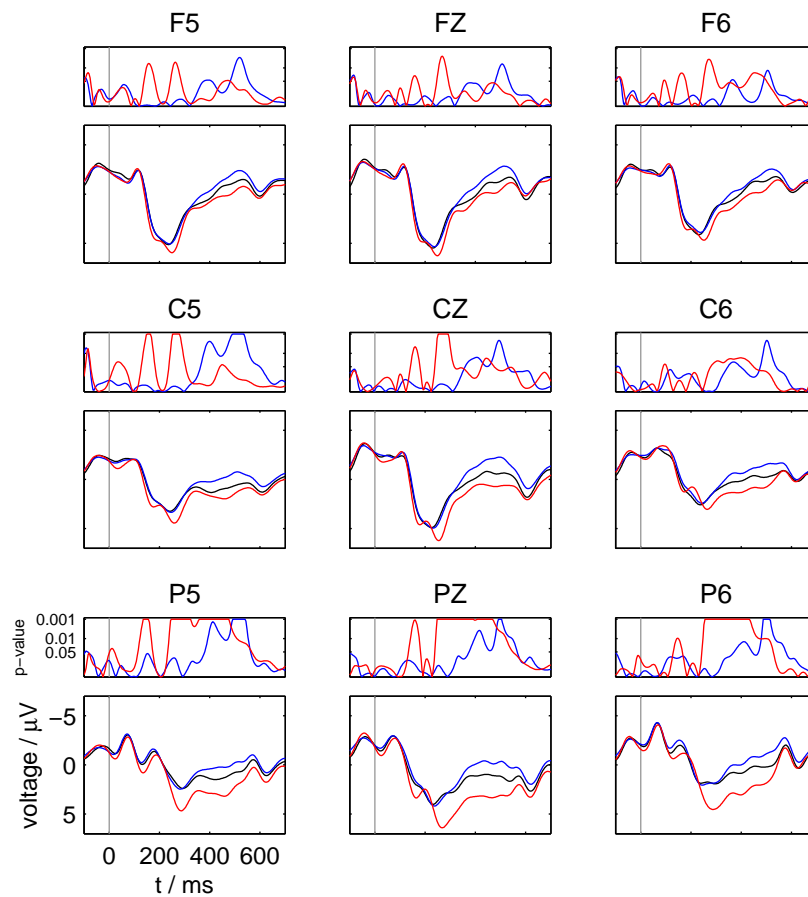


Figure 6.2: Average ERPs at nine electrodes, displayed in their topographic arrangement. The lower panels show the average ERPs (mean over subjects) for the control (black), semantic incongruity (blue), and physical mismatch (red) conditions. In the upper panels, p -values of the statistical difference between an experimental condition and the control condition are plotted (in corresponding colors), calculated with respect to a pointwise two-sided paired t -test (over subjects). Averages were filtered with a low-pass at 10 Hz and baseline-corrected (300 ms prestimulus).

The experiment was performed with 16 subjects. They were right-handers, university students, and grown up monolingually (German). The subjects differed in gender (male / female) and reading span³ (low: 2.5–3 / high: 4–6); for each combination there were four subjects. They were between 20 and 27 years old, and had normal or corrected to normal vision.

EEG was recorded with a sampling rate of 250 Hz from 59 scalp electrodes. After application of the spherical spline Laplacian algorithm (Sec. 3.1), out of these 27 electrodes were selected for the analysis to further diminish the likelihood of spurious correlations (for an electrode chart, see Fig. 6.6d). For those trials in which the subject had given the correct response to the probe word, artifact-free epochs from –600 to 1300 ms relative to the presentation of the critical item (the verb closing the sentence) were selected for processing, resulting in 85 to 103 epochs per condition and subject. To determine frequency-specific instantaneous phases, the Morlet wavelet transform (Sec. 3.2) was used with $\eta = 7$. The phase data were reduced to shorter epochs before further processing to remove boundary effects.

For each subject, experimental condition, frequency, and time instant separately, the phases ϕ_{ik} at an electrode i of an epoch k were taken as input for the phase synchronization analysis. The results for the single subjects were aggregated by calculating the mean over subjects for one condition, or measures of the statistical difference between two conditions based on the variance over subjects.

To check if the replication actually reproduced the results of Kutas and Hillyard (1980b), ERP averages were computed. Figure 6.2 shows the results for nine electrodes. As expected, the semantic incongruity elicited a negativity from 300 to 500 ms relative to the stimulus presentation, the known N400 component. It is broadly distributed but seems to be strongest in the left parietal area (electrode P5). Distinct from this, the effect of the physical mismatch was found to be a long lasting P300-like positivity (250–550 ms) that appears to be strongest in the parietal region (electrode PZ). Though the morphology of this effect (with a peak latency of about 300 ms) seems to be different from the “P560” found by Kutas and Hillyard (see Fig. 2.8), such a variation was to be expected because of the different implementation of the physical mismatch (color instead of font size). The fundamental finding of Kutas and Hillyard was reproduced, namely that a semantic incongruity elicits an N400 component that is clearly different from the effect of a comparable manipulation regarding the physical properties of the stimulus.

6.2 Results

To get a first overview of the different frequency bands, it is useful to look at time-frequency plots of measures of overall synchronization. The following two indices were computed:

- 1) The *bivariate mean*

$$\frac{2}{N(N-1)} \sum_{i,j>i} \bar{R}_{ij}, \quad (6.1)$$

introduced in Sec. 5.2, and

- 2) the *cluster mean*, the mean of the indices of oscillator-cluster synchronization strength (Sec. 5.1),

$$\frac{1}{N} \sum_i \bar{R}_{iC}. \quad (6.2)$$

³The “reading span” (Daneman and Carpenter, 1980) is a measure of a subject’s reading-related memory capacity.

The purpose of the latter measure is to obtain information on the overall synchronization state that is directly linked to the topographic data resulting from the synchronization cluster analysis (see below). In contrast to the index of cluster strength used before (Eq. 5.7), its definition does not include any specific features of the dynamical model of a synchronization cluster. We will see that bivariate and cluster mean give very similar results, which provides further evidence that the cluster analysis algorithm preserves the information given by the bivariate synchronization matrix \bar{R}_{ij} .

Figure 6.3 displays the results for the control condition. For both measures, the time-frequency plot gives a similar pattern: At low frequencies (below circa 4 Hz) there is a relatively strong sustained synchronization. It seems to slightly increase in response to the stimulus but has a base level that is apparently not related to stimulus presentation. This is supplemented by a transient increase in overall synchronization around 100–300 ms that extends up to circa 10 Hz. There is also an increased synchronization level in the prestimulus interval for frequencies around 10 Hz that disappears about 300 ms after presentation.

The evolution of the cluster topography (described by the index of participation \bar{R}_{iC}) corresponding to these processes is shown in Fig. 6.4 for two selected frequencies. At 6 Hz there is a pronounced transient increase of synchronization elicited by the stimulus. In the evolution of the topography over time (panel a) this appears as an increased left parieto-occipital participation at circa 120–300 ms. Additionally, there seems to be an increased right frontotemporal synchronization in the time window 480–660 ms that can not be observed in the overall measure, followed by a return to the prestimulus level. The topographies corresponding to the stimulus-related desynchronization at 10 Hz are shown in Fig. 6.4b. The higher participation in the left and right parieto-occipital areas found in the prestimulus interval is further enhanced by the stimulus until 180 ms, but is then followed by a short transient desynchronization (around 420 ms) in the left and a sustained desynchronization in the right area.

These plots for the control condition give a first insight into the frequencies and the time structure of synchronization processes, but there are no distinct events at specific time-frequency locations comparable to those found for the Kanizsa experiment presented in the previous chapter. In addition, from the viewpoint of cognitive science the relevant information is concerning differences between conditions (see Sec. 2.2). The time-frequency plots of Fig. 6.5 represent the statistical difference between the semantic incongruity and physical mismatch conditions, respectively, and the control condition. Taking the threshold corresponding to a two-sided t -test (over subjects, at a level of 1%) as an indicator of the relevant time windows and frequency bands, with respect to the bivariate mean there are three prominent effects related to the experimental manipulations:

- 1) The semantic incongruity condition exhibits a *decrease* of synchronization at 90–280 ms and 5.7–7 Hz.
- 2) The physical mismatch condition shows an *increase* of synchronization at 0–250 ms and 4–6.3 Hz as well as
- 3) a second *increase* at 120–270 ms and 8.3–12 Hz.

The effects for the cluster mean are almost identical.

To determine the scalp distribution of these effects, three specific time-frequency locations were chosen: For the semantic incongruity condition, $t = 188$ ms and $f = 7$ Hz; for the physical mismatch condition, $t = 128$ ms and $f = 5$ Hz, as well as $t = 200$ ms and $f = 10$ Hz. For these three cases, the synchronization topography \bar{R}_{iC} for the control condition, the respective experimental condition and the statistical difference of both is shown in Fig. 6.6. The effect of the semantic incongruity

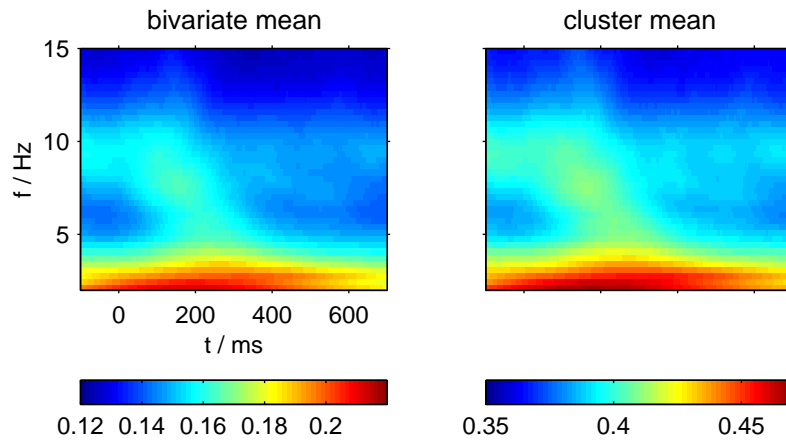


Figure 6.3: Time-frequency plots of the overall measures of synchronization, bivariate mean and cluster mean (Eq. 6.1 & 6.2), for the control condition (mean over subjects).

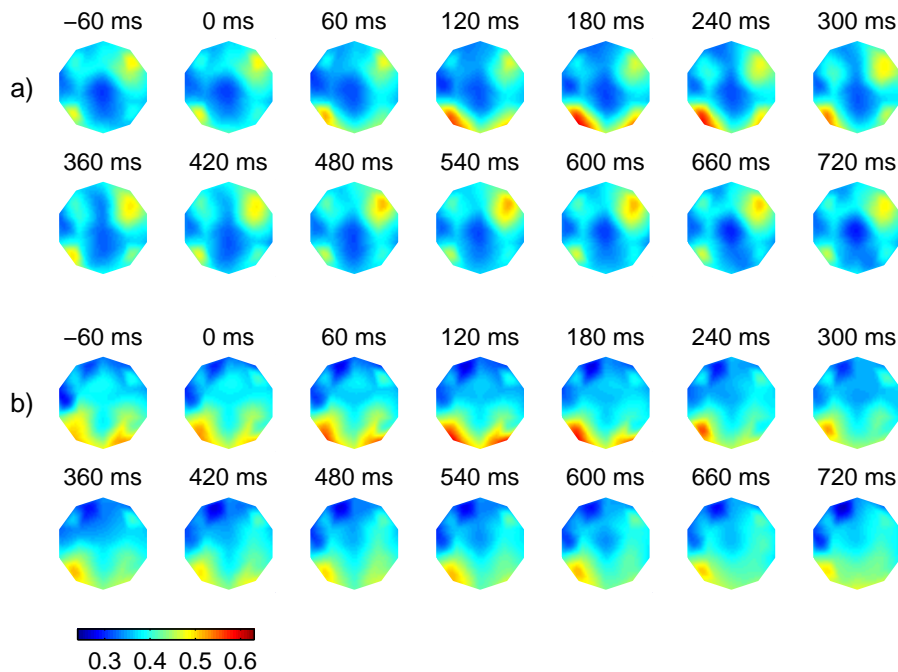


Figure 6.4: The evolution of the synchronization cluster topography over time for the control condition (mean over subjects), at 6 Hz (panel a) and 10 Hz (panel b). The colors correspond to an interpolation of the \bar{R}_{iC} -values attributed to the electrodes. For an electrode chart, see Fig. 6.6d.

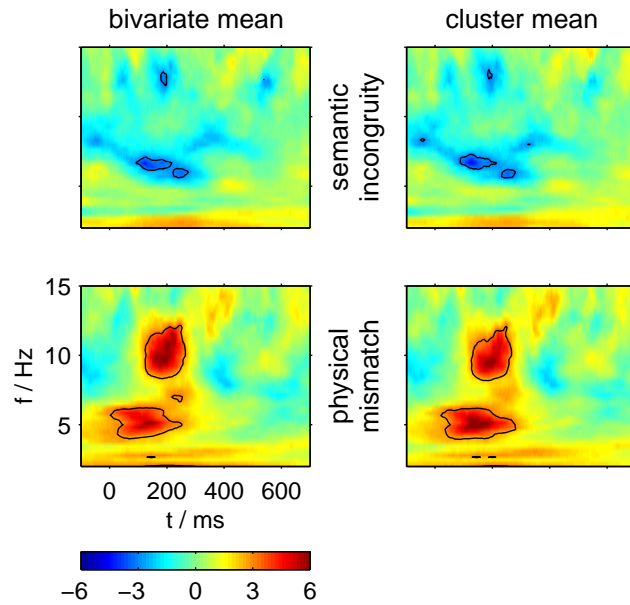


Figure 6.5: Time-frequency plots of the statistical difference between conditions for the overall measures of synchronization, bivariate mean and cluster mean (left and right column; Eq. 6.1 & 6.2). The upper row shows the difference between the semantic incongruity and the control condition, the lower row that between the physical mismatch and the control condition. The plotted quantity is the pointwise paired t statistic (over subjects); contours indicate the threshold corresponding to a two-sided test at a level of 1%.

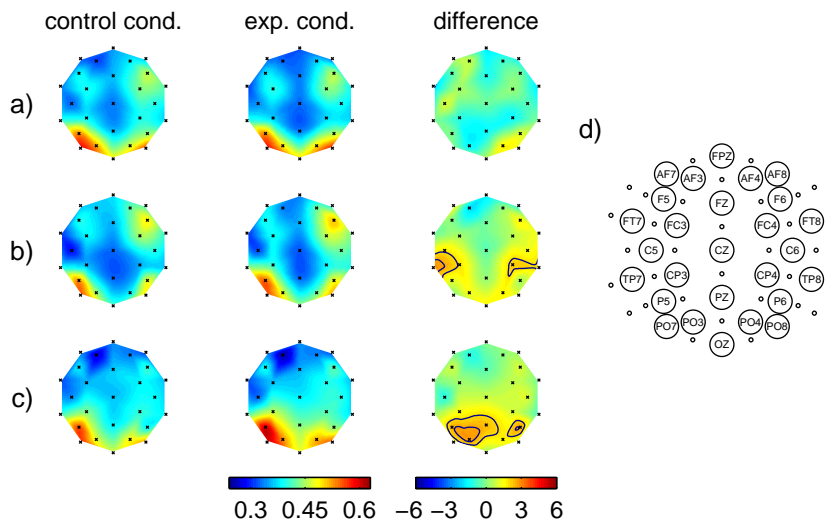


Figure 6.6: Synchronization topographies (first and second column) and statistical difference between conditions (third column) for: a) semantic incongruity vs. control condition at 188 ms and 7 Hz, b) physical mismatch vs. control condition at 128 ms and 5 Hz, and c) physical mismatch vs. control condition at 200 ms and 10 Hz. The difference measure is a statistic based on a pointwise paired permutation test (over subjects); contours indicate the threshold for a two-sided test at levels 5% and 1%.—Panel d) shows the locations of all electrodes included in the recording. Those retained for analysis after the decorrelation step are labeled with their MCN names.

can not be attributed to a specific location, it appears to be broadly distributed. For the physical mismatch at 5 Hz, there is an increased participation in the left and right temporoparietal areas ($p < 0.01$ at TP7); at 10 Hz, an increase mainly in the left parieto-occipital area ($p < 0.01$ at PO3).⁴

6.3 Discussion

The results reported above indicate that ERP average and synchronization analysis deliver comparable but not identical information about the underlying processes. The synchronization indices allow one to observe the modification of the neuronal process that is brought about by the semantic and physical deviations. Similar to the ERP components, the responses to both types of variation are clearly distinct from each other and point to opposite directions, decreased and increased synchronization.

However, the processes underlying the synchronization effects can not be simply identical to those observed in the ERP average. This is already indicated by the fact that the waveforms of the ERP components correspond to oscillations with frequencies that are lower ($< \text{ca. } 4 \text{ Hz}$) than those readily accessible by the wavelet transform (using the given epoch length). Moreover, all of the effects of decreased or increased synchronization take place *before* the effects in the ERP average. While the earliest onset of an ERP component observed in this experiment takes place at about 250 ms poststimulus, at this time the synchronization effects are almost over. Apparently, with the new analysis method processes are observed that precede and probably prepare for those visible in the averages.

The findings regarding the synchronization topography also fit into this picture. For the physical mismatch, both methods identify effects located in the temporoparietal region. This is consistent with the location of secondary visual cortex areas, that can be expected to be involved in the processing of the color change. The symmetrically increased participation may be interpreted as indicating the functional integration of homologous areas in the left and right hemispheres. For the semantic incongruity, unfortunately there is no information on the location of the decreased synchronization that appears in the overall measures. This may be because this effect is generally weaker than that of the physical deviation, so that the topographic resolution overstrains the statistical power of the data. Also, the difficulty to localize this effect is consistent with the broad distribution of the N400 ERP component (Sec. 2.2).

Regarding frequency, the synchronization effects reported here belong to the EEG theta and alpha bands (see Sec. 2.1). Higher frequencies than those shown in the time-frequency plots were originally included in the analysis, but the results above 15 Hz proved to be statistically unstable. The indications found there were confined to very small regions of the time-frequency plane and scattered about in a way that did not allow a clear identification, let alone interpretation. Therefore they have been left out of the presentation.

A study that is in some respects similar to the research reported in this chapter was recently performed by Weiss and Müller (2003).⁵ They auditorily presented

⁴For the determination of statistical differences between conditions in the ERP average (Fig. 6.2) and the bivariate and cluster mean (Fig. 6.5), the standard t statistic was applied (cf. Sheskin, 1997) because these quantities can be expected to be normally distributed in a good approximation. Since this does not necessarily hold for the \bar{R}_{iC} as a result of the synchronization cluster analysis, the p -values given here were computed by the quantile estimation underlying a permutation test (cf. Good, 1994). For the visualization (Fig. 6.6) the estimated quantile was transformed into a statistic that under H_0 follows a standard normal distribution, so that the usual thresholds of a Gauss test can be applied.

⁵This overview article only briefly describes the study (Sec. 3.2.2.1, pp. 336–337) in the context of a

German sentences with or without a semantic incongruity. EEG was recorded at 19 electrodes and processed to obtain a time- and frequency-dependent coherence.⁶ The authors found a decrease in coherence for the semantic incongruity compared to normal sentences around 30 Hz at 300–500 ms after presentation of the critical stimulus.

The study of Weiss and Müller exhibits some methodical shortcomings. Their experimental design does not include a physical mismatch condition, so that it is not possible to check whether the observed effect is caused specifically by a semantic deviation. Secondly, the EEG signals were filtered with an analog band-pass at 0.3–35 Hz before sampling. Such an analog filter is very likely to distort the phase component, especially if one takes into account that the frequency band of the main effect lies only shortly below the upper cut-off frequency of the band-pass. And finally, the validity of the bivariate ARMA approach of Schack et al. (2000) used by the authors to compute the time-frequency coherence is problematic (for a short comment, see Sec. 3.2).

Irrespective of this criticism, the finding of Weiss and Müller is materially different from the results obtained by the synchronization analysis presented here: The effect appears at a much higher frequency, and it occurs concurrently to the N400 ERP component. This disagreement may be due to the fact that stimuli were presented auditorily instead of visually, but those aspects of language processing targeted in the experiments should be largely independent of the modality. From the viewpoint of synchronization theory taken in this thesis, which argues that coherence is not to be regarded as a genuine measure of synchronization, a more likely explanation is that the coherence measure simply quantifies a different aspect of the neuronal dynamics than the phase synchronization indices employed here (see Sec. 1.2). The temporal coincidence suggests that the decreased coherence found by Weiss and Müller is more directly linked to the known N400 than the decreased synchronization effect demonstrated above.

In conclusion, the synchronization analysis has shown to provide information that can be related to the findings of the conventional method, but that goes beyond what has been known before. Especially the observation of an effect of the semantic incongruity preceding the N400 suggests that first hints at a semantic processing problem are available earlier than the time window 300–500 ms poststimulus inferred from the ERP average (Friederici, 2002). An interpretation of this finding is that the decreased synchronization marks the beginning of an attempt to the semantic integration of the verb into the sentence context, whose final failure is indicated by the N400 ERP component. Further research will be necessary to clarify this issue.

general report on the use of coherence for the investigation of language processing; the full details are not published at the time being. See also Weiss et al. (2004).

⁶Classically, coherence is the linear correlation of signals computed in the frequency domain (Sec. 1.2) and does not depend on time. The authors used a generalization of this quantity resulting from a time-frequency analysis of the signals based on a bivariate ARMA model. For details, see Weiss and Müller (2003), Sec. 2 and Schack et al. (2000).

Chapter 7

Conclusion and Outlook

The aim of the present thesis has been to contribute to the methods of phase synchronization analysis and to apply these methods to event-related potentials.

The topic of Ch. 4 have been statistical tests to detect a change in the strength of bivariate synchronization, with the aim to obtain procedures improved in theoretical validity and applicability over the approaches known from the literature. The key elements to achieve this have been a two-samples test setup, the use of a test statistic with a background in directional statistics, as well as the application of modern statistical methodology (resampling techniques). Several tests have been presented that differ in precision and applicability, but also in the computational cost of the underlying algorithm. The tests have been checked in numerical simulations, finding that an approach based on a permutation test delivers the best results. In the last section, the application of the tests to partially dependent sample data (time series) has been discussed.

Chapter 5 has motivated the need for a multivariate phase synchronization analysis (not only) for EEG data and has described a specific approach to this problem. Starting from a first notion of a statistical synchronization cluster, the consideration of clustering in coupled noisy phase oscillators has led to a straightforward specification of the data analysis algorithm. Because this approach incorporates relatively few theoretical assumptions, the author has argued for it to represent a generic multivariate phase synchronization analysis. The algorithm has been applied to event-related potentials from a visual attention experiment, detecting the transient formation of a synchronization cluster elicited by the stimulus presentation.

In the last chapter (Ch. 6), the method of synchronization cluster analysis has been applied to event-related potentials from a language processing experiment. A replication of a classic study comparing the effect of a semantic and a physical deviation was performed and has been shown to reproduce the known effects in the average ERP. The application of phase synchronization analysis to this data set has proved to provide information on the neuronal processes that can be related to the established findings but that goes beyond, identifying effects that are preceding those known from the conventional method. The cluster analysis has been shown to reveal the topographic distribution of the effect of the physical deviation. A similar study using coherence has been discussed, arguing that its results do not provide the additional information found by synchronization analysis.

In the following the author wants to comment on some topics that are related to the work presented, but that are beyond the scope of this thesis. In part these comments are concerned with methodical improvements and further research that may be addressed in the future; the other briefly discuss the results of this work in

a broader context or give remarks of a more speculative nature.

Generic decorrelation methods

A serious problem for the synchronization analysis of EEG is the strong linear correlation (due to the low spatial resolution of scalp potentials) between signals recorded from neighboring electrodes. This issue has already been treated in Sec. 3.1; the remedy described there was the spherical spline Laplacian algorithm, an approach that has a good theoretical background and works well in practice. Still, there are methods to reduce linear dependencies in multivariate data that are not specific to EEG, and that therefore do not incorporate any assumptions that may only be approximately fulfilled. Regarding these generic methods, the classic principal component analysis (that is restricted to orthogonal transforms) has in the last years been complemented by approaches trying to obtain statistically independent signals, so-called independent component analysis (ICA; cf. Ziehe and Müller, 1998). A drawback of these methods with respect to synchronization analysis is that algorithms generating independent signals are likely not only to reduce unwanted correlations, but also those corresponding to dynamical relations like synchronization. However, ongoing research (Meinecke, 2004) suggests that it is possible to avoid this effect by adapting ICA methods to the specific properties of phase synchronization. Therefore, phase synchronization analysis may in the future be combined with an ICA-based decorrelating step instead of the spherical spline Laplacian or similar methods.

Performance comparison of coherence and synchronization measures

In the introduction (Sec. 1.2) the preference for a genuine measure of phase synchronization in contrast to coherence has been established theoretically, based on a specific interest in neuronal synchronization. On the other hand, from a pragmatic viewpoint of EEG analysis it is important which of the measures provides more information on the underlying neuronal processes—a question that can only be answered empirically. Though there are studies using coherence as well as those employing synchronization analysis, because of the multitude of possible experimental subjects there are only single cases in which both methods have been applied in exactly the same context.¹ A first empirical comparison has been given by Quian Quiroga et al. (2002). The authors apply several linear and nonlinear measures to rat EEG and report that the separation between different levels of synchronization is “more pronounced with nonlinear measures” including phase synchronization. This opinion speaks in favor of the theoretical argumentation. However, it is based on a visual inspection of the analysis results and there is no quantitative measure of separation that would allow an objective rating. Further work will try to derive such a quantification based on statistical considerations.

Significance testing on time-frequency measures

Chapter 6 has shown time-frequency plots of the statistical difference between conditions for the measures of overall synchronization, along with a contour indicating the threshold corresponding to a pointwise hypothesis test at a level of 1% (see Fig. 6.5). If the statistical difference compared to the threshold was to be interpreted as actually representing a statistical test for each (t, f) -point separately, the nominal significance level of all these tests taken together would be far higher than 1%. Therefore the measure of statistical difference has been shown as such,

¹This is not the case for the experiment of Ch. 6 and the study of Weiss and Müller (2003) because of the different modality of presentation, data preprocessing, etc.

the contour being just an indication of the possibly relevant regions of the time-frequency plane.² This practice, to report exact p -values or equivalent quantities without explicitly deciding on a hypothesis, is advocated by some statisticians (cf. Cohen, 1994). In this way, the decision if the effects “are significant” is left to the reader. Still, it would be preferable if the assessment that comes to mind in interpreting these plots—that there is a significant increase in overall synchronization in certain regions—could be formulated in conformance with the traditional procedure of hypothesis testing. This may be possible by defining the compound H_0 for the whole plot not as a conjunction of elementary null hypotheses corresponding to each (t, f) -point (the compound alternative not as a disjunction), but for instance by regarding contiguous areas where a threshold is exceeded.

“40 Hz” versus lower frequency bands

The findings reported in Ch. 5 and 6 belong to the EEG frequency bands theta and alpha. In contrast to this, the synchronized oscillations found by single cell and multi-unit recordings in the cat visual cortex (Engel et al., 1991; Eckhorn et al., 1991) were in the range 40–60 Hz, and accordingly most early EEG studies aimed at synchronization focused on the EEG gamma band (above 30 Hz; see Ch. 1 for references). However, neuronal oscillations on the microscopic and macroscopic level are of a substantially different nature (see Sec. 2.1), and as Habeck and Srinivasan (2000) point out, there is little reason to expect direct agreements between data obtained at different scales. Though there actually is a large number of findings on synchronization in the gamma band, this may largely be because in many studies effects in the lower frequency bands were “not investigated, not reported, or dismissed as an epiphenomenon” (Habeck and Srinivasan). Hopefully, this attitude will change in the future. An indication of such a change is the review of von Stein and Sarnthein (2000), who propose a framework for the interpretation of effects in the different frequency bands from theta to gamma, including a relation between the scale and the frequency of synchronization-related interaction.

The nature of neuronal oscillators

As has been explained in Ch. 1, the interest in synchronization analysis of neurophysiological data including EEG was motivated by findings with microelectrode recordings in the visual cortex. The extension of this approach from single cell and multi-unit recordings to other types of data presupposes that synchronization processes can be found on multiple different scales of neuronal activity. In particular, in the application of synchronization analysis to EEG data this thesis assumes that—after decorrelation and band-pass filtering—the signals recorded at different electrodes can approximately be attributed to different autonomous oscillators. As has been mentioned in Sec. 2.1, according to the observation of Nunez (1995) that the spatial resolution of decorrelated EEG lies in the order of magnitude of a macrocolumn, the natural theoretical candidate for the macroscopic neuronal oscillator whose dynamics can be observed in the EEG is the macrocolumn.

In this context, a recent finding by Montbrió et al. (2004) may become relevant. The authors show that an ensemble of mutually coupled oscillators in the synchronized regime behaves like a single macro-oscillator, and as such can be synchronized to another macro-oscillator. Interestingly, the natural frequency of a macro-oscillator may be substantially lower than that of the single oscillators it is constituted of. This finding may provide theoretical backup for the notion of

²The alternative of selecting only specific (t, f) -pairs for statistical analysis was not taken because this research is of an explorative character and at the time being there is no prior evidence to guide such a selection.

neuronal synchronization at different spatial scales, and also account for the observation that these scales are associated with different frequencies (see previous section).

Investigation of synchronization effects in sentence comprehension

Until now, there are only few studies on neuronal synchronization related to sentence processing (cf. Weiss and Müller, 2003). For phase synchronization analysis, to the author's knowledge the research reported in Ch. 6 is the very first contribution. Because of this lack of context, at the time being it is hardly possible to give a detailed interpretation of the results. Further experiments will be necessary to achieve a deeper insight into synchronization processes related to sentence comprehension.

Even now, phase synchronization analysis has shown to be able to provide information that is not present in the ERP average, and therefore to contribute to the investigation of language comprehension. A possible use of this supplementary information is the dissociation of ERP components. For instance, the N400 component that was elicited by a semantically incongruous verb in the experiment of Ch. 6 can also be observed with many other types of semantic violation, and even with manipulations that do not represent a semantic violation in the proper sense. Röhm et al. (2004) have recently shown that it is possible to distinguish different types of the N400 by a frequency band analysis of the event-related potential at single electrodes. Further work will try to establish whether a similar dissociation of the N400 or other ERP components can be achieved by synchronization analysis.

Acknowledgements

This thesis was prepared under supervision of Prof. Jürgen Kurths. The work on it was financed by Deutsche Forschungsgemeinschaft (German Research Foundation) within the context of the research unit 375, “Conflicting Rules and Strategies for the Resolution of Conflicts in Cognitive Science”, part B1: “Diagnosis in Language Processing”. EEG experiments were performed at the Max Planck Institute of Cognitive Neuroscience, Leipzig. The language processing experiment of Ch. 6 was planned, designed and prepared in cooperation with Stefan Frisch.

A doctoral thesis can not come into existence without the help of many others. The following people supported me in different ways and to different extent, from close cooperation and extensive proofreading, over inspiring discussion or performing the EEG recordings, to listening to my worries and lending out the manual for the 100th time (in alphabetical order): Bernd Blasius, Sandra Böhme, Ina Bornkessel, Eva Brehm, Mario Chavez, Sébastien Clodong, Heiner Drenhaus, Angela D. Friederici, Stefan Frisch, Peter beim Graben, Jette Krause, Jürgen Kurths, Nina Kuckländer, Frank Meinecke, Anja Meinke, Marije Michel, Ernest Montbrió, Klaus Oberauer, Tim Rättig, Michael Rosenblum, M. Carmen Romano, Douglas Saddy, Matthias Schlesewsky, Udo Schwarz, Marco Thiel, Ruben van de Vijver, and Kristin Wittich. I sincerely want to thank you all. For the unfortunate case that I forgot someone who needed to be mentioned here: please forgive me.

Appendix A

Language Material

This appendix gives the language material of the experiment described in Sec. 6.1. It was adopted in modified form from Friederici et al. (1999). Each table row gives two sentences that are meaningful as they are. By exchanging the verbs between them, sentences with a semantic incongruity are constructed. The correct probe words for each sentence are its noun and its verb. Alternative incorrect probe words are given in the second column of the table; they were chosen to be semantically related to the correct words.

1	Die Straße wurde asphaltiert. Der Priester wurde geholt.	Weg, betoniert Pfarrer, gerufen
2	Die Wand wurde bemalt. Die Suppe wurde versalzen.	Mauer, gestrichen Soße, verdorben
3	Das Beet wurde bepflanzt. Die Maus wurde gejagt.	Feld, bebaut Ratte, verfolgt
4	Die Wolke wurde durchflogen. Die Tinte wurde vergossen.	Nebel, durchstoßen Farbe, verschüttet
5	Die Sprache wurde entschlüsselt. Das Eis wurde geschleckt.	Code, verstanden Lutscher, geleck
6	Der Docht wurde entzündet. Die Sitzung wurde vertagt.	Kerze, angesteckt Treffen, verschoben
7	Der Besucher wurde erschreckt. Die Torte wurde gezuckert.	Gast, schockiert Kuchen, verziert
8	Der Bär wurde ertränkt. Die Aufgabe wurde verlesen.	Löwe, erschossen Auftrag, verkündet
9	Die Frau wurde erwürgt. Die Flagge wurde gehisst.	Dame, erdrosselt Wimpel, aufgezogen
10	Die Luft wurde geatmet. Der Stein wurde geschleppt.	Brise, eingesogen Brocken, getragen
11	Die Mauer wurde gebaut. Der Briefträger wurde gebissen.	Wand, errichtet Postbote, angeknurrt
12	Das Fleisch wurde gebraten. Das Gestell wurde verschraubt.	Filet, gegrillt Gestänge, verschweißt
13	Die Bluse wurde gebügelt. Die Katze wurde umsorgt.	Hemd, gewaschen Hund, gepflegt
14	Das Schiff wurde geentert. Die Kuh wurde geschlachtet.	Kahn, erobert Kalb, gemästet
15	Die Zitrone wurde geerntet. Das Flugzeug wurde gelandet.	Orange, gepflückt Hubschrauber, gestartet

16	Das Abwasser wurde gefiltert. Der Strafzettel wurde zerrissen.	Abfall, gereinigt Strafmandat, verlegt
17	Das Baby wurde gefüttert. Das Metall wurde verzinkt.	Säugling, gestillt Karosserie, vergoldet
18	Die Marmelade wurde gegessen. Das Kriegsschiff wurde torpediert.	Konfitüre, gekocht Zerstörer, bombardiert
19	Das Papier wurde geheftet. Das Klavier wurde gestimmt.	Dokument, einsortiert Piano, justiert
20	Das Brett wurde gehobelt. Der Urlaub wurde genossen.	Balken, abgeschliffen Ausflug, gebucht
21	Das Haar wurde gekämmt. Die Bank wurde überfallen.	Bart, geschnitten Geschäft, ausgeraubt
22	Der Kaffee wurde gekocht. Der Leser wurde verwirrt.	Tee, zubereitet Zuhörer, abgelenkt
23	Das Kabel wurde gelötet. Der Strumpf wurde gestrickt.	Draht, angeschlossen Socke, gehäkelt
24	Das Gebäude wurde gemauert. Die Mahlzeit wurde verdaut.	Haus, gebaut Essen, genossen
25	Der Felsen wurde gemeißelt. Der Pudding wurde gerührt.	Granit, gesprengt Brei, gekocht
26	Das Bonbon wurde genascht. Die Liste wurde geschrieben.	Schokolade, gelutscht Aufstellung, aufgestellt
27	Der Ofen wurde geputzt. Der Autofahrer wurde verwarnt.	Kamin, angezündet Taxifahrer, geblitzt
28	Die Polizei wurde gerufen. Die Hecke wurde verpflanzt.	Notarzt, alarmiert Busch, beschnitten
29	Das Holz wurde gesägt. Der Autor wurde zitiert.	Material, zugeschnitten Schriftsteller, rezensiert
30	Der Apfel wurde geschält. Die Harfe wurde gezupft.	Birne, geschnitten Zither, gestimmt
31	Der Sand wurde geschaufelt. Der Helfer wurde verständigt.	Erde, ausgehoben Arzt, benachrichtigt
32	Die Abteilung wurde geschlossen. Der Sohn wurde verheiratet.	Filiale, erweitert Tochter, verlobt
33	Die Rose wurde geschnitten. Der Walzer wurde getanzt.	Blume, gebrochen Tango, geprobt
34	Die Strophe wurde gesungen. Der Reifen wurde zerstoßen.	Text, rezitiert Schlauch, aufgeschlitzt
35	Die Geisel wurde getötet. Die Massage wurde verschrieben.	Opfer, ermordet Behandlung, verordnet
36	Der Saft wurde getrunken. Der Teppich wurde gewebt.	Wasser, gepresst Matte, geklopft
37	Der Kaktus wurde gewässert. Der Vorschlag wurde verdeutlicht.	Pflanze, eingetopft Vorlage, erläutert
38	Die Hose wurde gewaschen. Der Vortrag wurde verstanden.	Rock, gebügelt Erklärung, abgesagt
39	Die Lampe wurde repariert. Die Gazelle wurde verletzt.	Fernseher, renoviert Antilope, getötet
40	Die Halle wurde vergrößert. Der Mörder wurde verurteilt.	Raum, ausgebaut Täter, bestraft
41	Der Baum wurde gefällt. Das Buch wurde kopiert.	Wald, abgeholzt Werk, vervielfältigt

42	Das Brot wurde gebacken. Die Zeitung wurde abonniert.	Brötchen, geschnitten Zeitschrift, bestellt
43	Der Computer wurde eingeschaltet. Die Flasche wurde ausgetrunken.	Rechner, hochgefahren Glas, geleert
44	Das Geschenk wurde verpackt. Die Krankheit wurde geheilt.	Gabe, eingepackt Leiden, behandelt
45	Der Verdächtige wurde befragt. Der Rasen wurde gemäht.	Zeuge, vernommen Wiese, gewässert
46	Das Geschirr wurde gespült. Der Gast wurde begrüßt.	Besteck, abgewaschen Besucher, empfangen
47	Die Glocke wurde geläutet. Die Zitrone wurde ausgepresst.	Klingel, betätigt Orange, ausgedrückt
48	Der Ball wurde geworfen. Das Haus wurde abgerissen.	Speer, getreten Gebäude, gesprengt
49	Die Zigarette wurde geraucht. Der Beamte wurde beleidigt.	Zigarre, gepafft Angestellte, bestochen
50	Das Essen wurde verdaut. Der Verbrecher wurde bestraft.	Mahl, verschlungen Sünder, verurteilt
51	Die Pizza wurde aufgetaut. Das Problem wurde gelöst.	Lasagne, bestellt Schwierigkeit, umgangen
52	Der Braten wurde serviert. Das Märchen wurde erzählt.	Steak, aufgetragen Geschichte, vorgelesen

Bibliography

C. Allefeld and J. Kurths. An approach to multivariate phase synchronization analysis and its application to event-related potentials. *International Journal of Bifurcation and Chaos*, 14(2), 2004a.

C. Allefeld and J. Kurths. Testing for phase synchronization. *International Journal of Bifurcation and Chaos*, 14(2), 2004b.

E. O. Altenmüller and C. Gerloff. Psychophysiology and the EEG. In E. Niedermeyer and F. Lopes da Silva, editors, *Electroencephalography: Basic Principles, Clinical Applications, and Related Fields*, chapter 32, pages 637–655. Lippincott Williams & Wilkins, 4th edition, 1998.

The American Electroencephalographic Society. Guidelines for standard electrode position nomenclature. *Journal of Clinical Neurophysiology*, 8(2):200–202, 1991.

P. beim Graben. *Symbolische Dynamik ereigniskorrelierter Gehirnpotentiale in der Sprachverarbeitung*. Shaker, 2001.

P. beim Graben, J. D. Saddy, M. Schlesewsky, and J. Kurths. Symbolic dynamics of event-related brain potentials. *Physical Review E*, 62(4):5518–5541, 2000.

J. Bhattacharya, E. Pereda, R. Kariyappa, and P. P. Kanjilal. Application of nonlinear analysis to intensity oscillations of the chromospheric bright points. *Solar Physics*, 199:267–290, 2001.

J. Bhattacharya and H. Petsche. Enhanced phase synchrony in the electroencephalograph γ band for musicians while listening to music. *Physical Review E*, 64:012902, 2001.

B. Blasius, A. Huppert, and L. Stone. Complex dynamics and phase synchronization in spatially extended ecological systems. *Nature*, 399:354–359, 1999.

S. Boccaletti, J. Kurths, G. Osipov, D. L. Valladares, and C. S. Zhou. The synchronization of chaotic systems. *Physics Reports*, 366:1–101, 2002.

S. Braeutigam, A. J. Bailey, and S. J. Swithenby. Phase-locked gamma band responses to semantic violation stimuli. *Cognitive Brain Research*, 10:365–377, 2001.

M. Breakspear. Nonlinear phase desynchronization in human electroencephalographic data. *Human Brain Mapping*, 15:175–198, 2002.

D. T. Campbell and J. C. Stanley. *Experimental and Quasi-Experimental Designs for Research*. Houghton Mifflin, 1963.

R. Carmona, W.-L. Hwang, and B. Torrésani. *Practical Time-Frequency Analysis. Gabor and Wavelet Transforms with an Implementation in S*. Academic Press, 1998.

- M. Chavez, D. Cosmelli, J.-P. Lachaux, M. Le Van Quyen, and J. Martinerie. Plasticity of neural networks during ongoing perception: Phase synchronization and clustering in magnetoencephalographic dynamics. submitted, 2003.
- J. Cohen. The earth is round ($p < .05$). *American Psychologist*, 49:997–1003, 1994.
- M. G. H. Coles and M. D. Rugg. Event-related brain potentials: an introduction. In M. D. Rugg and M. G. H. Coles, editors, *Electrophysiology of Mind: Event-Related Potentials and Cognition*, pages 1–26. Oxford University Press, 1995.
- A. R. Damasio. Synchronous activation in multiple cortical regions: a mechanism for recall. *The Neurosciences*, 2:287–296, 1990.
- M. Daneman and P. A. Carpenter. Individual differences in working memory and reading. *Journal of Verbal Learning and Verbal Behavior*, 19(4):450–466, 1980.
- D. J. DeShazer, R. Breban, E. Ott, and R. Roy. Detecting phase synchronization in a chaotic laser array. *Physical Review Letters*, 87:044101, 2001.
- H. Drenhaus. *Minimalism, Features and Parallel Grammars: On the acquisition of German ditransitive structures*. PhD thesis, University of Potsdam, 2003.
- R. Eckhorn, T. Schanze, M. Brosch, W. Salem, and R. Bauer. Stimulus-specific synchronizations in cat visual cortex: Multiple microelectrode and correlation studies from several cortical areas. In E. Başar and T. H. Bullock, editors, *Induced Rhythms in the Brain*. Birkhäuser, 1991.
- B. Efron and R. J. Tibshirani. *An Introduction to the Bootstrap*. Chapman & Hall, 1993.
- A. K. Engel, P. Fries, and W. Singer. Dynamic predictions: Oscillations and synchrony in top-down processing. *Nature Reviews Neuroscience*, 2(10):704–716, 2001.
- A. K. Engel, P. König, A. K. Kreiter, C. M. Gray, and W. Singer. Temporal coding by coherent oscillations as a potential solution to the binding problem: Physiological evidence. In H. G. Schuster, editor, *Nonlinear Dynamics and Neuronal Networks*, pages 3–25. VCH, 1991.
- A. K. Engel and W. Singer. Temporal binding and the neural correlates of sensory awareness. *Trends in Cognitive Sciences*, 2001.
- A. D. Friederici. The time course of syntactic activation during language processing: A model based on neuropsychological and neurophysiological data. *Brain and Language*, 50:259–281, 1995.
- A. D. Friederici. Towards a neural basis of auditory sentence processing. *Trends in Cognitive Sciences*, 6(2):78–84, 2002.
- A. D. Friederici, K. Steinhauer, and S. Frisch. Lexical integration: Sequential effects of syntactic and semantic information. *Memory & Cognition*, 27(3):438–453, 1999.
- D. Gabor. Theory of communication. *The journal of the Institution of Electrical Engineers. Part 3, Radio and Communication Engineering*, 93(26):429–457, 1946.
- P. Good. *Permutation Tests. A Practical Guide to Resampling Methods for Testing Hypotheses*. Springer, 1994.
- C. G. Habeck and R. Srinivasan. Natural solutions to the problem of functional integration. *Behavioral and Brain Sciences*, 23(3):402–403, 2000.

- A. R. Haig, E. Gordon, J. J. Wright, R. A. Meares, and H. Bahramali. Synchronous cortical gamma-band activity in task-relevant cognition. *Neuroreport*, 11(4):669–675, 2000.
- C. S. Herrmann and A. Mecklinger. Magnetoencephalographic responses to illusory figures: Early evoked gamma is affected by processing of stimulus features. *International Journal of Psychophysiology*, 38:265–281, 2000.
- C. S. Herrmann, A. Mecklinger, and E. Pfeifer. Gamma responses and ERPs in a visual classification task. *Clinical Neurophysiology*, 110:636–642, 1999.
- W. Härdle, J. Horowitz, and J.-P. Kreiß. Bootstrap methods for time series. *International Statistical Review*, 71(2):435–459, 2003.
- K. K. Jerger, T. I. Netoff, J. T. Francis, T. Sauer, L. Pecora, S. L. Weinstein, and S. J. Schiff. Early seizure detection. *Journal of Clinical Neurophysiology*, 18(3):259–268, 2001.
- G. K. Kanizsa. Subjective contours. *Scientific American*, 235:48–52, 1976.
- H. Kantz and T. Schreiber. *Nonlinear Time Series Analysis*. Cambridge University Press, 1997.
- Y. Kuramoto. *Chemical Oscillations, Waves and Turbulence*. Springer, 1984.
- M. Kutas and S. A. Hillyard. Event-related brain potentials to semantically inappropriate and surprisingly large words. *Biological Psychology*, 11:99–116, 1980a.
- M. Kutas and S. A. Hillyard. Reading senseless sentences: Brain potentials reflect semantic incongruity. *Science*, 207:203–204, 1980b.
- J.-P. Lachaux, E. Rodriguez, J. Martinerie, C. Adam, D. Hasboun, and F. J. Varela. A quantitative study of gamma-band activity in human intracranial recordings triggered by visual stimuli. *European Journal of Neuroscience*, 12:2608–2622, 2000.
- J.-P. Lachaux, E. Rodriguez, J. Martinerie, and F. J. Varela. Measuring phase synchrony in brain signals. *Human Brain Mapping*, 8:194–208, 1999.
- T. D. Lagerlund, F. W. Sharbrough, C. R. Jack, Jr., B. J. Erickson, D. C. Strelow, K. M. Cicora, and N. E. Busacker. Determination of 10-20 system electrode locations using magnetic resonance image scanning with markers. *Electroencephalography and clinical Neurophysiology*, 86:7–14, 1993.
- A. R. Laird, B. P. Rogers, J. D. Carew, K. Arfanakis, C. H. Moritz, and M. E. Meyerand. Characterizing instantaneous phase relationships in whole-brain fMRI activation data. *Human Brain Mapping*, 16:71–80, 2002.
- M. Le Van Quyen, J. Foucher, J.-P. Lachaux, E. Rodriguez, A. Lutz, J. Martinerie, and F. J. Varela. Comparison of Hilbert transform and wavelet methods for the analysis of neuronal synchrony. *Journal of Neuroscience Methods*, 111:83–98, 2001a.
- M. Le Van Quyen, J. Martinerie, V. Navarro, M. Baulac, and F. J. Varela. Characterizing neurodynamic changes before seizures. *Journal of Clinical Neurophysiology*, 18(3):191–208, 2001b.
- K.-H. Lee, L. M. Williams, M. Breakspear, and E. Gordon. Synchronous Gamma activity: a review and contribution to an integrative neuroscience model of schizophrenia. *Brain Research Reviews*, 41:57–78, 2003.
- E. L. Lehmann. *Testing Statistical Hypotheses*. Springer, 1997.

- F. Lopes da Silva. EEG analysis: Theory and practice. In E. Niedermeyer and F. Lopes da Silva, editors, *Electroencephalography: Basic Principles, Clinical Applications, and Related Fields*, chapter 61, pages 1135–1163. Lippincott Williams & Wilkins, 4th edition, 1998a.
- F. Lopes da Silva. Event-related potentials: Methodology and quantification. In E. Niedermeyer and F. Lopes da Silva, editors, *Electroencephalography: Basic Principles, Clinical Applications, and Related Fields*, chapter 52, pages 947–957. Lippincott Williams & Wilkins, 4th edition, 1998b.
- F. Lunkeit. Synchronization experiments with an atmospheric global circulation model. *Chaos*, 11:47–51, 2001.
- W. Lutzenberger, F. Pulvermüller, and N. Birbaumer. Words and pseudowords elicit distinct patterns of 30-Hz EEG responses in humans. *Neuroscience Letters*, 176:115–118, 1994.
- S. Makeig, M. Westerfield, T.-P. Jung, S. Enghoff, J. Townsend, E. Courchesne, and T. J. Sejnowski. Dynamic brain sources of visual evoked responses. *Science*, 295: 690–694, 2002.
- S. Mallat. *A Wavelet Tour of Signal Processing*. Academic Press, 1998.
- E. Mammen and S. Nandi. Change of the nature of a test when surrogate data are applied. submitted, 2004.
- K. V. Mardia. *Statistics of Directional Data*. Wiley, 1972.
- K. V. Mardia and P. E. Jupp. *Directional Statistics*. Wiley, 2000.
- F. Meinecke. Measuring phase synchronization on superimposed signals. draft, 2004.
- W. H. R. Miltner, C. Braun, M. Arnold, H. Witte, and E. Taub. Coherence of gamma-band EEG activity as a basis for associative learning. *Nature*, 397:434–436, 1999.
- M. M. Müller. Hochfrequente oszillatorische Aktivitäten im menschlichen Gehirn. *Zeitschrift für experimentelle Psychologie*, 47(4):231–252, 2000.
- E. Montbrió, J. Kurths, and B. Blasius. Synchronization between populations of nonidentical phase oscillators. draft, 2004.
- F. Mormann, K. Lehnertz, P. David, and C. E. Elger. Mean phase coherence as a measure for phase synchronization and its application to EEG of epilepsy patients. *Physica D*, 144:358–369, 2000.
- E. Niedermeyer. The normal EEG of the waking adult. In E. Niedermeyer and F. Lopes da Silva, editors, *Electroencephalography: Basic Principles, Clinical Applications, and Related Fields*, chapter 9, pages 149–173. Lippincott Williams & Wilkins, 4th edition, 1998.
- P. L. Nunez. *Electric Fields of the Brain. The Neurophysics of EEG*. Oxford University Press, 1981.
- P. L. Nunez. Quantitative states of neocortex. In P. L. Nunez, editor, *Neocortical Dynamics and Human EEG Rhythms*, pages 3–67. Oxford University Press, 1995.

- P. L. Nunez, R. Srinivasan, A. F. Westdorp, R. S. Wijesinghe, D. M. Tucker, R. B. Silberstein, and P. J. Cadusch. EEG coherency I: Statistics, reference electrode, volume conduction, Laplacians, cortical imaging, and interpretation at multiple scales. *Electroencephalography and clinical Neurophysiology*, 103:499–515, 1997.
- G. V. Osipov and J. Kurths. Regular and chaotic phase synchronization of coupled circle maps. *Physical Review E*, 65:016216, 2001.
- G. V. Osipov, A. S. Pikovsky, M. G. Rosenblum, and J. Kurths. Phase synchronization effects in a lattice of nonidentical Rössler oscillators. *Physical Review E*, 55(3): 2353–2361, 1997.
- M. Paluš. Detecting phase synchronization in noisy systems. *Physics Letters A*, 235:341–351, 1997.
- M. Paluš and D. Hoyer. Detecting nonlinearity and phase synchronization with surrogate data. *IEEE Engineering in Medicine and Biology*, 17:40–45, 1998.
- M. Paluš, J. Kurths, U. Schwarz, D. Novotná, and I. Charvátová. Is the solar activity cycle synchronized with the solar inertial motion? *International Journal of Bifurcation and Chaos*, 10(11):2519–2526, 2000.
- U. Parlitz, L. Junge, and W. Lauterborn. Experimental observation of phase synchronization. *Physical Review E*, 54(2):2115–2117, 1996.
- L. M. Pecora and T. L. Carroll. Synchronization in chaotic systems. *Physical Review Letters*, 64(8):821–824, 1990.
- W. D. Penny, S. J. Kiebel, J. M. Kilner, and M. D. Rugg. Event-related brain dynamics. *Trends in Neurosciences*, 25(8):387–389, 2002.
- F. Perrin, O. Bertrand, and J. Pernier. Scalp current density mapping: Value and estimation from potential data. *IEEE Transactions on Biomedical Engineering*, 34(4): 283–288, 1987.
- F. Perrin, J. Pernier, O. Bertrand, and J. F. Echallier. Spherical splines for scalp potential and current density mapping. *Electroencephalography and clinical Neurophysiology*, 72:184–187, 1989. see also Corrigenda. *ibid.*, 76:565–566, 1990.
- G. Pfurtscheller. EEG event-related desynchronization (ERD) and event-related synchronization (ERS). In E. Niedermeyer and F. Lopes da Silva, editors, *Electroencephalography: Basic Principles, Clinical Applications, and Related Fields*, chapter 53, pages 958–967. Lippincott Williams & Wilkins, 4th edition, 1998.
- A. Pikovsky, M. Rosenblum, and J. Kurths. *Synchronization: A Universal Concept in Nonlinear Sciences*. Cambridge University Press, 2001.
- A. S. Pikovsky, M. G. Rosenblum, and J. Kurths. Synchronization in a population of globally coupled chaotic oscillators. *Europhysics Letters*, 34(3):165–170, 1996.
- A. S. Pikovsky, M. G. Rosenblum, G. V. Osipov, and J. Kurths. Phase synchronization of chaotic oscillators by external driving. *Physica D*, 104:219–238, 1997.
- F. Pulvermüller, C. Eulitz, C. Pantev, B. Mohr, B. Feige, W. Lutzenberger, T. Elbert, and N. Birbaumer. High-frequency cortical responses reflect lexical processing: an MEG study. *Electroencephalography and clinical Neurophysiology*, 98:76–85, 1996.
- R. Quian Quiroga, A. Kraskov, T. Kreuz, and P. Grassberger. Performance of different synchronization measures in real data: a case study on electroencephalographic signals. *Physical Review E*, 65:041903, 2002.

- E. L. Reilly. EEG recording and operation of the apparatus. In E. Niedermeyer and F. Lopes da Silva, editors, *Electroencephalography: Basic Principles, Clinical Applications, and Related Fields*, chapter 7, pages 122–142. Lippincott Williams & Wilkins, 4th edition, 1998.
- D. Röhm, M. Schlesewsky, I. Bornkessel, S. Frisch, and H. Haider. Fractionating language comprehension via frequency characteristics of the human EEG. *Neuroreport*, 15(3):409–412, 2004.
- E. Rodriguez, N. George, J.-P. Lachaux, J. Martinerie, B. Renault, and F. J. Varela. Perception's shadow: Long-distance synchronization of human brain activity. *Nature*, 397:430–433, 1999.
- E. Rosa, Jr., W. B. Pardo, C. M. Ticos, J. A. Walkenstein, and M. Monti. Phase synchronization of chaos in a plasma discharge tube. *International Journal of Bifurcation and Chaos*, 10(11):2551–2563, 2000.
- M. G. Rosenblum, A. S. Pikovsky, and J. Kurths. Phase synchronization of chaotic oscillators. *Physical Review Letters*, 76:1804–1807, 1996.
- M. G. Rosenblum, A. S. Pikovsky, and J. Kurths. From phase to lag synchronization in coupled chaotic oscillators. *Physical Review Letters*, 78:4193–4196, 1997.
- J. Sarthain, H. Petsche, P. Rappelsberger, G. L. Shaw, and A. von Stein. Synchronization between prefrontal and posterior association cortex during human working memory. *Proceedings of the National Academy of Sciences*, 95:7092–7096, 1998.
- B. Schack, P. Rappelsberger, C. Anders, S. Weiss, and E. Möller. Quantification of synchronization processes by coherence and phase and its application in analysis of electrophysiological signals. *International Journal of Bifurcation and Chaos*, 10(11):2565–2586, 2000.
- C. Schäfer, M. G. Rosenblum, H.-H. Abel, and J. Kurths. Synchronization in human cardiorespiratory system. *Physical Review E*, 60:857–870, 1999.
- D. J. Sheskin. *Handbook of Parametric and Nonparametric Statistical Procedures*. CRC Press, 1997.
- W. Singer. Response synchronization: A universal coding strategy for the definition of relations. In M. S. Gazzaniga, editor, *The New Cognitive Neurosciences*, chapter 23, pages 325–338. MIT Press, 2nd edition, 2000.
- W. Singer. Consciousness and the binding problem. *Annals of the New York Academy of Sciences*, 929:123–146, 2001.
- S. H. Strogatz. From Kuramoto to Crawford: Exploring the onset of synchronization in populations of coupled oscillators. *Physica D*, 143:1–20, 2000.
- C. Tallon-Baudry, O. Bertrand, C. Delpuech, and J. Pernier. Stimulus specificity of phase-locked and non-phase-locked 40 Hz visual responses in human. *Journal of Neuroscience*, 16(13):4240–4249, 1996.
- P. Tass, M. G. Rosenblum, J. Weule, J. Kurths, A. Pikovsky, J. Volkman, A. Schnitzler, and H.-J. Freund. Detection of $n : m$ phase locking from noisy data: Application to magnetoencephalography. *Physical Review Letters*, 81(15):3291–3294, 1998.

- J. Theiler, S. Eubank, A. Longtin, B. Galdrikian, and J. D. Farmer. Testing for nonlinearity in time series: the method of surrogate data. *Physica D*, 58(77), 1992.
- E. Thompson and F. Varela. Radical embodiment: Neural dynamics and consciousness. *Trends in Cognitive Sciences*, 5(10):418–425, 2001.
- F. Varela, J.-P. Lachaux, E. Rodriguez, and J. Martinerie. The Brainweb: Phase synchronization and large-scale integration. *Nature Reviews Neuroscience*, 2:229–239, 2001.
- F. J. Varela. Resonant cell assemblies: A new approach to cognitive functions and neuronal synchrony. *Biological Research*, 28:81–95, 1995.
- C. von der Malsburg. Nervous structures with dynamical links. *Berichte der Bunsengesellschaft für Physikalische Chemie*, 89:703–710, 1985.
- C. von der Malsburg. Binding in models of perception and brain function. *Current Opinion in Neurobiology*, 5:520–526, 1995.
- C. von der Malsburg and W. Schneider. A neural cocktail-party processor. *Biological Cybernetics*, 54:29–40, 1986.
- A. von Stein and J. Sarnthein. Different frequencies for different scales of cortical integration: from local gamma to long range alpha/theta synchronization. *International Journal of Psychophysiology*, 38:301–313, 2000.
- W. Wang, I. Z. Kiss, and J. L. Hudson. Experiments on arrays of globally coupled chaotic electrochemical oscillators: Synchronization and clustering. *Chaos*, 10(1): 248–256, 2000.
- S. Weiss and H. M. Müller. The contribution of EEG coherence to the investigation of language. *Brain and Language*, 85:325–343, 2003.
- S. Weiss, H. M. Müller, and P. Rappelsberger. Processing concepts and scenarios: Electrophysiological findings on language representation. In A. Riegler, M. Peschl, and A. von Stein, editors, *Understanding Representation in the Cognitive Sciences*, pages 237–245. Kluwer Academic / Plenum Publishers, 1999.
- S. Weiss, P. Rappelsberger, B. Schack, and H. M. Müller. Kohärenz- und Phasenuntersuchungen und ihre Bedeutung für die Untersuchung von Sprachprozessen. In H. M. Müller and G. Rickheit, editors, *Neurokognition der Sprache*, pages 211–258. Stauffenburg, 2004.
- M. A. Zaks, E.-H. Park, M. G. Rosenblum, and J. Kurths. Alternating locking ratios in imperfect phase synchronization. *Physical Review Letters*, 82(21):4228–4231, 1999.
- C. Zhou and J. Kurths. Noise induced phase synchronization and synchronization transitions in chaotic oscillators. *Physical Review Letters*, 88:230602, 2002.
- A. Ziehe and K.-R. Müller. TDSEP – an efficient algorithm for blind separation using time structure. In L. Niklasson, editor, *ICANN 98: Proceedings of the 8th International Conference on Artificial Neural Networks*, pages 675–680. Springer, 1998.